AD-A051 126 LOGICON INC LEXINGTON MA F/G 4/1
ANALYSIS AND RESEARCH FOR INTEGRATED SYSTEMS IN PHYSICS OF THE --ETC(U)
NOV 77 J N BASS, K H BHAVNANI, B J GUZ F19628-76-C-0304
UNCLASSIFIED AFGL-TR-77-0265 NL

1 OF 2
AD
A051126

(2)

AFGL-TR-77-0265

ANALYSIS AND RESEARCH FOR INTEGRATED SYSTEMS IN PHYSICS OF THE ATMOSPHERE

James N. Bass
Krishin H. Bhavnani
Ben-Zion J. Guz
Robert R. Hayes
Shu T. Lai
Richard Pavelle
David C. Schwank
Donna L. Spiegelman
Leo A. Whelan

Logicon, Inc.
18 Hartwell Avenue
Lexington, Massacusetts 01731

30 November 1977

Final Report for Period 1 September 1976 - 30 September 1977

Approved for public release; distribution unlimited.

AIR FORCE GEOPHYSICS LABORATORY
AIR FORCE SYSTEMS COMMAND
UNITED STATES AIR FORCE
HANSCOM AFB, MASSACHUSETTS 01731

Unclassified

SECURITY CLASSIFICATION OF THIS PAGE (When Data Entered)

REPORT DOCUMENTATION PAGE

READ INSTRUCTIONS BEFORE COMPLETING FORM

1. REPORT NUMBER	2. GOVT ACCESSION NO.	3. RECIPIENT'S CATALOG NUMBER
AFGL-TR-77-0265		

4. TITLE (and Subtitle)
ANALYSIS AND RESEARCH FOR INTEGRATED SYSTEMS IN PHYSICS OF THE ATMOSPHERE.

5. TYPE OF REPORT & PERIOD COVERED
Final rept.
1 Sep 76 - 30 Sep 77

6. PERFORMING ORG. REPORT NUMBER

7. AUTHOR(s)
James N. Bass, Robert R. Hayes, Shu T. Lai, Krishin H. Bhavnani, Richard Pavelle, Donna L. Spiegelman, Ben-Zion J. Guz, David Schwank, Leo A. Whelan

8. CONTRACT OR GRANT NUMBER(s)
F19628-76-C-0304

9. PERFORMING ORGANIZATION NAME AND ADDRESS
LOGICON, INC.
18 Hartwell Avenue
Lexington, MA., 02173

10. PROGRAM ELEMENT, PROJECT, TASK AREA & WORK UNIT NUMBERS
P- n/a-Tn/a-WUn/a
PE 61102F

11. CONTROLLING OFFICE NAME AND ADDRESS
Air Force Geophysics Laboratory
Hanscom AFB, Massachusetts, 01731
Contract Monitor: Edward C. Robinson/SUA

12. REPORT DATE
30 Nov 77

13. NUMBER OF PAGES
168 Pages

14. MONITORING AGENCY NAME & ADDRESS (if different from Controlling Office)

15. SECURITY CLASS. (of this report)
Unclassified

15a. DECLASSIFICATION/DOWNGRADING SCHEDULE

16. DISTRIBUTION STATEMENT (of this Report)
Approved for Public release; distribution unlimited.

DDC RECEIVED MAR 13 1978 B

17. DISTRIBUTION STATEMENT (of the abstract entered in Block 20, if different from Report)

18. SUPPLEMENTARY NOTES
Tech, Other

19. KEY WORDS (Continue on reverse side if necessary and identify by block number)

Computer Programs	Geopotential Models	Satellite Orbits
Astronomical Ephemeris	Ionospheric Research	Scintillations
Data Packing Routines	Multi-Spectral Measurement	Steepest Descent Method
DMSP Project	Orbit Determination	Topside Plasma Monitor
Electric Fields	Plasma Motion	Worldmap

20. ABSTRACT (Continue on reverse side if necessary and identify by block number)
This report describes significant analyses and computer programming problems performed in support of Air Force Geophysics Laboratory scientists. Mathematical and logical procedures are discussed; reference material and samples of results are presented.

Various AFGL rapid orbit generation programs have been modified for satellite observation by aircraft, for prediction of longitude drift due to resonances, and for improved estimation of solar eclipsing.

DD FORM 1 JAN 73 1473 EDITION OF 1 NOV 65 IS OBSOLETE

next page

Unclassified

SECURITY CLASSIFICATION OF THIS PAGE (When Data Entered)

409 990

Geopotential model studies were conducted to identify significant terms and evaluate results in operational orbit determination programs.

Ionospheric research programs include data reduction and analyses for plasma motion and electric field mapping, topside plasma monitoring on a Univac 1110, and scintillations modeling for equatorial and high latitude station coverage. A geographic-geomagnetic background continental outline plot program is also described.

Analysis and data processing for the Multi-Spectral Measurement Program includes calibrations and initial flight data base design.

A general data compaction routine for use with large data bases is described.

A revised astronomical ephemeris program which uses the new JPL planetary system was developed.

Acknowledgements

The coordination, guidance and encouragement of our Contract Monitor, Mr. Edward Robinson of the Analysis and Simulation Branch, is deeply appreciated.

Mr. Robert McInerney, Branch Chief, and earlier, Ms. Eunice Cronin, ably supported by Mrs. Isabel Hussey, Mr. John Kotelly, and Dr. Paul Tsipouras, all of the Analysis and Simulation Branch, provided invaluable help through their involvement and interest in many of the projects.

Thanks are also due to the initiators and investigators on the various projects, whose technical motivation and direction has consistently benefited our participation in AFGL research.

For Logicon, Ms. Kim Terrell coordinated the technical typing and compilation admirably with the efficient help of Ms. Karen Favreau and Ms. Kathleen Lecaroz.

Dr. Shu Lai, Logicon Project Leader, edited this report.

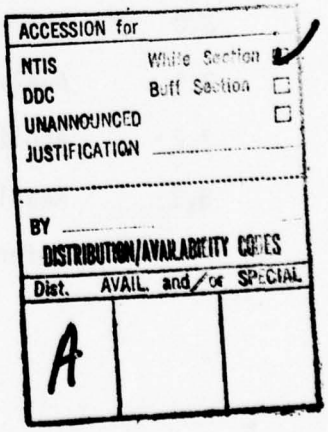

Table of Contents

Table of Contents (cont.)

Table of Contents (cont.)

List of Figures

List of Figures (cont.)

List of Figures (cont.)

List of Tables

Section 1. Satellite Orbits

Authors: K. H. Bhavnani

B. J. Guz

D. L. Spiegelman

1.1 Observing Satellite from Aircraft

Initiator: J. Buchau

Project No: 4643 Problem No: 4714

The capability of program LOKANGL to produce the position of a satellite with respect to an observation station was augmented by adding subroutine CORFL. This addition allows program LOKANGL to observe a satellite from an aircraft as a moving station. Subroutine CORFL calculates for any moment of time the corresponding aircraft position, given a sequence of its path segments and its flying altitude. Input information describing the path of an aircraft may be given either in the regular format provided for stations in LOKANGL, or in the format used by the researcher. In this latter case the special service program FLTRANS was created to transfer such information to the format acceptable by LOKANGL. Figure 1 reflects the updated input format.

1.1.1 Functional Description

The path of the aircraft consists of a number of segments. Each segment is considered a part of a great circle and is given by its starting and ending coordinates (longitude, latitude), as well as the flight altitude. Each flight segment is thus given as two stations. Subroutine CORFL interpolates the aircraft position at any desired instant, and this location is then considered by LOKANGL as an observation station position for output calculations. When a number of flight segments is given, program LOKANGL should be provided with a corresponding number of pairs of station cards for starting and ending positions. Number of stations in LOKANGL input should be equal to the number of flight segments.

```
*****************************************************************  LOKANG
   INPUT FORMAT FOR PROGRAM LOKANGL                                  LOKANG
*****************************************************************  LOKANG
   DATA DECK SETUP                                                   LOKANG
                                                                     LOKANG
   CARD     COLS                  DESCRIPTION                        LOKANG
   1        1      CODE OF ORBITAL DETERMINATION FORM                LOKANG
                   1=FORM NO. 3 :   SCF 2-CARD POS.-VEL. SET        LOKANG
                   2=FORM NO. 2 :   AOC 2-CARD ELEMENT DATA SET     LOKANG
                   3=3-CARD ELEMENT DATA SET                        LOKANG
                   4=OSCULATING ELEMENTS                            LOKANG
                   5=FORM NO.1: AOC 5-CARD DATA SET                 LOKANG
                                                                    LOKANG
   2+              ONE OR MORE ELEMENT SETS                         LOKANG
           8-9     X OR U ON FIRST CARD OF ALL SUBSEQUENT ELEMENT SETS LOKANG
                                                                    LOKANG
   3       1-3     NO. OF STATIONS. IF NO STATIONS USE 0            LOKANG
           4       CODE 1 OR 0 FOR PRINT CONTROL OF STATION DATA    LOKANG
                   0=PRINT BY TIME ONLY                             LOKANG
                   1=PRINT BY STATIONS                              LOKANG
           7-10    0=STANDARD                                       LOKANG
                   IONOHT=SUB-IONOSPHERIC ALTITUDE (KM)    I3       LOKANG
           13-15   MINELV= MIN ELEVATION FOR SAT VIEWING  I3       LOKANG
                                                                    LOKANG
   3+              STATION LOCATION CARDS,IF NMS.GT.0               LOKANG
           1-5     I.D. OF STATION (NUMBER)                         LOKANG
           7-8       2=GEODETIC SYSTEM                              LOKANG
                     -1=INDICATES MOVING STATION (AIRCRAFT)         LOKANG
           9-23    STATION GEODETIC LATITUDE. DEGREES               LOKANG
           24-38   STATION LONGITUDE (POSITIVE WEST). DEGREES       LOKANG
           39-53   STATION HEIGHT. METERS                           LOKANG
           61-72   NAME OF STATION                                  LOKANG
                                                                    LOKANG
   4       1-16    TIME INCREMENT IN SECONDS. F15.5                 LOKANG
           17-59   TIME INTERVAL FOR PRINT OR TAPE 3 WRITE          LOKANG
                   START COLS: 17-18;20-21;23-24;26-29;31-34;36-41  LOKANG
                   FINAL COLS: 43-44;46-47;49-50;52-55;57-60;62-67  LOKANG
                   TIME        MONTH;  DAY; YEAR; HOUR;  MIN;  SEC  LOKANG
                   FORMAT         I2;   I2;   I2; F3.1; F3.1; F5.3  LOKANG
                                                                    LOKANG
   5               CODE FOR PRINT-OUT: 0=NO PRINT: 1=PRINT  FOLLOWING: LOKANG
           2       1=POSITION AND VELOCITY                          LOKANG
           4       1=SUB-SATELLITE DATA                             LOKANG
           6       1=OSCULATING ELEMENTS                            LOKANG
           8       1=OBSERVATION DATA                               LOKANG
           9-10    0=STANDARD BINARY ON TAPE3                       LOKANG
                   -1=PERIGEE-APOGEE DATA ON TAPE7                  LOKANG
           11-13   1.0=SINGLE PASS PERTRAC. CORRECTION (STANDARD)   LOKANG
   6       1-14    "END OF PROBLEM"                                 LOKANG
                                                                    LOKANG
   ABOVE MAY BE REPEATED N TIMES                                    LOKANG
   LAST CARD: "9" IN COL. 1                                         LOKANG
                                                                    LOKANG
   COMMENT 1: USAGE OF MOVING OBSERVATION STATION STMULATING        LOKANG
       AIRCRAFT REQUIRES INPUT OF SEVERAL (N_2) CONSECUTIVE AIRCRAFT LOKANG
       POSITION COORDINATE CARDS                                    LOKANG
                                                                    LOKANG
   COMMENT 2: EACH FLIGHT SEGMENT MUST BE SUPPLIED WITH TWO         LOKANG
       POSITION COORDINATE CARDS SIGNIFYING START AND END OF        LOKANG
       SEGMENT. FOR EACH PAIR, NUMBER OF STATIONS(NMS) IS           LOKANG
       INCREASED BY ONE(NMS=NMS+1)                                  LOKANG
*****************************************************************  LOKANG
```

Figure 1. Input Format for Program LOKANGL

Input format provided by the initiator consists of a number of cards, each of which provides the coordinates and times of turning points along the flight path. Program FLTRANS uses this information to create starting and ending points for each flight segment, as well as all other parameters required by LOKANGL.

1.1.2 Mathematical and Logical Procedures

Given the total time of flight T along the flight segment, starting and ending coordinates $(\phi_1 \lambda_1)$ and $(\phi_2\ \lambda_2)$ of the flight segment, height of the flight H, and earth radius R; the position of aircraft (ϕ,λ) at the time t is determined as follows:

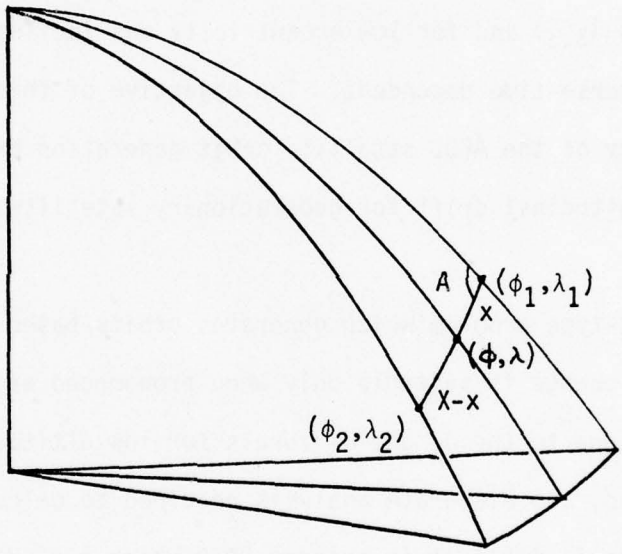

1. $X = \arccos(\sin\phi_1 \sin\phi_2 + \cos\phi_1 \cos\phi_2 \cos(\lambda_1-\lambda_2))$.

2. $A = \arccos((\sin\phi_2 - \cos X \sin\phi_1)/(\sin X \cos\phi_1))$.

3. $x = Xt/T$.

4. $\phi = \arcsin(\sin\phi_1 \cos X + \cos\phi_1 \sin x \cos A)$.

5. $\lambda = \lambda_1 + \arcsin(\sin A \sin x/\cos\phi)$.

1.2 Long Term Ephemeris for Near-geostationary Satellites

Initiator: J. Klobuchar

Project No: 4643 Problem No: 4887

The orbits of near-geostationary satellites are significantly influenced by resonant perturbations due to the lower order tesseral terms in the geopotential, and to a lesser extent also by the luni-solar gravitational forces. These effects show up only over a period of months, and some analyses are available in the literature [1-6] for the lowest tesserals ($J_{2,2}$ and $J_{3,3}$) and for low eccentricity and inclination. Luni-solar forces are of course time dependent. The objective of this work was to improve the capability of the AFGL satellite orbit generation programs to predict long term longitudinal drift for geostationary satellites.

A LOKANGL-type program which generates orbits based on elements and their rates of change is suitable only when pronounced effects are involved such as those due to the J_2 and J_3 zonals for low altitude polar orbits. On the other hand, the elaborate analysis required to calculate geostationary resonances is implicit in program ROPP which includes tesserals thru $J_{6,6}$, lunar and solar perturbations, and an atmospheric drag model.

Program ROPLOK was accordingly developed by removing the drag calculations of ROPP, simplifying to a no-overlay program capable of executing in 77K (octal), and with input similar to LOKANGL. (See Figure 2. LOKANGL-type output not available). Accurate knowledge of the mean motion and the semi-major axis is essential to predict the long term resonance amplitude in

```
RAPID ORBIT PREDICTION PROGRAM ROPLOK
VERSION NOV., 1976     LOGICON, INC.

DATA DECK SETUP

    NAMELIST INPUT FOR CHECK-OUT MAY PRECEDE NORMAL INPUT
    THIS DATA IS ENTERED BETWEEN $INPUT AND $END CARDS

CARD    COLS                  DESCRIPTION
1       1       ORBITAL DETERMINATION FORM CODE
                1=FORM NO. 3 :   SCF 2-CARD POS.-VEL. SET
                2=FORM NO. 2 :   ADC 2-CARD ELEMENT DATA SET
                5=FORM NO. 1 :   ADC 5-CARD DATA SET

2*              ONE OR TWO ELEMENT SETS
        8-9     X OR U ON FIRST CARD OF EACH ELEMENT SET
                NOTE: IF TWO ELEMENT SETS ARE INPUT,
                MEAN MOTION OF THE FIRST SET IS ADJUSTED
                TO MATCH TRUE ANOMALY OF THE SECOND SET.

3       1-3     NO. OF STATIONS. IF NO STATIONS USE 0
        6       CODE 1 OR 0 FOR PRINT CONTROL OF STATION DATA
                0=PRINT BY TIME ONLY
                1=PRINT BY STATIONS
        7-10    0=STANDARD
                IONOHT=SUB-IONOSPHERIC ALTITUDE (KM)     I3

3*              STATION LOCATION CARDS,IF NMS.GT.0
        1-5     I.D. OF STATION (NUMBER)
        11-25   STATION GEODETIC LATITUDE, DEGREES
        26-40   STATION LONGITUDE (POSITIVE EAST), DEGREES
        41-55   STATION HEIGHT, METERS
        61-72   NAME OF STATION

4       1-5     TIME INCREMENT IN MINUTES.               I5
        11-47   TIME SPAN FOR PRINT OR TAPE3 WRITE
                START COLS: 11-12;14-15;17-18;20-21;23-24;26-27
                FINAL COLS: 31-32;34-35;37-38;40-41;43-44;46-47
                TIME          YEAR;MONTH;  DAY; HOUR;  MIN;  SEC
                FORMAT          I2;   I2;   I2;   I2;   I2;   I2

5               CODE FOR PRINT-OUT; 0=NO PRINT; 1=PRINT  FOLLOWING:
        2       1=POSITION AND VELOCITY
        4       1=SUB-SATELLITE DATA
        6       1=MEAN KEPLERIAN ELEMENTS
        8       1=OBSERVATION DATA
        9-10    TAPE 3 CONTROL; STANDARD=0

6       1-14    "END OF PROBLEM"

ABOVE MAY BE REPEATED N TIMES
LAST CARD: "9" IN COL. 1
```

Figure 2. Input Format for Program ROPLOK

longitude. This facility was achieved by accepting and adjusting to two sets of elements which would ideally be provided separated by a number of weeks. Subsequently, the tesseral selecting subroutine RESON was also incorporated into ROPP.

Subroutine RESON determines whether the net motion specified by the elements approaches any resonance commensurability IB/IA revolutions per day, where IA,IB may be any integers from 1 thru 6. If such a ratio of integers is found, a search is conducted for all L,M tesserals where the allowable P,Q subscripts result in significant geopotential contributions. Thus, solve for L,M,P,Q from

$$IB(L-2P+Q) = IA(M)$$

for the following ranges:

L=2 thru 6

M=0 thru L

P=0 thru L

Q=-1 thru 1 for eccentricity $<$ .08

-2 thru 2 for eccentricity $<$ .16

-3 thru 3 for ecentricity $\geq$ .16

The corresponding inclination function FLMP and eccentricity function GLPQ are obtained using existing routines FINK and FECC respectively.

The contributing geopotential field is then given by

$$VLMPQ = \frac{\mu}{\alpha^{L+1}} \cdot J_{L,M} \cdot FLMP \cdot GLPQ$$

where μ = 398603.15 km^3/sec^2

and α is the semi-major axis in earth radii.

Program ROPP is set to always include the J_2 and J_3 zonals because of their usual importance. In the sample tabulation below VLMPQ values are also listed for all cases greater than 10^{-8} for a satellite with mean motion n=1.00273 (and a=6.6109), e=0.00907, i=2.5°.

	L	M	P	Q	VLMPQ
*	2	2	0	0	$+7.34\times10^{-3}$
*	3	1	1	0	-6.09×10^{-4}
	3	2	0	-1	-2.32×10^{-7}
	3	2	1	1	-6.95×10^{-7}
*	3	3	0	0	$+6.75\times10^{-6}$
*	4	0	2	0	$+1.93\times10^{-5}$
	4	1	1	-1	-1.56×10^{-8}
	4	1	2	1	$+7.81\times10^{-8}$
*	4	2	1	0	-3.44×10^{-5}
	4	3	0	-1	-5.61×10^{-8}
	4	3	1	1	-1.68×10^{-7}
*	4	4	0	0	$+2.21\times10^{-5}$
	5	1	2	0	$+3.52\times10^{-7}$
	5	2	2	1	$+1.77\times10^{-8}$
*	5	3	1	0	-2.70×10^{-6}
*	5	5	0	0	$+5.37\times10^{-6}$
	6	0	3	0	$+1.43\times10^{-7}$
	6	2	2	0	$+3.52\times10^{-7}$

For a selection level of 1.0×10^{-6} the terms starred are significant; a sample of the corresponding print-out is shown in Figure 3.

```
      MEAN
TWO CARD SPACATS INPUT

                        MEAN ELEMENTS DEFIND AT MODIFIED JULIAN DATE    196.69444444
   CARD 1 YIELDS EPOCH YR AND EPOCH DAY ONLY
   CARD 2
              MEAN ANOMALY      RTA OF ASC NODE     ARG OF PER.          ECCEN.       INCLINATION(DEG)
              .29000600E+03   0.                  .18000000E+03     .90700000E-02     .25000000E+01
              MEAN MOTION
              1.002739E+00
         ADJUSTED SEMI MAJOR AXIS   AND   ECCENTRICITY
                   6.610918E+00           .90700000E-02
```

20

```
THE J(L,M) COEFFICIENTS --
     J( 2, 0) =  -.10826450E-02     J( 2, 2) =   .17768800E-05     J( 3, 0) =   .25460000E-05
     J( 3, 1) =   .19549900E-05     J( 3, 2) =   .37486700E-06     J( 3, 3) =   .21614500E-06
     J( 4, 0) =   .16490000E-05     J( 4, 1) =   .67020700E-06     J( 4, 2) =   .14634700E-06
     J( 4, 3) =   .57087800E-07     J( 4, 4) =   .66778900E-08     J( 5, 0) =   .12100000E-06
     J( 5, 1) =   .39860000E-07     J( 5, 2) =   .90012300E-07     J( 5, 3) =   .18846100E-07
     J( 5, 4) =   .91364700E-09     J( 5, 5) =   .11937500E-08     J( 6, 0) =  -.64600000E-06
     J( 6, 1) =   .15825200E-06     J( 6, 2) =   .37786200E-07     J( 6, 3) =   .25826200E-08
     J( 6, 4) =   .18019500E-08     J( 6, 5) =   .50115800E-09     J( 6, 6) =   .66298500E-10

THE LAMDA(L,M) COEFFICIENTS --
     LAMDA( 2, 1) =   .71969802E+02     LAMDA( 2, 2) =  -.14576848E+02     LAMDA( 3, 1) =   .76166144E+01
     LAMDA( 3, 2) =  -.20874658E+02     LAMDA( 3, 3) =   .22826696E+02     LAMDA( 4, 1) =  -.14306699E+03
     LAMDA( 4, 2) =   .28596897E+02     LAMDA( 4, 3) =  -.40938637E+01     LAMDA( 4, 4) =   .24322746E+02
     LAMDA( 5, 1) =  -.17410067E+03     LAMDA( 5, 2) =  -.15773356E+02     LAMDA( 5, 3) =  -.59347541E+02
     LAMDA( 5, 4) =  -.21258224E+02     LAMDA( 5, 5) =  -.16061153E+02     LAMDA( 6, 1) =   .11694470E+03
     LAMDA( 6, 2) =  -.44536296E+02     LAMDA( 6, 3) =   .12332917E+02     LAMDA( 6, 4) =  -.27339999E+02
     LAMDA( 6, 5) =  -.23354612E+02

THE SUBSCRIPTS -- 11 SETS
     L =  2, 3, 3, 2, 3, 3, 4, 4, 4, 5, 5
     M =  0, 0, 0, 2, 1, 3, 0, 2, 4, 3, 5
     P =  1, 1, 2, 0, 1, 0, 2, 1, 0, 1, 0
     Q =  0,-1, 1, 0, 0, 0, 0, 0, 0, 0, 0
```

Figure 3. Selection of Resonance Terms in Program ROPLOK

In order to gauge the relative long term effect of these terms, a number of different combinations were run over a 200 day span for the above satellite, and for a satellite with e=0.01 and $i=5^{o}$. Table 1 shows longitude drift predictions. With no extra terms, the drift is small. As expected, inclusion of $J_{2,2}$ shows the resonance drift well, with the $J_{3,1}$ and $J_{3,3}$ tesserals essentially completing the picture. The remaining terms contribute little. The selection threshold for VLMPQ is adjustable in ROPP, but the default value is set at 1.0×10^{-4}.

Finally, a study was made for future use on a SCATHA type satellite. For n=1.018965, e=0.17907 and $i=2.5^{o}$ the satellite drifts eastward at 6^{o}/day. Thus no resonance commensurability exists, but the same combinations of terms as before were forced in for testing. After 200 days a minor effect of including the (2,2,0,0) term was evident, giving a longitude 1.5^{o} East of the longitude with no extra terms. Additional terms produced no tangible effects. Since the higher mean motion tends towards the (2,2,0,-1) term, this was also tested. The CP execution time was unexpectedly quadrupled, but again there was no effect on the longitudinal drift. A SCATHA type satellite is not near-geostationary, and additional terms are properly excluded.

GEOSYNCHRONOUS SATELLITES

L,M,P,Q TEST (200 day run)

Terms	n=1.002730	
Included	i=2.5,e=.00907	i=5.0,e=.01
(2,0),(3,0) always present	East Longitude	
Initial	285.86	285.81
All (2,2)(3,1)(3,3)(4,0) (4,2)(4,4)(5,3)(5,5)	266.51	266.63 (also 3,2)
(2,2),(3,1),(3,3)	266.65	266.76
(2,2) alone	262.10	262.25
(2,2),(3,1)	263.29	263.41
(2,2),(3,3)	265.43	265.56
No Extra	288.35	288.43

Table 1. Longitude Drift Due To Selected Geopotential Terms

1.3 Subroutine ECLIPS

Initiator: E. Robinson

Project No: 0001 Problem No: 4517

Subroutine ECLIPS was written to be called by rapid orbit prediction program ROPP to produce in-out eclipse times of a satellite. Subroutine ECLIPS was developed in order to replace the existing subroutine which produced in-out eclipse times using iteration methods which required unnecessarily long execution times and was not able to produce smooth and reasonably exact in-out eclipse time calculations. The new subroutine ECLIPS is based on an analytical approach developed in chapter 5 of Reference 7 which resolves the above difficulties.

1.3.1 Functional Description

Subroutine ECLIPS determines the entrance and exit true anomalies of the satellite into the shadow of the earth, and the duration of eclipse. It assumes no flattening of the earth and no shift of the earth in its orbit. Umbra and penumbra effects are also neglected. These assumptions will result in a quartic equation in the cosine of the entrance and exit true anomalies.

A given orbital ellipse is fully defined as to dimensional size and orientation in the equatorial or right ascension-declination coordinate system by semi-major axis-a, eccentricity-e, inclination-i, longitude of the ascending node-Ω, argument of perigee ω and the time of perifocal passage T. Given the above information, the shadow function ξ is calculated and composed into the quartic equation for determination of entrance and exit true anomalies of the satellite into the shadow of the earth. To solve this equation subroutine POLRT is used.

Based on true anomalies, the mean anomalies for entrance and exit from the shadow and therefore in-out times are calculated.

1.3.2 Mathematical and Logical Procedures

Given: a,e,i, Ω, ω, T we calculate first the orthogonal set of vectors :-

P_x = Cos ω Cos Ω -Sin ω Sin Ω Cosi

P_y = Cos ω Sin Ω +Sin ω Cos Ω Cosi

P_z = Sin ω Sini

(P is taken as pointing toward perifocus.)

Q_x = Sin ω Cos Ω -Cos ω Sin Ω Cosi

Q_y = Sin ω Sin Ω +Cos ω Cos Ω Cosi

Q_z = Cos ω Sin i

(Q is in the orbit plane advanced to P by a right angle in the direction of increasing time anomaly.)

We calculate then

$$\beta = \frac{X_s P_x + Y_s P_y + Z_s P_z}{(X_s^2 + Y_s^2 + Z_s^2)^{\frac{1}{2}}} \qquad \xi = \frac{X_s Q_x + Y_s Q_y + Z_s Q_z}{(X_s^2 + Y_s^2 + Z_s^2)^{\frac{1}{2}}}$$

where X_s, Y_s, Z_s are coordinates of the sun.

Shadow function of the Earth is produced by

$$S \equiv \alpha_e^2 (1 + e \text{ Cos } 0)^2 + P^2 (\beta \text{Cos}\theta + \xi \text{Sin}\theta)^2 - P^2$$

where S = 0 is the condition for entrance or exit from the shadow and $P = \alpha(1-e^2)$ is the semi-parameter of the orbit. 0 is the true anomaly.

Satellite enters the shadow if S changes sign from "-" to "+". Exit from shadow is determined by changing of sign of S from "+" to "-".

Rejection of spurious roots is accomplished by

$$\text{Cos } \psi = \beta \text{Cos} \theta + \xi \text{ Sin } \theta < 0$$

since ψ is the angle between the radius vector to the sun and the radius vector to the satellite at entrance or at exit points.

Solution of the equation S = 0

$$A_0 \text{Cos}^4 \theta + A_1 \text{Cos}^3 \theta + A_2 \text{Cos}^2 \theta + A_3 \text{Cos} \theta + A_4 = 0$$

with

$$A_0 = \left[(\alpha_e/p)^4 e^4 - 2(\alpha_e/p)(\xi^2-\beta^2)e^2 + (\beta^2 + \xi^2)^2 \right]$$

$$A_1 = \left[4(\alpha_e/p)^4 e^3 - 4(\alpha_e/p)^2 (\xi^2-\beta^2)e \right]$$

$$A_2 = \left[6(\alpha_e/p)^4 e^2 - 2(\alpha_e/p)^2 (\xi^2-\beta^2) - 2(\alpha_e/p)^2(1-\xi^2)e^2 + 2(\xi^2-\beta^2)(1-\xi^2) - 4\beta^2\xi^2 \right]$$

$$A_3 = \left[4(\alpha_e/p)^4 e - 4(\alpha_e/p)^2(1-\xi^2)e \right]$$

$$A_4 = \left[(\alpha_e/p)^4 - 2(\alpha_e/p)^2(1-\xi^2) + (1-\xi^2)^2 \right]$$

REFERENCES

1) Wexler, D.M., "Rapid Orbit Prediction Program (ROPP)", TRW-09967-6001-RO-00, prepared under AFCRL Contract No. F19628-68-C-0170, October 1968.

2) Sparks, S.T., "Users' Manual for the TRW Rapid Orbit Prediction Program", TRW-09967-6002-RO-00, prepared under AFCRL Contract No. F19628-68-C-0170, October, 1968.

3) Kaula, W.M., Theory of Satellite Geodesy, Blaisdell Publishing Co. (1966)

4) Blitzer, L.; Boughton, E.M.; Kang, G.; and Page, R.M., "Effect of Ellipticity of the Equator on 24-Hour Nearly Circular Satellite Orbits", J. Geophysical Research, Vol. 67, No. 1, January 1962.

5) Allan, R.R., "Perturbations of a Geostationary Satellite by the Longitude-Dependent Terms in the Earth's Gravitational Field", Planetary Space Science, Vol. 11, 1963.

6) Allan, R.R., "Satellite Resonance with Longitude-Dependent Gravity-II", Planetary Space Science, Vol. 15, 1967.

7) Escobal, P.R., Methods of Orbit Determination, John Wiley & Sons, Inc., N.Y./London/Sydney (1965)

Section 2. Ionospheric Research Support

Author: B. J. Guz

2.0 New Worldmap (WRLDMAP)

Initiator: J. Buchau

Project No: 4643 Problem No: 4714

Program WRLDMAP is designed to provide the user with 12 or 30-inch wide plots of the land mass outlines within desired limits. These limits are represented by geographic or geomagnetic longitude and latitude. Together with a reference longitude, this provides full information for plotting a map of specific areas of either hemisphere of the Earth. Program WRLDMAP is able to plot maps with a given scale up to the maximum size allowed by the plotting facilities. The geographic or corrected geomagnetic coordinate backgrounds can be superimposed if desired. A sample plot is reproduced in Figure 1.

2.1 Functional Description

Input for the program consists of particular values of longitude and latitude, factors indicating the scale of maps, and the desired coordinate background, either geographic or geomagnetic. Table 1 shows the card input format.

After initialization, the continental outline data file is used and the land mass outlines are plotted within specified bounds. Then subroutine SUBMAP plots, if desired, the coordinate lines of geographic or geomagnetic longitude and latitude. The plot is supplied with a framed label.

Program WRLDMAP possesses four options for confining the geographic or the geomagnetic plot with the geographic or the geomagnetic coordinate background.

The program has the capability of plotting a map for each data card provided.

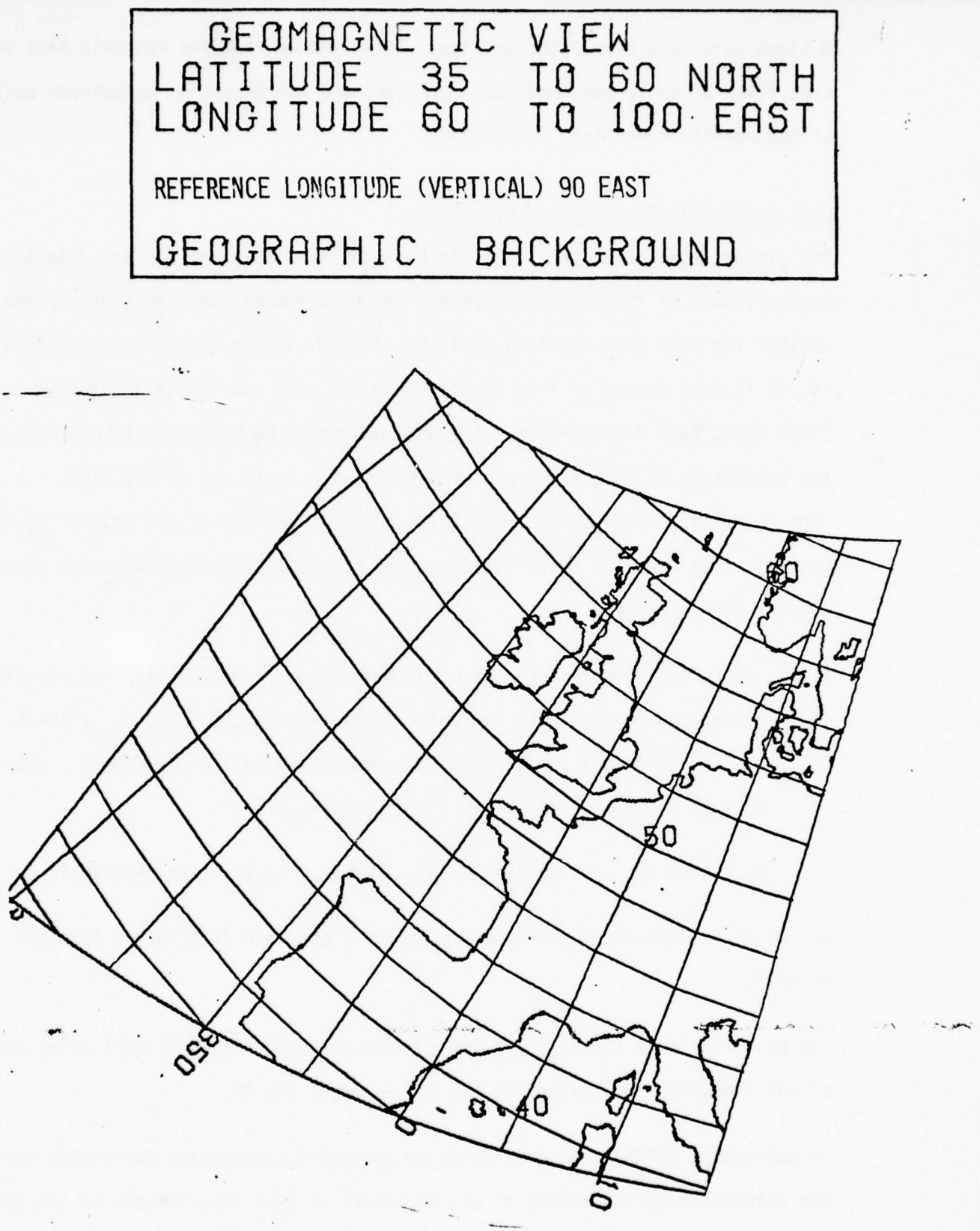

Figure 1. Sample Plot by WRLDMAP

A blank data card terminates the job. This program requires magnetic tape or disk files of digitized land mass outlines, and the Hakura or Gustafsson table of geomagnetic coordinate conversions.

2.2 Mathematical or Logical Procedures

The proper data (permanent) files to be read into the array AAA are determined by the values of K3. FACTOR determines the proper plot size, WRLD determines whether the land mass outlines shall be plotted. If the land mass coordinate (X, Y) is such that X or Y is greater than 900, the coordinate is ignored. (Tape 2 and Tape 3 coordinates were obtained from the Geophysical Institute of the University of Alaska and are compatible with their use of 999.9998 as a "non-coordinate" abcissa or ordinate). CORRGM is called if and only if K3 is equal to 1 in order to convert from geographic to corrected geomagnetic coordinates when necessary.

If (X, Y) is the "ordered set" of coordinates under consideration for plotting, the plotting pen is lifted if and only if $SQRT((X_i-X_{i-1})^2 + (Y_i-Y_{i-1})^2) > .1$, or $(X_{i-1})^2 + (Y_{i-1})^2 > 100$; and the pen is moved if and only if $X_i^2+Y_i^2 \leq 100.$, where:

$X_i = X_b \cos y_b$, $Y_i = X_b \sin y_b$, $X_b = (90.- x_a)/5.$,

$Y_b = AMOD\ (y_a - 90., 360)* \pi/180.$, and $(x_a,\ y_a)$ is the geographic or corrected geomagnetic coordinate (in degrees) obtained from Tape 2 (or Tape 3) or CORRGM.

The pen moves only to $(\pm X_i, Y_i)$ for a north or south (respectively) polar view of the hemisphere determined by the values of K1 and K2.

In subroutine SUBMAP, the geographic or corrected geomagnetic coordinate system map determined by the values of K1, K2 and K3 is then superimposed on the existing polar coordinate system if the value of MAP is not "NO".

Card No.	Variable Name	Card Col.	Format	Variable Description
1	K1	1-3	I3	"1" for northern hemisphere
				"40"for southern hemisphere
	K2	4-6	I3	"50"for northern hemisphere
				"89"for southern hemisphere
	K3	7-9	I3	"1" for geomagnetic bounds on geographic background
				"2" for geographic bounds on geographic background
				"3" for geomagnetic bounds on geographic background
				"4" for geographic bounds on geographic background
	VIEW	11	A1	"N" for north polar view
				"S" for south polar view
	WRLD	13-14	A2	"NO" to suppress plot of land mass outlines
	MAP	16-17	A2	"NO" to suppress plot of coordinate background
	BLAT	21-17	F7.2	Beginning latitude of plotted region
	ELAT	28-35	F7.2	Ending latitude of plotted region
	BLON	36-43	F7.2	Beginning longitude (east) of region
	ELON	44-51	F7.2	End longitude (east) of the region
	CLON	52-53	F7.2	Reference longitude-vertical on the plot
	FACTOR	60-67	F7.2	"1" for 12 inch plot
				"2" for 30 inch plot
	FACT	68-75	F7.2	"0" indicates that region will be plotted in the maximal possible scale, otherwise given scale should be entered as degrees latitude/inch.

Table 1. Card Input Format for Program WRLDMAP.

The major part of subroutine SUBMAP is devoted to calculating the intersection points of the boundaries of the plotted region with lines of constant longitude and latitude. Since these lines could intersect with more than one boundary line and come from unpredictable directions, fairly complicated logic is involved. Algorithms for calculating polar coordinates for intersection points consists of four parts. They check whether the intersection of the given longitude (latitude) line with one of four bounds ("upper" and "lower" latitude bound and "right" and "left" longitude bound) does exist. For this purpose a value is calculated showing whether the two consecutive points of latitude (longitude) line are on both sides of the boundary or not. Then, if intersection with a "latitude" bound has occurred, the intersection points (polar coordinates) are calculated by the formulas

$$\theta = \theta_1 \frac{P_2 - P}{P_2 - P_1} + \theta_2 \frac{P - P_1}{P_2 - P_1} \quad \text{and} \quad P = \text{RMAX or } P = \text{RMIN}$$

where RMIN and RMAX are beginning and ending boundary latitude. For the intersection with "longitude" boundaries the following formulas are used.

$$P = \frac{P_1 P_2 \text{ Sin } (\theta_2 - \theta_1)}{P_1 \text{ Sin } (\theta - \theta_1) + P_2 \text{ SIN } (\theta_2 - \theta)} \quad \text{and } \theta = \theta\text{MIN or } \theta\text{MAX}$$

where θMIN and θMAX are beginning and ending boundary longitude.

Section 3. Geopotential Model Term Selection For Satellite Orbit Computations

Author: J. N. Bass

3. Geopotential Model Term Selection For Satellite Orbit Computations

Initiator: K. S. W. Champion

Project No: 427M Problem No: 4867

3.0 Introduction

Among the most time consuming tasks in most modern earth satellite orbit computations is the computation of the earth's gravitational attraction. This is because geopotential models, as derived from analysis of artificial satellite tracking data, surface gravity data and other data, contain up to several hundred terms (usually spherical harmonics). An analysis of the perturbing effect of these terms on a satellite orbit, such as that carried out by Kaula[1] shows that for any given satellite only a few terms will be important. Furthermore atmospheric drag (for low-altitude satellites) and in some cases tracking data errors (noise, biases such as station location errors, etc.) will overshadow the effects of many geopotential terms[2,3]. Thus it seems worthwhile to develop a selection procedure for particular satellites to select only the most important terms of a given geopotential such that the remaining terms will not have an appreciable effect on the accuracy in orbit determination and prediction.

In this report we therefore give an error analysis of the effect of model changes on determination of orbit parameters from tracking data and the subsequent effects on predicted orbit positions. This is used with various simplifications to select a subset of terms from a given geopotential model

to yield a specified r.m.s. predicted position difference relative to the given model at a specified time beyond the tracking fit span. Applications are given for 3 low-altitude satellites and one medium altitude satellite using the Smithsonian Standard Earth III (SEIII) geopotential model.[4]

Slowey, et al,[5] have also given a selection procedure which uses only the first-order perturbation amplitudes on the orbit due to individual harmonics without relating these to prediction accuracy.

3.1 Analysis

The analysis of the effects of individual harmonic terms on satellite orbit determination is given elsewhere.[3] Briefly, each spherical harmonic gives rise to a series of secular and oscillating perturbations to a given unperturbed orbit.[1] The secular contributions are limited to zonal harmonics (those independent of longitude). The frequencies and amplitudes of the periodic contributions can be computed in straight-forward fashion. Although the number of such terms is infinite, one may obtain a finite series by limiting the expansion to low powers in the eccentricity.

The effect of each perturbation on a satellite orbit obtained by least squares fitting of tracking data are:

1) The change in an orbit of specified initial conditions, which can be computed using the theory of Reference 1.

2) The change in the orbit's initial conditions, which can be computed from a least-squares fit to the perturbation.

Considering only the in-track component of the orbit, assuming a second degree polynomial

$$s(t) = \sum_{i=1}^{3} P_i t^{i-1}$$

where P_1 represents the original orbital position, P_2 the original mean motion, and P_3 the time derivative of mean motion (as produced by drag), and assuming uniform time distribution of the tracking data, we obtain, for the changes dP_i due to a periodic orbital perturbation A cos $(at + q_o)$:

$$dP_1 = -\frac{A}{aT}\left[12\,(2\sin q - 3\sin q_o) + \frac{1}{aT}\,(2\cos q + 3\cos q_o) \right.$$
$$\left. \frac{-60}{(aT)^2}\,(\sin q - \sin q_o)\right],$$

$$dP_2 = \frac{A}{aT^2}\left[12\,(2\sin q - 3\sin q_o) + \frac{1}{aT}\,(168\cos q + 192\cos q_o)\right.$$
$$\left. \frac{-360}{(aT)^2}\,(\sin q - \sin q_o)\right],$$

$$dP_3 = -\frac{A}{aT^3}\left[30(\sin q - \sin q_o) + \frac{180}{aT}\,(\cos q + \cos q_o)\right.$$
$$\left. \frac{-360}{(aT)^2}\,(\sin q - \sin q_o)\right],$$

where

T = length of fit span,
$q = aT + q_o$

From this the r.m.s. prediction error at any time can be plotted as a function of the ratio of the fit span to the perturbation period. A series of maxima are found, the largest occurring for fit span nearly equal to perturbation period. In particular very long period resonances do not always produce the largest effects.

3.2 Applications

The preceding results were applied to the SEIII geopotential for satellites DB-7, DB-8, DB-9 and OV1-17 (See Table 1). The longer fit span and

Satellite	Perigee (km)	Eccentricity	Inclination Deg.	Mean Motion Revs/day	Fit Span Days	Predict Time Days*
DB-7	157	.009	96	16.2	1.1	0.625
DB-8	160	.009	96	16.2	1.1	0.625
DB-9	162	.009	96	16.2	1.1	0.625
OV1-17	400	.0035	99	15.4	1.75	3.0

*.5km prediction error effect used as criterion.

Table 1. Satellites Used

prediction time used for OV1-17 is customary for the higher altitude satellites with less drag.

Radial and cross-track amplitudes due to perturbations in semi-major axis, eccentricity and inclination[1] were added vectorially to the in-track components to produce the total error estimates shown in Tables 2 and 3. For low altitude satellites it was found that periodic perturbations in the perigee height ($\sim$1% of the density scale height) due to perturbations in the semi-major axis, argument of perigee, and eccentricity could sometimes produce significant effects on in-track error, so these have been included.

The geopotential model was reduced in each case by rejecting the terms with the smallest errors such that the sum of squares of their errors is less than the square of the indicated criterion. Thus we aim to limit the r.m.s. error at a specified prediction time to a specified tolerance. The terms remaining (those not rejected) are underlined in Tables 2 and 3. Computations were carried out with program TESAMP, originally written to compute first-order tesseral perturbation amplitudes.[5] This program was modified to include the computations described here. A total of 12 cases for the 3 DB satellites was processed using program CELEST[6] and Doppler Beacon data. CELEST's geopotential routine was modified to take better account of the structure of the selected geopotentials, as in its original form termination of recursive computational loops is determined solely by the maximum L index and no tests are made for vanishing coefficients. Since maximum L is nearly as large for the selected as for the original geopotential

L	M=1	2	3	4	5	6	7	8	9	10	11	12	13	14	15	16	17
2	0	28	31														
3	548	79	103														
4	1428	714	151	140													
5	46	70	33	7	67												
6	225	346	6	90	93	23											
7	164	26	28	24	5	24	2										
8	193	103	28	77	35	19	29	27									
9	160	3	9	3	4	10	12	18	7								
10	484	33	48	13	29	6	20	1	6	21							
11	76	4	4	9	4	5	7	3	3	10	17						
12	421	21	43	6	23	2	5	5	8	5	4	5					
13	36	3	7	4	4	1	5	1	4	1	3	13	32				
14	252	6	34	2	16	1	8	3	4	3	6	2	8	15			
15	37	4	9	1	3	1	2	5	5	5	4	5	3	16	87		
16	250	21	18	7	10	1	0	5	6	2	2	1	3	2	54	225	
17	44	3	2	4	4	2	2	2	3	4	6	3	5	5	9	259	2164
18	310	21	12	10	1	1	1	3	0	2	2	1	6	4	23	90	209
19	0	0	0	0	0	0	0	0	0	0	0	3	18	13	0	0	0
20	0	0	0	0	0	0	0	0	0	0	0	0	5	10	0	0	0
21	0	0	0	0	0	0	0	0	0	0	0	0	12	5	0	0	0
22	0	0	0	0	0	0	0	0	0	0	0	0	1	5	0	0	0
23	0	0	0	0	0	0	0	0	0	0	0	0	5	3	0	0	0
24	0	0	0	0	0	0	0	0	0	0	0	0	0	3	0	0	0

Table 2. R.M.S. Prediction Error Effects in Meters for Terms of SEIII, as Function of Their Subscripts L, M; Satellites DB-7, DB-8, DB-9 (Selected Terms Underlined)

L	M=1	2	3	4	5	6	7	8	9	10	11	12	13	14	15	16	17	18
2		06582																
3	151		85	107														
4	123	214	13	483		33												
5	13		53	36		7	81											
6	174	522		20		20	144		97									
7	47		18	31		20		5	38		3							
8	130		85	78		18		50	53		36		15					
9	41		1		9		2		4		13		12		20		13	
10	277		15	115		3		35		6		23		0		10		24
11	17		3		3		6		5		5		10		3		4	
12	196		90		84		3		23		2		5		2		14	
13	6		8		5		4		5		1		7		1		11	
14	92		42		52		1		12		4		7		2		7	
15	5		8		5		1		3		2		3		3		12	
16	57		79		18		3		5		4		0		4		7	
17	3		4		1		4		3		4		2		2		7	
18	30		53		5		2		0		5		0		2		0	
19	0		0		0		0		0		0		0		0		0	
20	0		0		0		0		0		0		0		0		0	
21	0		0		0		0		0		0		0		0		0	
22	0		0		0		0		0		0		0		0		0	
23	0		0		0		0		0		0		0		0		0	
24	0		0		0		0		0		0		0		0		0	

L	M=1	2	3	4	5	6	7	8	9	10	11	12	13	14	15	16	17	18
2																		
3																		
4																		
5																		
6																		
7																		
8																		
9																		
10																		
11																		
12																		
13																		
14																		
15																		
16																		
17																		
18																		
19																		
20																		
21																		
22																		
23																		
24																		

Table 3. R.M.S. Prediction Error Effects in Meters for SEIII, Satellite OV1-17 (Selected Terms Underlined)

little savings is gained in CP time. Improvements of over 50% were gained however by early termination of recursive loops and avoiding unnecessary computation for zero coefficients.

OV1-17 skin-track data from ADCOM was used with program CADNIP for fits, and BADMEP[7] for prediction errors. Unlike CELEST these programs test for zero coefficients and hence the geopotential computation time is proportional to the number of terms with non-zero coefficients. Programs CADNIP and BADMEP were utilized by Dorothy Gillette (LKB).

3.3 Results and Discussion

Tables 4 and 5 compare the selected and the full SE111 prediction errors for the DB satellites and OV1-17, respectively. For many of the DB runs the resulting prediction error differences between full and selected geopotentials lie within the .5 km target. The others are all within 1 km. The OV1-17 prediction differences are considerably larger as are the total errors. Hence in both cases the prediction accuracies of the selected and full geopotentials are nearly identical.

The larger prediction differences for OV1-17 are due to several possible effects; non-uniform time density of observations, variations in fit span, non-linear effects, and the use of only 3 orbital parameters, combined with the longer prediction time - fit span ratio. In particular data gaps of up to 3 hours occured in the ADCOM data, sometimes at the beginning or end of a fit span. This would effectively shorten the fit span to which the prediction error effect is highly sensitive for larger prediction times. Non-linearities in the orbit relative to the adjustable parameters can also be

Case #	Full SE111	Selected SE111
1	-3.2	-2.9
2	-3.3	-2.3
3	16.0	16.1
4	0.7	1.6
5	1.3	1.7
6	-3.8	-3.1
7	-0.5	-0.9
8	-1.1	-0.4
9	0.3	0.3
10	-0.2	0.3
11	3.5	3.7
12	-2.5	-1.5

Table 4. 15 Hour Prediction Errors (km)
Satellites DB-7, DB-8, DB-9

Case #	Full SE111	Selected SE111
1	30.3	29.0
2	121.8	112.5
3	-5.0	-2.4
4	12.0	14.5
5	-32.4	-25.9
6	14.2	22.1
7	-15.3	-10.4
8	-24.8	-14.8
9	-5.3	6.7
10	-31.6	-26.6
11	2.6	0.9

Table 5. 3 Day Prediction Errors (km)
Satellite OV1-17

expected to increase for larger time periods. It was for these reasons that the relatively small (compared to overall prediction accuracy) prediction difference criterion was used for OV1-17. Alternatively, one can develop a model to include the above mentioned effects. It was not the intention to do so in this work, but rather to develop as simple a method as possible to achieve a desired goal.

The method of geopotential term selection described here is not put forth as the "best" method to be used in all circumstances. Certainly different goals (such as accuracy in the orbit parameters, or the orbit itself over the fit span) would suggest different criteria. It is believed, however, to represent a good starting point and is certainly adequate for satellites where errors from other sources dwarf those due to the geopotential. The analysis presented in Section 3.1 should also serve as a good starting point for rapidly estimating modeling error effects on orbit determination and other analyses such as atmospheric density determination from satellite drag.

References

1. Kaula, W. M., Theory of Satellite Geodesy, Blaisdell Publishing Co., Waltham, Massachusetts, 1966.

2. Garret, H. B. (1st Lt., USAF), Forbes, J. M. and Champion, K. S. W. (U), "Geopotential Effects on Low-Altitude Satellite Orbit Prediction", AFGL-TR-76-0176, 1975.

3. Bass, J. N., Bhavnani, K. H., and Hussey, I. M. (U), "Geopotential Effects on Low-Altitude Satellite Ephemeris Prediction Accuracy - A Comparison Study for Various Sets of Tracking Data", AFGL-TR-77-0097, 1977.

4. Gaposchkin, E. M., ed., The 1973 Smithsonian Standard Earth (3) SAO Spec. Report 353; SAO-311-002, 1973.

5. Slowey, J. W., "Reduction in the Number of Terms in Geopotential Models Used in Satellite Orbit and Ephemeris Computation", Unpublished.

6. O'Toole, J. W., "Naval Surface Weapons Center Reduction and Analysis of Doppler Satellite Receivers Using the CELEST Computer Program", Proceedings of the International Geodetic Symposium on Satellite Doppler Positioning, Vol. 2, Cosponsored by U. S. Defense Mapping Agency and National Ocean Survey, Oct., 1976.

7. Bramson, A. S., and Slowey, J. W. "Some Recent Innovations in Atmospheric Density Programs", AFCRL-TR-74-0370, 1974.

Section 4. Scintillations

Authors: K. H. Bhavnani
B. J. Guz
L. A. Whelan

4.0 Scintillations

Initiator: J. Aarons

Project No: 4643 Problem No: 4844

4.1 Low Latitude Study

The system of programs developed for creation and analyses of the high latitude scintillations data base (References 1 and 2) were adapted and applied to the equatorial scintillations data base for two stations--Huancayo (LES-6 and ATS-3 satellites) and Ghana (ATS-3 satellite). The following programs comprise the scintillations data processing system:

1. An Edited Raw Data file is created using program SEQCHK. The raw data cards are previously read in time sequence and catalogued. Format and sequence errors as well as duplicates and invalid ranges are checked. Corrections are made over the Intercom System.

2. Program DABASE creates the data base with complete environmental information for each 15-minute sample. Each sample was recorded in BCD as follows:

IDSTA, IDSAT, IFREQ, IYR, IMO, IDA, UT, SCIN, DB, XKP, LF2

I2, A2, I3, I2, I2, I2, F5.2, F4.1, A2, F3.1, I3

where

IDSTA: Huancayo = 20, Ghana = 17

IDSAT: ATS3 = A3, LES6 = L6

IFREQ = 137 MHz for A3, 254 MHz for L6

All 0dB SI values were discarded. Ghana A3 data were converted to dB values by setting SI $\geq$ 0.1 and $\leq$ 94.24, and then

$$SCIN\ (dB) = 15.23077 - \sqrt{231.9763 - 2.46154SI}$$

Kp and 2.7 GHz solar flux (LF2) files were provided by members of the Space Physics Laboratory.

Subsequently all data were compacted into one 60-bit word with common identifier characters entered in a leader. The format and some details are described in Section 4.3, but the programs below have not yet been revised to operate with data in this format.

3. All further analyses of the data were done in local rather than universal time. The sub-ionospheric longitudes used were

HA3 = 75° W, HL6 = 72.6° W, GA3 = 10° W.

Program SIDIST provides distributional breakdowns in a form which covers most cross-sections of interest. Figure 1 shows a typical print-out for HA3 for month 2, the lowest K_p range, and all solar flux ranges combined. Percentage occurrences by local time intervals and SI ranges are calculated after sorting the data. The following divisions are used:

Months	1, 3(Season), 12 (all)
Solar Flux	0 to 95, 96 to 120, 121 up, all
K_p	0 to 1-, 1 to 2-, 2 to 3+, 4- to 5+, 6- up, all.
Local Time	1, 3, 24 (all)

4. The analytical modeling effort requires that the data be divided into moderate size partitions in each of which the average or median is obtained. Program SIPART used 4 K_p ranges: 0 to 1+, 2- to 3+, 4- to 5+, 6- up and 3 S_f ranges: 0 - 95, 96 - 120, 121 up for each month and hour of local time. Within each partition S_f and SI were averaged and a total count was also kept for possible future weighting. This averaged file was saved.

HUANCAYO A3 137 MHZ

MONTH(S) 2 KP 0 1- SF ALL

LT=UT-5.00	AVE	0 1-	1 3-	3 6-	6 9-	9 12-	12 UP	COUNT
00-01	8.4	13.2	16.2	22.1	13.2	5.9	29.4	68
01-02	8.1	21.1	18.4	10.5	13.2	3.9	32.9	76
02-03	5.8	41.8	7.5	10.4	14.9	6.0	19.4	67
03-04	1.8	55.7	20.0	17.1	5.7	0.0	1.4	70
04-05	1.0	50.0	44.4	3.7	0.0	1.9	0.0	54
05-06	.4	71.7	28.3	0.0	0.0	0.0	0.0	53
06-07	.4	74.5	25.5	0.0	0.0	0.0	0.0	55
07-08	1.0	25.9	72.4	1.7	0.0	0.0	0.0	58
08-09	1.4	18.3	73.3	6.7	1.7	0.0	0.0	60
09-10	1.3	14.5	80.6	4.8	0.0	0.0	0.0	62
10-11	1.2	21.8	77.0	1.1	0.0	0.0	0.0	87
11-12	1.2	12.9	87.1	0.0	0.0	0.0	0.0	85
12-13	1.3	12.0	86.7	1.2	0.0	0.0	0.0	83
13-14	1.4	15.3	81.9	2.8	0.0	0.0	0.0	72
14-15	1.2	19.4	80.6	0.0	0.0	0.0	0.0	72
15-16	1.2	34.2	61.8	3.9	0.0	0.0	0.0	76
16-17	1.3	19.2	76.9	3.8	0.0	0.0	0.0	52
17-18	.9	39.2	60.8	0.0	0.0	0.0	0.0	51
18-19	.5	74.5	21.6	2.0	2.0	0.0	0.0	51
19-20	3.7	45.6	25.0	7.4	7.4	2.9	11.8	68
20-21	13.7	10.1	10.1	5.8	4.3	1.4	68.1	69
21-22	16.8	1.4	2.8	8.3	1.4	0.0	85.1	72
22-23	15.4	0.0	3.1	9.4	7.8	10.9	68.8	64
23-24	13.4	0.0	4.5	16.4	11.9	7.5	59.7	67
23-02	9.9	11.8	13.3	16.1	12.8	5.7	40.3	211
02-05	3.0	49.2	22.5	11.0	7.3	2.6	7.3	191
05-08	.6	56.6	42.8	.6	0.0	0.0	0.0	168
08-11	1.3	18.7	77.0	3.8	.5	0.0	0.0	209
11-14	1.3	13.3	85.4	1.3	0.0	0.0	0.0	240
14-17	1.2	25.0	72.5	2.5	0.0	0.0	0.0	200
17-20	1.9	52.4	34.7	3.5	3.5	1.2	4.7	170
20-23	15.3	3.9	5.4	7.8	4.4	3.9	74.6	205
00-24	4.4	27.1	45.4	5.9	3.5	1.7	16.3	1592

Figure 1. Typical Print-out of Distributional Characteristics of Scintillations for Huancayo ATS3.

5. Program SIMED obtained the median scintillation index rather than the average. This required sorting of the data in each partition. The median and the average were shown to be similar for any of the data bases, and no further studies were conducted using medians.

6. Program TABSIN used the catalogued file to tabulate average or median SI values by partition, 3 months per page. This concise format is identical to the output from the modeling program.

7. Program MODEL used the partition-averaged file to develop an analytical model of scintillation index as a function of day of the year, local time, K_p and S_f. Out of a maximum of 3456 blocks (12 months x 4 K_p x 3 S_f x 24 local time) the averaged files with at least 5 observations in the block were as follows:

Huancayo	A3	2838 blocks
Huancayo	L6	2461 blocks
Ghana	A3	2615 blocks

The empty blocks generally occur in the high K_p and occasionally the high S_f range.

The development and application of program MODEL has been described earlier[1]. An additional feature now available is a tabulation of the correlation coefficients for all the variables in the search. Highly correlated variables can suggest reformulation of the model expression. The final expression selected was similar in form to the high-latitude version[2], and Figure 2 summarizes all three cases. The standard deviation of the residuals in each case was as follows:

Huancayo A3	1.77
Huancayo L6	1.30
Ghana A3	1.34

DA = Day Number
HL = Local Time (Hrs.)
As = $S_f/100$, where
S_f = 2695 MHz Solar Flux

Huancayo ATS3

$$FD = \cos(DA - 4.4) - .5\cos(2(DA - 4))$$

$$FA = (-2.9 + .6\,FD)As \qquad FB = (.3 + FD) + (.1 - .2\,FD)\,K_p \qquad FC = (1.6 - .4\,FD)As + .2\,K_p$$

$$SI(dB) = 1. + 2\left[FA + FB + \{(-1.3\,FA + 2.1\,FB)\cos(HL + .1 - .25K_p)\} + FC\{\cos(2(HL + 3.3)) - .4\cos(3(HL + 1.5))\}\right]$$

Huancayo LES6

$$FD = \cos(DA + 1.3) - .6\cos(2(DA - 4))$$

$$FA = (-2.7 - .3\,FD)As \qquad FB = (.2 + FD) + (.1 - .1\,FD)K_p \qquad FC = (1.6 + .7\,FD)As + .1K_p$$

$$SI(dB) = 2\left[FA + FB + \{(-1.5\,FA + .8\,FB)\cos(HL - .2 - .25K_p)\} + FC\{\cos(2(HL + 3.3)) - .4\cos(3(HL + 1.5))\}\right]$$

Ghana ATS3

$$FD = \cos(DA - 10.3) - .5\cos(2(DA - 4))$$

$$FA = (-.7 + .2\,FD)As \qquad FB = (.4 + .5\,FD) + (0.)K_p \qquad FC = (.7 - .4\,FD)As + .15K_p$$

$$SI(dB) = -.05 + 2\left[FA + FB + \{(-3.6\,FA + 1.9\,FB)\cos(HL - .25K_p)\} + FC\{\cos(2(HL + 3.3)) - .4\cos(3(HL + 1.2))\}\right]$$

Figure 2. Equatorial Scintillation Index (dB) Models

Since the equatorial scintillations are lower than those encountered in the auroral regions, the lower residuals that were obtained were to be expected.

8. Program SIPLT was used to simultaneously present the model and the averaged data which had been used as the basis. Figures 3-8 show typical plots for months 2 and 6 for the three stations.

4.2 High Latitude Data Extension and Analysis

The existing high-latitude data base was extended by including the additional year of data acquired for Narssarssuaq, Goose Bay and Sagamore Hill since the original data base was created. Programs SEQCHK and DABASH were used; where DABASH was modified from the original program to include estimation of near-geostationary satellite ephemerides using inclination and ascending node information from widely separated element sets. Sub-ionospheric latitude and longitude, and geomagnetic latitude and time are obtained using routine SILL2 provided by the Space Physics Laboratory, followed by CORRGM2 and MAGTIM based on Gustafsson's 1970 Revised Corrected Geomagnetic Coordinate System.

Program SIDIST was used to provide distributional breakdowns as were done for the equatorial cases (Figure 1).

The Narssarssuaq - Goose Bay - Sagamore Hill based global model of Reference 1, P. 193 which had been derived from the individual models for the three stations was found to possess a singularity near 54° geomagnetic latitude. The model was therefore corrected using a revised form which avoids this problem. The revised model is shown in Figure 9.

4.3 Packed Data Bases

The limited resolution of all parameter values in the data base, and the extensiveness of the samples warranted packing the full data bases

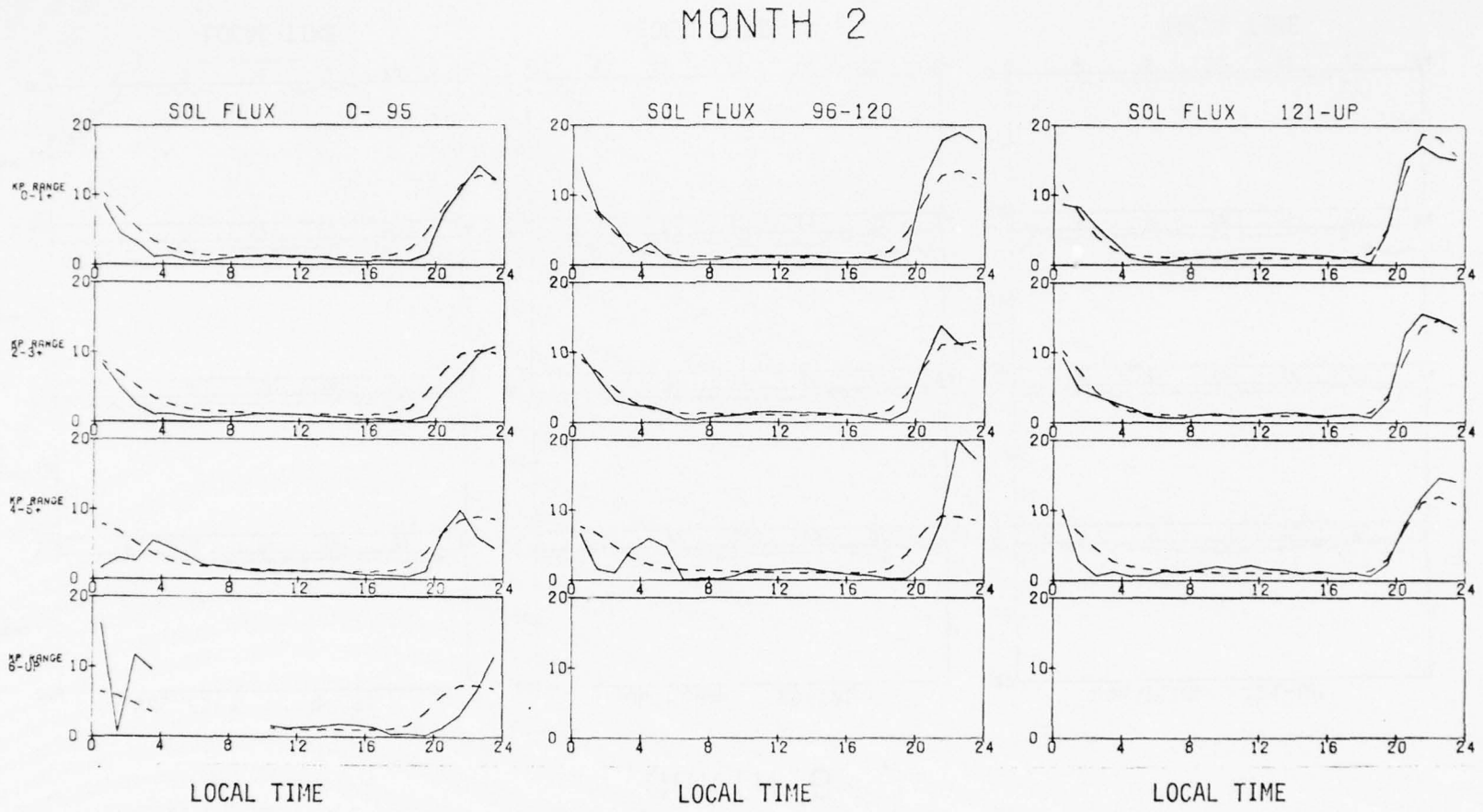

Figure 3. Average SI Data and Model Plots for Huancayo A3 for February.

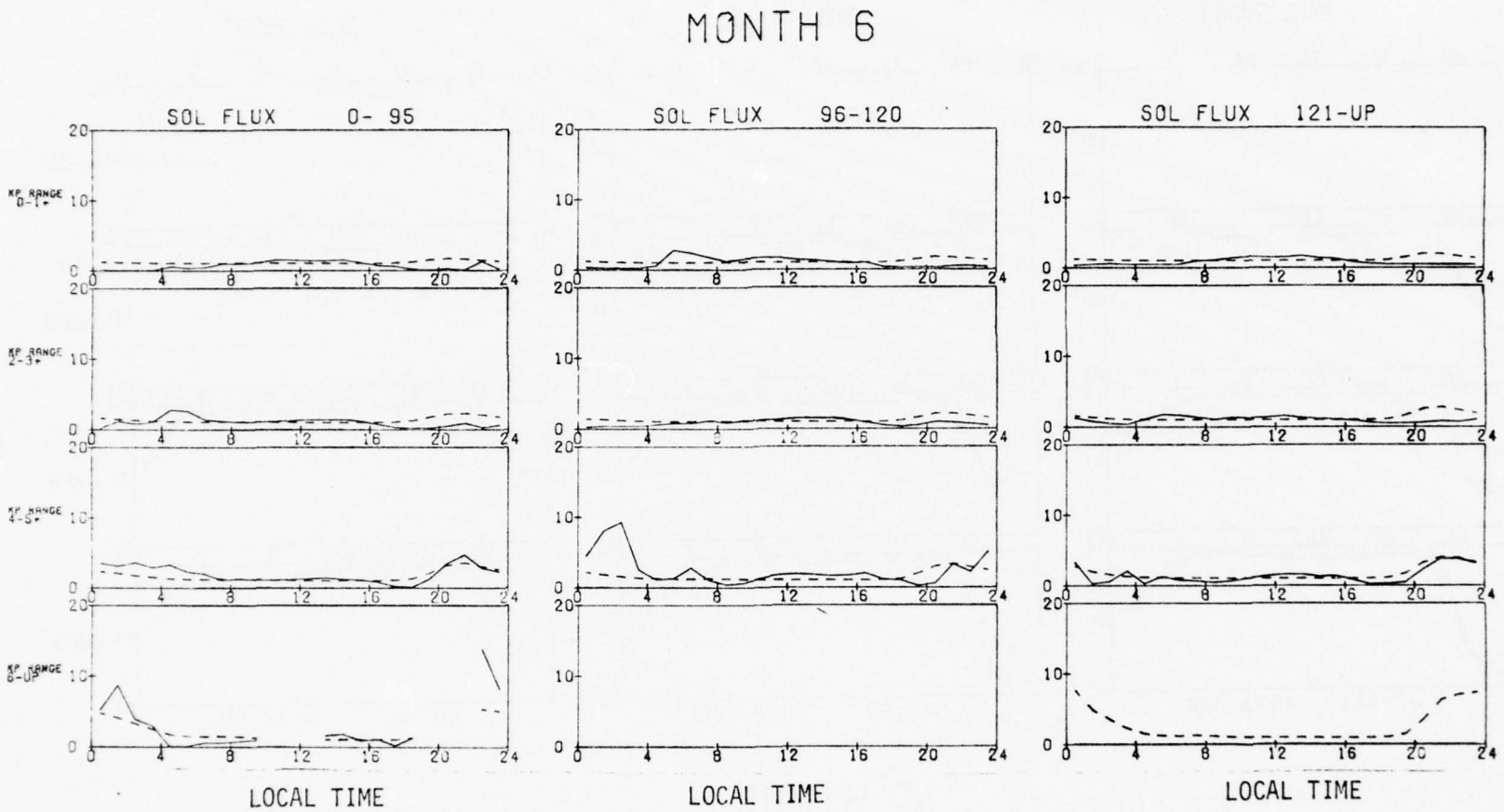

Figure 4. Average SI Data and Model Plots for Huancayo A3 for June.

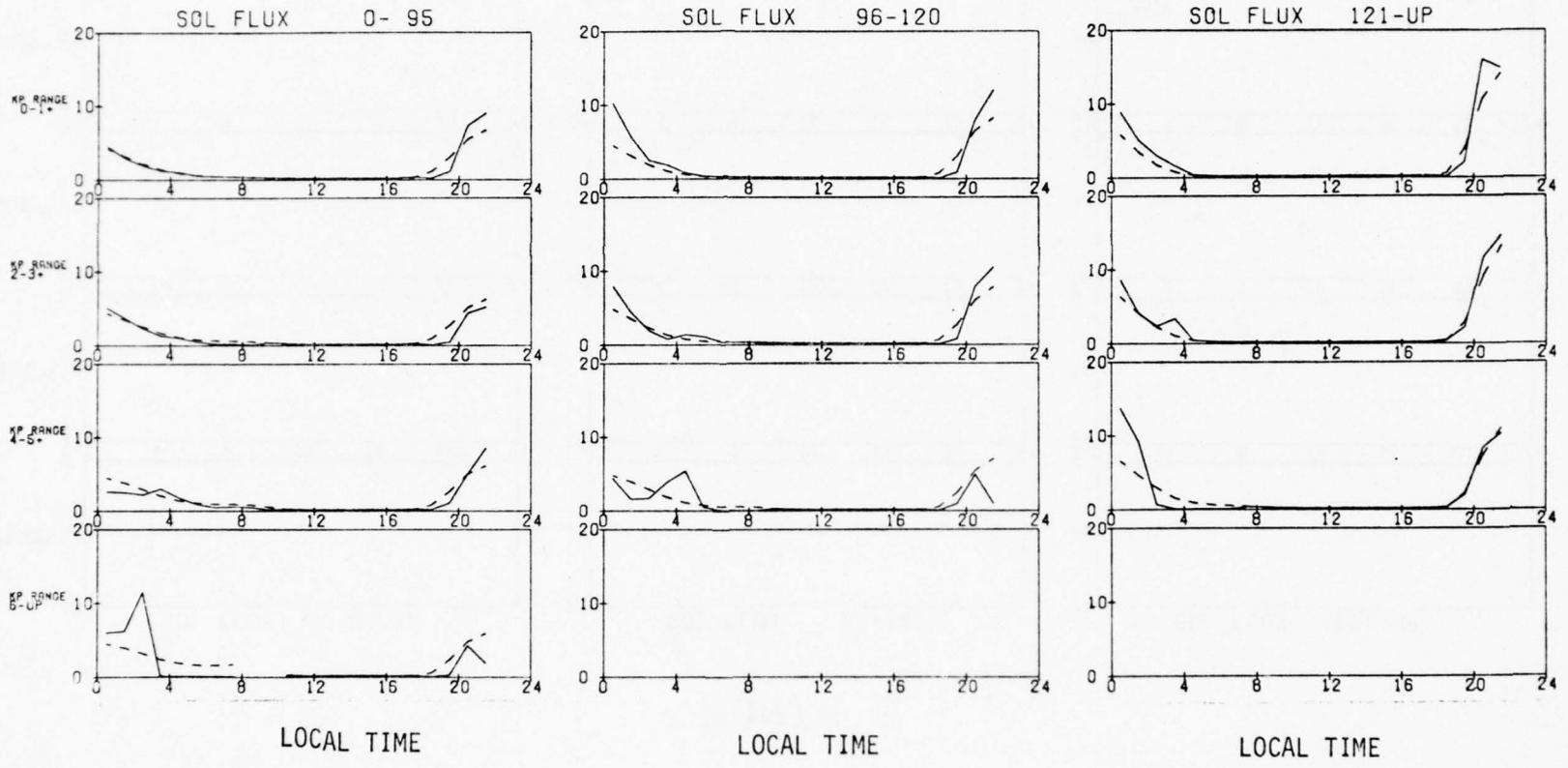

Figure 5. Average SI Data and Model Plots for Huancayo L6 for February.

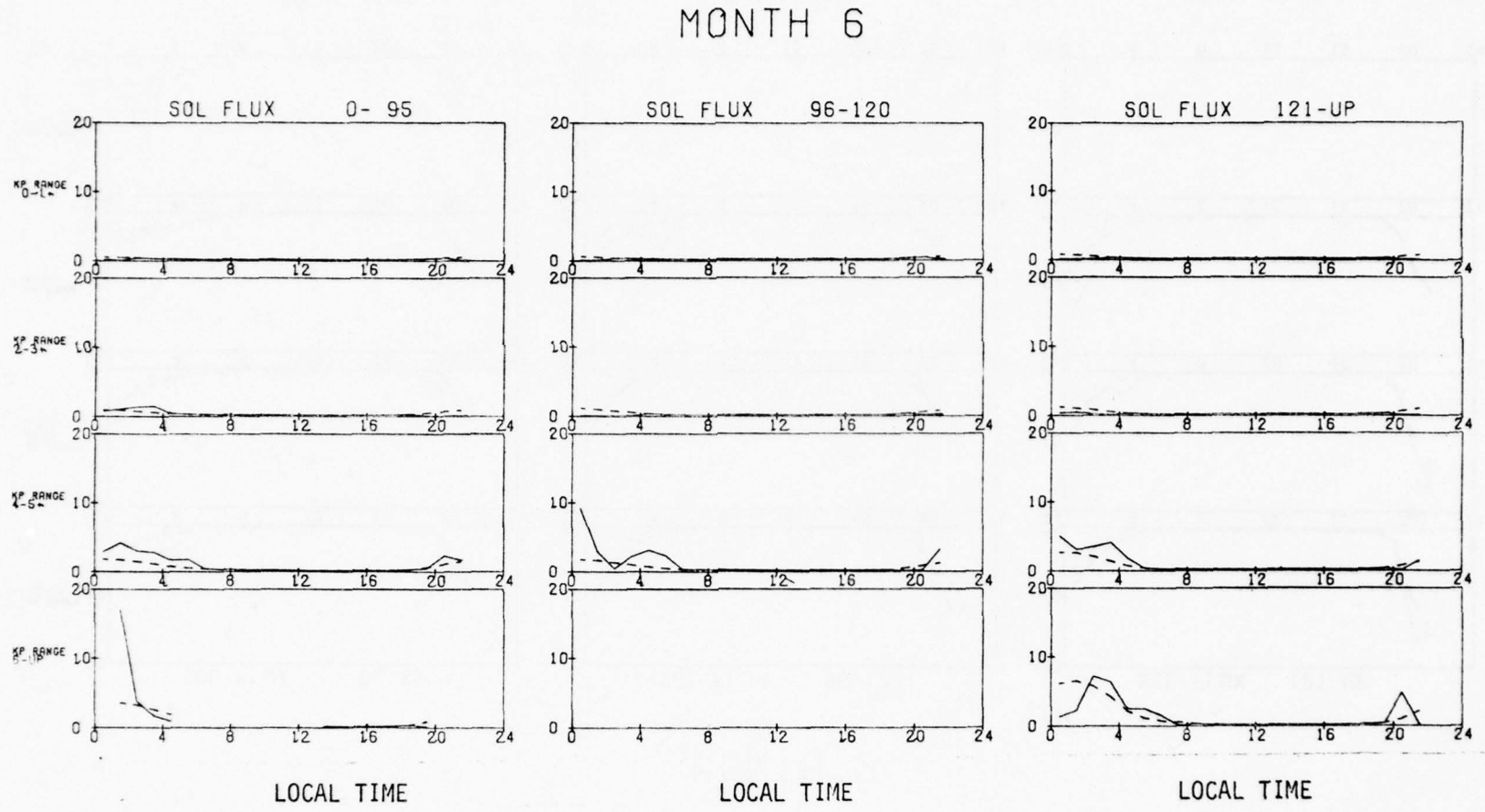

Figure 6. Average SI Data and Model Plots for Huancayo L6 for June.

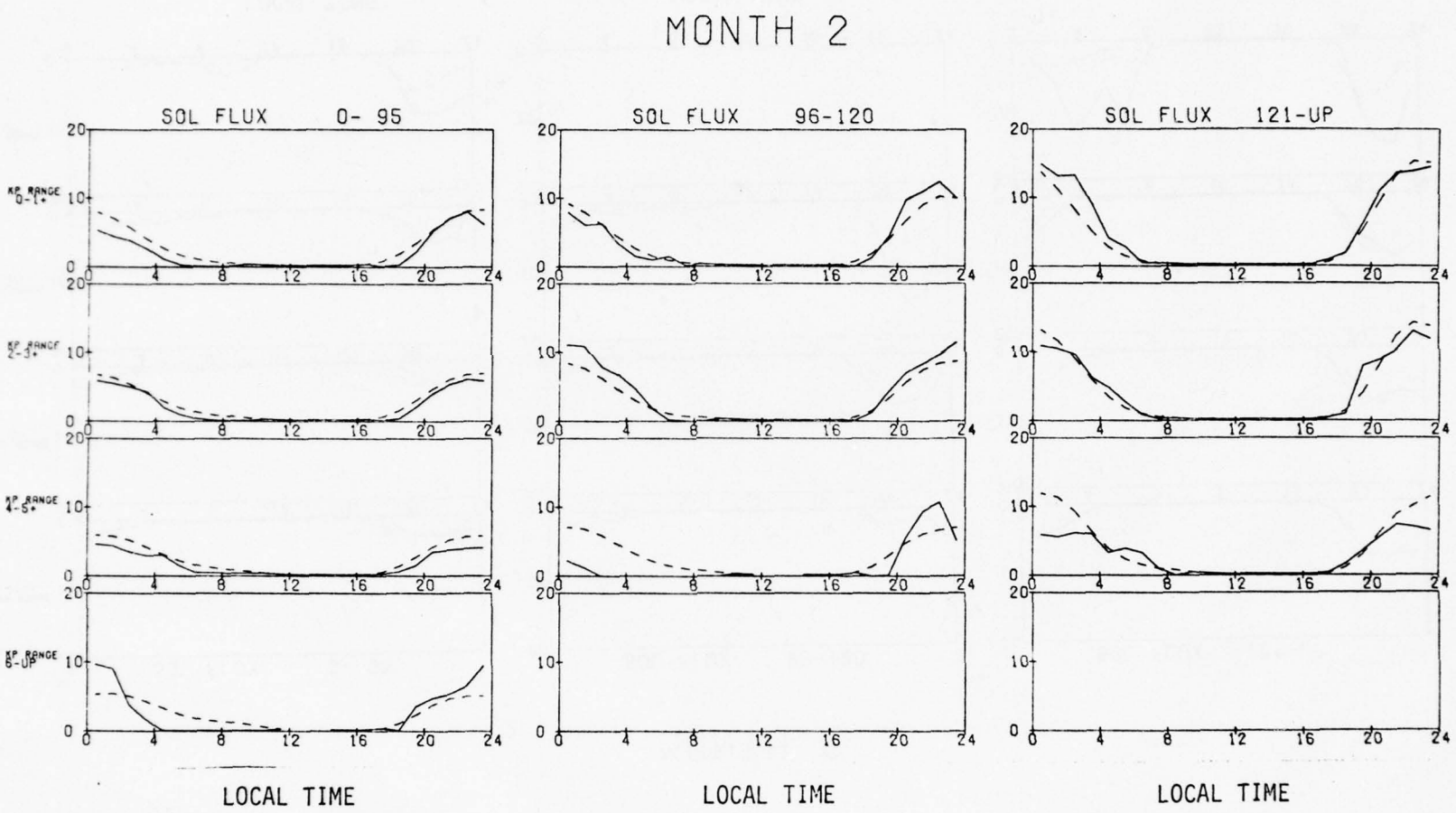

Figure 7. Average SI Data and Model Plots for Ghana A3 for February.

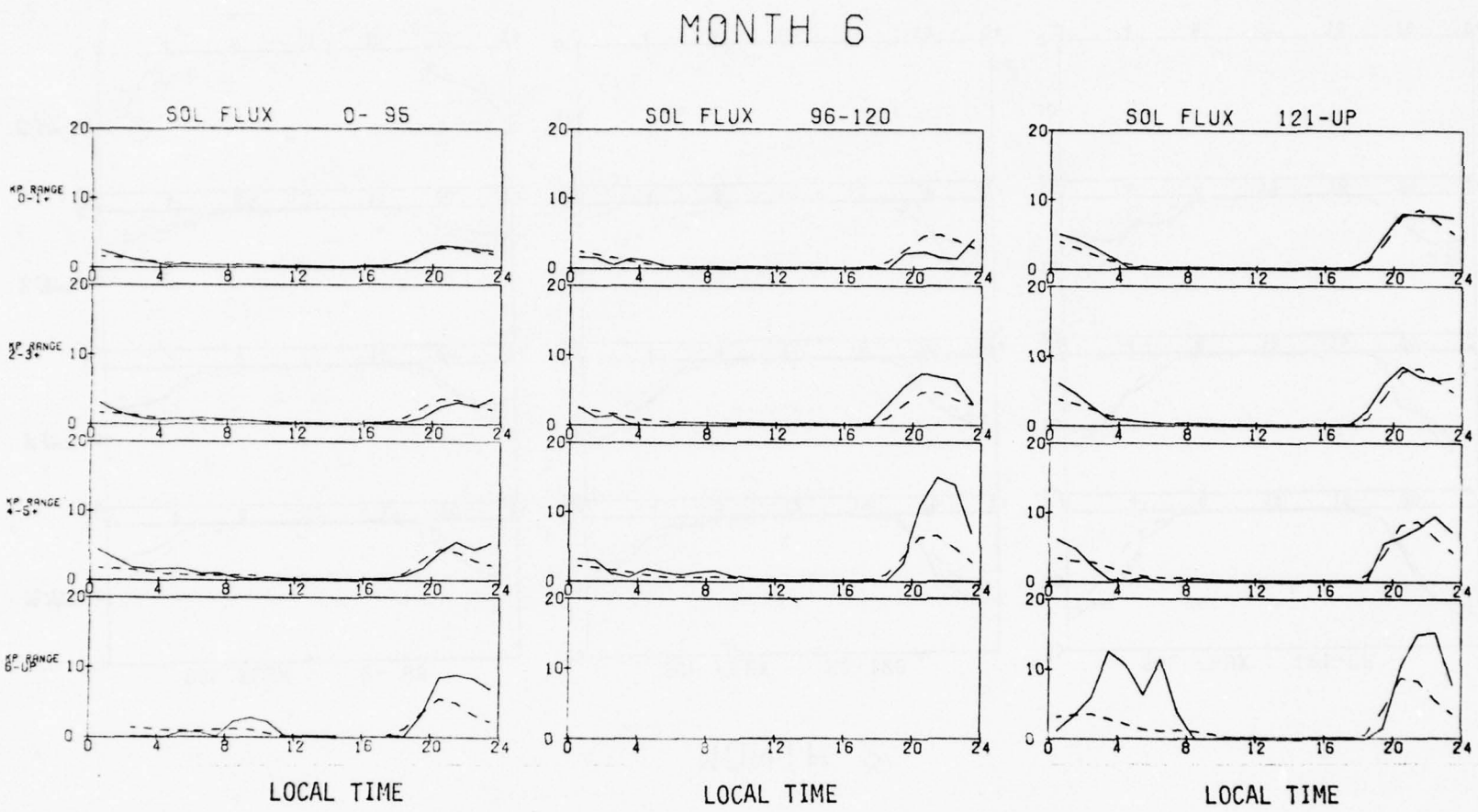

Figure 8. Average SI Data and Model Plots for Ghana A3 for June.

with high efficiency. Each of the bases for the equatorial study were collected into files with headers and stored on one magnetic tape. The same was done for all the high latitude data.

All data are in integer form, obtained by multiplying the orginal values by the scale factors described in the file headers (see Figures 10 and 11). Information common to all samples in the file, such as station ID, satellite ID, Frequency, Preparation Date, and the number of bits per variable is also contained in the headers. Each sample is described in a CDC 60-bit word by time(UT), SI(dB), K_p and 2.7 GHz solar flux. The special key is presently unassigned and contains zero. The high latitude data requires an additional CDC word for sub-ionospheric geographic latitude and longitude, geomagnetic latitude and geomagnetic local time. A system of routines PACKUP (2123/03/02/4937) for handling these data is described in Section 9.

Periods covered and total number of 15-minute sample records that have been collected into the data base are as follows:

DATA BASES	SPAN	#RECORDS
Narssarssuaq	Sep. 68-Jul. 76	196388
Goose Bay	Jan. 72-Jul. 76	120507
Sagamore Hill	Dec. 69-Jan. 76	165009
Huancayo A3	May 69-Apr. 76	1644427
Huancayo L6	Dec. 70-Mar. 76	123715
Ghana A3	Oct. 71-Apr. 76	154222

PF - Geomagnetic Latitude

DA - Day Number

HL - Local Time (hrs.)

AS = (2.7 GHz Solar Flux)/100.

$$SI = -2.0+1.2CL+6.5(1-.2FD)\{1+.6(1-.16FD)(1-.45SL)\cos(HL+2-.4K_p)$$

$$+.05\cos(2(HL-.9))+.02\cos(3(HL+3.5))\}(EXL)\ EXA$$

$$\text{where } EXA = 2^{\{.2K_p(1+.25CL)(1-.1XD)+AS(1-.8SL)(1+.45FD)\}}$$

$$\text{and } EXL = 2^{\{.32(PF-66.1)\}}$$

where $\begin{cases} CL=\cos((PF-54.4)\ \pi/25) & CDL = 1+.75SL \\ SL=\sin((PF-54.4)\ \pi/25) & SDL = 1-3SL \end{cases}$

$PD=\cos(DA+16)+.3\cos(2(DA-30))$; $FD=CDL \times PD$ $XD=SDL \times PD$

Figure 9. Revised Model of Scintillation Based Upon Narssarssuaq, Goose Bay, and Sagamore Hill Data

HUANCAYO L6 IDSTA 20 IDSAT L6 IFREQ 254 SCINDEX DB PREPARED 07/27/77

FORMAT PER RECORD	VARIABLE	SCALE	BITS
	IYR	1	9
	IMO	1	6
	IDA	1	6
	UT	16	9
	SI	10	9
	KP	3	6
	SF2.7	1	9
	SP KEY	1	6

Figure 10. Header for Huancayo L6 Equatorial Data Base.

Tape EQSIDB contains three files of the equatorial SI data bases for Huancayo A3, Huancayo L6 and Ghana A3. Each file starts with the heater which may be printed out as 80-column card images.

GOOSE BAY IDSTA 33 IDSAT A3 IFREQ 137 SCINDEX DB PREPARED 08/5/77

FORMAT PER RECORD	VARIABLE	SCALE	BITS
	IYR	1	9
	IMO	1	6
	IDA	1	6
	UT	16	9
	SI	10	9
	KP	3	6
	SF2.7	1	9
	SP KEY	1	6
SUB-IONOSPHERIC PARAMETERS FOR HIGH LATITUDE DATA			
	LAT	16	12
	ELON	8	12
	MLA	16	12
	MT	16	9

Figure 11. Header for Goose Bay A3 Polar Data Base

Tape PLSIDB contains three files of the polar SI data bases for Narssarssuaq, Goose Bay and Sagamore Hill. Each file starts with the header which includes data on the station ID, satellite ID, Frequency and Preparation Date, as well as a description of the record format. These may be printed out as 80-column card images.

References

1) "Analysis and Programming for Research in Physics of the Upper Atmosphere," Logicon, Inc. Final Report, AFGL-TR-76-0231, September 1976.

2) Aarons, J., Mullen, J., Whitney, H., Martin, E., Bhavnani, K., and Whelan, L., "A High-Latitude Empirical Model of Scintillation Excursions: Phase 1," AFGL-TR-76-0210, Air Force Surveys in Geophysics, No. 353; September 1976.

Section 5. Defense Meterological Systems Project (DMSP)

Author: L. A. Whelan

5.0 Defense Meteorological Systems Project (DMSP)

Initiator: R. C. Sagalyn

Project No: DMSP Problem No: 4836

Program SSIE was written to process special ion and electron sensor data from a series of polar orbiting satellites of the SAMSO DMSP (Defense Meteorological Systems Project). The program will be run to process real time data as it is received at the Air Weather Service, Offutt Air Force Base, Nebraska, but it has been written and tested at Air Force Geophysics Laboratory. It has therefore been necessary to simulate the AWS Univac 1110 real-time system on the AFGL CDC 6600 computer. There were two principal programming tasks; data management and analysis.

5.1 Data Management

Preprocessed and Processed Data Files

Preprocessed ion and electron sensor data resides on a sector addressable circular file at GWC (addressing starts at sector 0). The SSIE processing program uses the preprocessed file as input, and constructs a file of similar structure for output. The output file contains the same information as the input file, but in different order and with the results of the analysis added.

A sector is 28 words long, and the file size is determined by the number of satellite readouts (usually a readout is one orbit's worth of data) which are to be retained in the file (usually about a day's worth). Both input and output files are from 20000-25000 sectors long. The following description is for the input file, but much of it applies to the

output file as well. Notes on the output file are included as Section 5.6.

The file is circular in operation in that new readouts received are inserted where the last readout ended. Should a readout begin near the end of the file and attempt to overflow the file, the data will continue writing at sector number 4. (Sectors 0-3 are reserved for the directory). This scheme assures constant collection of the most current data, since only the oldest readouts are being overwritten.

5.2 General File Structure

Figure 1 shows the general structure of the circular file. Figure 1 is intended to depict the general file structures and how they might appear within a circular file after it has been operational for some time. Figure 2 details the contents of the circular file.

A. Directory - The main function of the directory is to maintain current information concerning the status, position and size of each readout contained in the file. The directory is located in sectors 0-3 (Figure 2). The first 2 words of the 112 word directory are used by the processing program to maintain file position information only for the most current readout received. The next 26 words are pointers and reflect the total file content. Each valid pointer word represents a readout. There are a larger number of pointers than there are readouts that the file could actually contain. Each pointer word consists of 3 subdivisions--1. four status bits, 2. the sector number where the readout begins, 3. the number of data sets in that readout. Whenever a readout is overwritten the first status bit for its pointer word is set, and that pointer becomes in effect, invalid. The remainder of the directory is unused at this time.

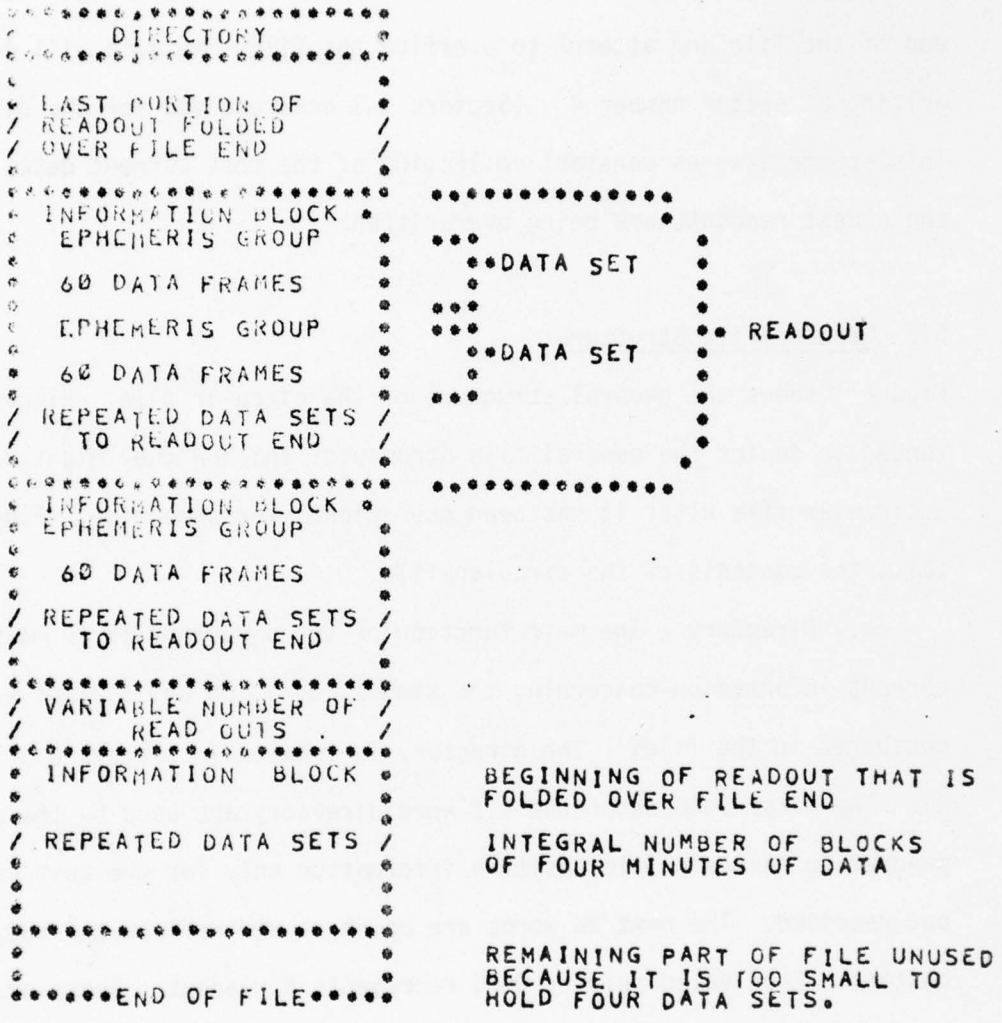

Figure 1. Circular File Structure

DIRECTORY

SECTOR WORD		DESCRIPTION (0 ... 17 18 ... 35)
0	1	BEGINNING SECTOR OF LAST READOUT (DIRECTORY) | POINTER WORD NUMBER IN THIS DIRECTORY (INTEGER)
THRU	2	BATCH NBR(1-99) ASSIGNED TO LAST READOUT(INTEGER) | BEGINNING SECTOR OF NEXT READOUT (INTEGER)
3	3 THRU 28	0•1•2•3•4 ... 19•20 ... 35 — BEGINNING SECTOR OF READOUT (INTE) | NUMBER OF DATA SETS IN READOUT (INTEGER)
	29 THRU 112	NOT ASSIGNED AT THIS TIME

BIT0 SET = READOUT OVERWRITTEN/POINTER NOT VALID
BIT1 SET = PROCESSED
BIT2 SET = READOUT ARCHIVED
BIT3 SET = PROCESSED

INFORMATION BLOCK

SECTOR WORD		
N	1	BATCH NBR(1-99) ASSIGNED TO READOUT (INTEGER)
N	2	MISSION ID, 6 ALPHANUMERIC CHARACTERS (HOLLERITH)
N	3	READOUT REV NUMBER (INTEGER)
N	4	LONGITUDE (IN TENTHS) OF ASCENDING NODE (INTEGER) +EAST (0-360DEGREES)X 10 I.E. 0-3600
N	5	AFGWC SYSTEM TIME (JULHR) OF NODAL CROSSING CUMULATIVE HOURS SINCE 0000 31 DEC 67 (INTEGER)
N	6	DATE TIME GROUP OF NODAL CROSSING (INTEGER) 0 ... 5•6 ... 11•12 ... 23•24 ... 35 — DAY (1-31) | MONTH (1-12) | YEAR (00-99) | TIME (0000-2359)
N	7	BEGINNING SECTOR OF THIS READOUT (INTEGER)
N	8	BEGINNING SECTOR OF NEXT READOUT (INTEGER)
N	9	NUMBER OF DATA SETS IN READOUT (INTEGER)
N	10	TIME OF FIRST MESSAGE IN READOUT (INTEGER) 0 ... 11• ... •18 ... 23•24 ... 29•30 ... 35 — JULIAN DAY (1-366) | HOUR | MINUTES | SECONDS
N	11	TIME OF LAST MESSAGE IN READOUT (INTEGER) (FORMAT AS WORD 10)
N	12 • • N+3 28	NOT ASSIGNED AT THIS TIME

Figure 2. Contents of the Circular File

DATA SET

EPHEMERIS GROUP

SECTOR	WORD	
N+4	1	LATITUDE, RADIANS, 0 -PI/2 (FLOATING POINT) +=NORTH, -=SOUTH
N+4	2	LONGITUDE, RADIANS, 0 -2PI (FLOATING POINT) +=EAST
N+4	3	ALTITUDE ABOVE SUBSATELLITE POINT, NM (INTEGER)
N+4	4	JULIAN DATE OF DATA, 1-366 (INTEGER)
N+4	5	NUMBER OF SECONDS FROM 0000Z ON JULIAN DAT 0-86399 (INTEGER)
N+4	6	FORMAT SAME AS WORD 1 * WORDS 1-5 PERTAIN TO
N+4	7	FORMAT SAME AS WORD 2 * THE FIRST DATA IN THI
N+4	8	FORMAT SAME AS WORD 3 * DAT SET.
N+4	9	FORMAT SAME AS WORD 4 * WORDS 6-10 PERTAIN TO
N+4	10	FORMAT SAME AS WORD 5 * THE LAST DATA IN THE * DATA SET
		EARTH CENTER COORDS. UNIT VECTOR CENTER OF EARTH
N+4	11	X THRU EQUATOR AT 0E
N+4	12	Y THRU EQUATOR AT 90E *AT TIME IN WORD 5
N+4	13	Z THRU NORTH POLE
N+4	14	X EARTH CENTER COORDINATES
N+4	15	Y AT TIME IN WORD 10
N+4	16	Z
N+4	17	WORD 1, RADIANS * 10000 (INTEGER)
N+4	18	WORD 2, RADIANS * 10000 (INTEGER)
N+4	19	ALTITUDE(NM) AT TIME IN WORD 5 (FLOATING POINT)
N+4	20	WORD 6, RADIANS * 10000 (INTEGER)
N+4	21	WORD 7, RADIANS * 10000 (INTEGER)
N+4	22	ALTITUDE(NM) AT TIME IN WOR 10(FLOATING POINT)
N+4	23	ORBIT ANOMALY ANGLE, RAD (FLOAT PT) FOR TIME 5
N+4	24	ORBIT ANOMALY ANGLE, RAD (FLOAT PT) FOR TIME 10
N+4	25	
	.	
	.	NOT USED AT THIS TIME
	.	
N+5	4	

Figure 2. Contents of the Circular File (Continued)

		SENSOR DATA
		0 15 16 35
N+5	5	MSB LSB (LINE SYNC)
		TIME CODE 11 111 000 110 111 010 100
N+5	6	
	•	60 SECONDS OF SPECIAL SENSOR DATA WITH TIME/SYNC
	•	WORD EACH SECOND
N+17	28	
N+18	1	
	•	NEXT EPHEMERIS GROUP
N+19	4	
N+19	5	
	•	60 SECONDS OF SPECIAL SENSOR DATA WITH TIME/SYNC
	•	WORD EACH SECOND
N+31	28	
		REPEATING EPHEMERIS GROUPS AND DATA SETS TO END OF READOUT

Figure 2. Contents of the Circular File (Continued)

B. Readout--A readout is the variable quantity of data received during a particular satellite data acquisition period. Each readout begins at a variable sector location dependent upon the length of previous readouts. The file sector where a readout begins is given in the directory pointer word. Each readout consists of an information sector followed by a variable number of data sets. Readouts are placed in the circular file in the sequence in which they are received from the spacecraft. A spacecraft having relatively older data on its recorder could be readout after a spacecraft having more recent data, thus the readouts are not necessarily in time sequence.

C. Information Block--The first four sectors of each readout contain the information block. The function of this sector is to maintain parametric data peculiar to the readout. (Figure 2).

D. Data Set--A data set is defined in the preprocessed files to be one ephemeris group plus 60 seconds of sensor data. Each data set contains 392 words and occupies 14 sectors (or 420 words and 15 sectors for the output file).

E. Ephemeris Group--The first 32 words (60 words on output file) are defined as an ephemeris group. The first five words of the ephemeris group contain position information at the time of the first data message following the ephemeris group. The second five words contain position information at a time 60 seconds earlier than the time of the first data message following the ephemeris group. That is, the information corresponds to the time of the data in the last data message in the data set. This is true because the spacecraft tape recorders are not rewound prior to playback. The data frames, within each readout, will be inserted into the file in reverse time order, i.e, the first frame within each readout will be the last frame produced by the sensor. The ephemeris group for 180 bit/sec to 216 bit/sec sensors is contained in the first 28 words of the data set, thus the

sensor data begins with the first word of the next sector rather than word 5. The block 5D spacecraft has precise attitude control which maintains the sensor pointing accuracy to 0.01 degree, thus pitch, yaw, and roll corrections are not necessary.

F. Sensor Data--Following the ephemeris group are 60 one second data frames. The first word of each data frame contains the spacecraft 24 hour elapsed time counter followed by a synch code (Figure 2). The least significant bit of the time code corresponds to 2 seconds. The synch code is the following logical pattern =111110001101110101000. The time synch word is followed by the integral number of 36-bit words necessary to contain the total bit output for the sensor when interrogated by the spacecraft processor for that second. The sensor data words will not be in the same sequence in which they were generated by the sensor. The bit stream is received in reverse order at AFGWC, that is, least significant bit first. The data formatter (DF) reverses the bits in 36-bit groups (one Univac word). Thus the sensor words in the preprocessed circular file appear with the most significant bit first but in a different sequence. The data word sequence for various bit length words is given in Figure 3. Figure 4 shows the contents of a 180 bit data block.

5.3 File Conventions

A. If a data drop-out, i.e. time discontinuity, is encountered between data frames, the remainder, (if any) of the 60 second block of data frames will be zero filled, the ephemeris groups associated with that data set will still be 60 seconds apart as if the data had continued uninterrupted. The next data set generated will start with the first data frame following the discontinuity.

Six Bit Words	Nine Bit Words	Twelve Bit Words	Eighteen Bit Words
6	4	3	2
5	3	2	1
4	2	1	4
3	1	6	3
2	8	5	6
1	7	4	5
12	6	9	8
11	5	8	7
10	12	7	10
9	11	12	9
8	10	11	
7	9	10	
18	16	15	
17	15	14	
16	14	13	
15	13		
14	20		
13	19		
24	18		
23	17		
22			
21			
20			
19			
30			
29			
28			
27			
26			
25			

Figure 3. Data Word Sequence

B. Data will be written to the file by the preprocessor in blocks of 4 minutes of sensor data and associated ephemeris groups, or 56 sectors. The circular file will be wrapped, that is, cease writing at the end of the file and begin overwriting at the beginning of the file, whenever there is not sufficient room remaining in the file for a complete four minute data block (56 or 64 sectors). The remainder of the file, between the last block written and the physical end of the file, is not initialized or set to zeroes. It will contain whatever was left from previous writes.

C. If there are insufficient data at the end of a readout to completely fill a four minute block, the remainder of the last four minute block will be zero filled.

5.4 Univac 1110 Conventions

The following information is provided for those not familiar with the Univac 1110 system.

Word length is 36 bits

1 sector is 28 words, mass storage is sector addressable

Negative values are ones complemented

Mass storage I/O efficiency is achieved in groups of 112 words.

5.5 DMSP SSIE Data Output

The SSIE experiment provides a single digital NRZ (nonreturn to zero) data signal, designated as (SSIEDAT) to the OLS (Operational Linescan System). This data signal is transferred in phase with the OLS supplied bit clock in bursts of 180 contiguous bits at a bit rate of 1000 Hz $\pm$ 1 Hz. Upon command (SSIERED) from the OLS, the SSIE provides one 180 bit data block per second

with the least significant bit (LSB) occurring first in the first word.

The SSIE 180 bit data block consists of twenty, 9 bit data words as follows:

7 Samples Electron Data (Words 1, 4, 7, 10, 13, 16, 19)

7 Samples Ion Data (Words 2, 5, 8, 11, 14, 17, 20)

6 Samples Event Monitor (Words 3, 6, 9, 12, 15, 18)

All data is stored in SSIE shift registers. Once per second a read pulse (SSIERED) of 180 ms duration from the OLS allows the registers to shift out data acquired during the 1000 ms period prior to the END of the read period. Word 1 is shifted out first.

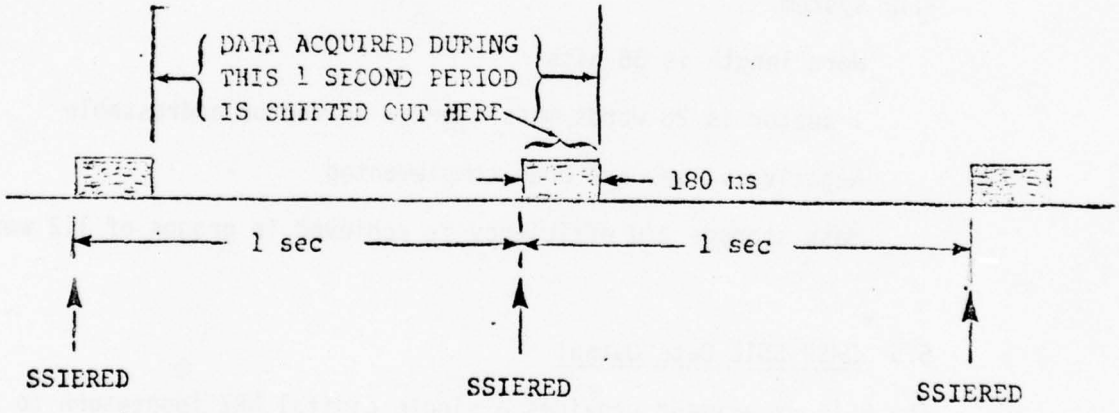

Figure 4. Contents of a 180 Bit Data Block

5.6 Output File Notes

The processed file (output) from the SSIE analysis program fits the description of the DMSP preprocessed circular file, with the following exceptions.

1. The processed file is 22016 sectors long, addressable 0-22015. Each data set is one minute of data, but is 420 words, or 15 sectors, long. The one additional sector is included in the emphemeris group (header) making that group 60 words in length, rather than 32 as in the preprocessed file.

2. As in the preprocessed file, one second of data is contained in six 36 bit words, the first being a time-synch word, and the remaining five containing 20 nine bit words of data. In the processed file, these words and the data sets data blocks are in time order, but within the blocks the data are in the same order as in the preprocessed file.

3. The 60 word data set header (ephemeris group) for the output file is as follows:

First Sector of Minute

Word	Contents	
1	Latitude, radians, 0-PI/2,fp.	
2	Longitude, " " "	First
3	Altitude, NM, tp.	data/time
4	Julian Date, 1-366,integer	in minute
5	Seconds from 0000Z on JD,0-86399	
6		
7		
8	As in words 1-5	Last
9		data/time
10		in minute

Word	Contents
	Earth center coordinates, time of word 5
11	X fp
12	Y fp
13	Z fp
	Earth center coordinates, time of word 10
14	X fp
15	Y fp
16	Z fp
17	Orbit anomaly angle, rad,fp. Time of word 5
18	" " " " " " " " " 10
19	JD of latest sweep pair start time, integer, 1-366.
20	Seconds from 0000Z, integer 0-86399.

t_0 designate time at midpoint of the electron sweep. If the start of an electron sweep occurs within a minute, the time in words 19-20 will be between the time in 4-5 and 9-10.

21	Electron density at t_0 for latest sweep not starting in current minute, CM^{-3},fp.
22	Electron density at t_0 for sweep starting in current minute if there is one - otherwise, same value as wd 21. CM^{-3},fp.
23	Ratio of electron density at t_0, to measured current at sensor potential equal to resting bias voltage for the same sweep as in word 21.
24	As in word 23 for same sweep as in word 22.
25	Electron temperature at t_0 for latest sweep - current minute sweep it one starts in it, deg K,fp.
26	Vehicle potential with respect to plasma at t_0, same sweep as in 25, volts, fp.

The parameters contained in the following eleven words take their values at t_0 + 17, midway into the ion sweep following the latest electron sweep - including the current minute. There are two cases a. 2 or 3 species present b. one specie present. In case b there are two ways to compute temperature, AMU, and vehicle potential with respect to plasma, depending on how the density is estimated. Both cases are carried - with subscripts (ss) 1 or 2.

27 NI number of species present, integer

	2 or 3 Species	One Specie
28	N(1) H + density	SS 1 density

Second Sector of Minute

1	N(2) He^+ density	SS 2 density
2	N(3) O^+ density	
3	T(1) Average ion temp.	SS 1 ion temp.
4	T(2)	SS 2 ion temp.
5	EM(1) Average ion mass	Ion mass for density N(1)
6	EM(2)	Ion mass for density N(2)
7	Vehicle pot wrt plasma	SS 1 vehicle pot
8		SS 2 vehicle pot
9	Current at 0 applied voltage	

The following, Scale height, is computed at t + 8.5, midway between the two sweeps.

10 Scale height for 2/3 specie case, or SS 1 of 1 specie case KM.

11 Scale height for 1 specie case, SS 2.

4. Directory sector is maintained for output file just as for input file.

5. Information block for a readout constructed for output file as for input file, except that words 10 and 11 are interchanged since time order is reversed.

6. Discontinuities in the data on the output file occur sporadically. They can be detected in two ways:

a. End time in header of one minute does not correspond to start time of the next. It may be earlier or later.

b. The data words will be all zeros at the beginning of a minute of data.

Conditions a. and b. may occur singly or simultaneously.

When discontinuities were detected on the input preprocessed file during a sweep pair, the sweep pair was considered invalid and the analysis not done for that pair.

General Reference:

Air Force Global Weather Control Data Acquisition and Processing Special Sensor Data Processing Section, Offut Air Force Base, Nebraska; "Special Sensor Data Preprocessed Circular File, Subsystem Specification", July 3, 1976, Nebraska

EVENT	APPLIED SIGNAL	EVENT MON LEVEL	DURATION (SEC)	TIME (SEC)	
				FIRST	REPEATS EVERY
CAL. NO. 1	$+5 \times 10^{-8}$a (ION) -1×10^{-6}a (ELEC)	0.2V	2	0-2	1024
CAL. NO. 2	$+5 \times 10^{-11}$a (ION) -1×10^{-9}a (ELEC)	0.4V	2	2-4	1024
ELECTRON SWEEP FLAG	NONE	0.6V	2	8-10	128
ELECTRON SWEEP (OUTER GRID)	+5V → -8V	+5V → +1V	10	10-20	128
ION SWEEP FLAG	NONE	0.8V	2	24-26	128
ION SWEEP (OUTER GRID)	-5V → +12V	+1V → +5V	12	26-38	128

BIAS MODE	RESTING BIAS ELECTRON DENSITY GRID	MODE MON. LEVEL
1	1.5V	3.5V
2	0V	1.5V

Table 1. SSIE Sequence of Events (DMSP)

Revised 13 May 77: (ELEC) Cal. 1 and Cal. 2 from (-10^{-5} and -10^{-8}a) to (-10^{-6} and -10^{-9}a) respectively

Section 6. Plasma Bulk Motion

Author: S. T. Lai

Figure 2. Contents of the Circular File

6.0 Plasma Bulk Motion

Initiator: P. Wildman

Project No: 2311 Problem No: 4701

Disturbances and irregularities in the ionosphere and magnetosphere, particularly in the polar and auroral regions, affect electromagnetic wave communications, detection, tracking, guidance, and early-warning defense systems. Ambient plasma bulk motion is an important factor in forecasting ionospheric and magnetospheric plasma meteorology and in understanding the processes leading to polar region irregularities (Figure 1). Such irregularities are already known to cause the scintillations in satellite signals received at ground stations (Reference 1). This work supports research projects at AFGL in situ satellite sensing of plasma bulk motion as well as plasma densities and temperatures. The satellites concerned are S3-2 and S3-3. Schematically, the sensors are divided into three groups: the planar ion sensor cluster, the non-planar ion sensor cluster, and the spherical Langmuir-type electron sensor.

6.1 Data Processing

For data processing, three types of data tapes are required, viz., the plasma data tape, the satellite attitude (OM) data tape, and the satellite ephemeris (ORMAG) data tape. The structures of these data are documented in the references (References 2, 3).

Figure 1. Plasma Flows in the Earth's Environment

The satellite signals consist of several patterns which have to be recognized. They are the TM applied voltage sweeps, electron sensor real sweeps, electron calibrates, ion calibrates, and range switchings. The flow chart of Figure 2 outlines the data processing and computational schemes.

6.2 Ionospheric Plasma Electron Properties

The technique used in this satellite project for measurements of ionospheric plasma electron properties is to analyze the Langmuir probe responses. A TM applied voltage sweep appears once every 128 sec. in the experiment. This voltage is also applied to every real sweep of the electron sensor in the following 128 sec. period. The voltage-current response characteristics of the sensor output gives information on the electron properties of the plasma environment. Physically, the electron sensor-current I in the Langmuir probe is proportional to the velocity, thermal distribution, and density of the electrons, i.e.

$$I(V) \propto NeA \sqrt{\frac{2kT}{m}} \exp\left[-\left(\frac{eV}{kT}\right)\right] \qquad (1)$$

where the square root term is due to the electron velocity, the exponential term is the Boltzmann distribution function, N is electron density, e is electron charge, and A is sensor aperture area. Therefore, the slope of $\log_e(I)$ plotted versus voltage V(t) should yield the electron temperature T, and, once T is found, N can be computed.

Analysis of the real data revealed that the sensor-current I(V) deviates from Langmuir's equation because of several reasons. They are: (1) vehicle potential is nonzero but an environmental dependent variable; (2) the effective aperture area is affected by the plasma sheath surrounding the sensor and the vehicle; (3) there often exist at the same region more than one species of electrons, characterized by their densities and temperatures; (4) geometry of grids in the sensor; (5) secondary electron emissions and also photo electron emissions from the sensor.

The vehicle potential variations in the ionosphere are related to the phenomenon of spacecraft charging (Reference 4). The plasma sheath is a result of the well known Debye shielding property of plasmas. The presence of multi-electron species is due to electron flows in the ionosphere, especially in events such as energetic electron precipitations in auroral and red arc regions and in polar plasma flow regions. Photoemissions and secondary emissions are due to solar photons and energetic electrons respectively.

Mathematically, the sensor current becomes expressed as the sum of contributions of I_1 and I_2 from the two species and I_3 from the secondary and photoemissions.

$$I(V) = I_1(N_1,T_1,V) + I_2(N_2,T_2,V) + I_3(V)$$

$$I(V) = \sum_{i=1}^{2} 4\pi r^2 \xi N_i e \sqrt{\frac{kT_i}{2\pi m}} \left[1 - \frac{r^2 - R^2}{r^2} \exp\left(-\frac{R^2}{r^2-R^2}\,\frac{eV}{kT_i}\right)\right]$$

$$+ \exp(a + bV)$$

Figure 2. Plasma Flow (Polar Wind) Data Flow

where $V = V_s + \Phi$, where Φ is the vehicle potential, and V_s is the applied voltage on the sensor, r is sheath radius, R grid radius, ξ transmission factor, k Boltzmann constant, e electron charge, N electron density, T electron density, and i labels the species. Each sweep pattern is the superposition of the sweep patterns corresponding to two single species. The expression I(V) is invariant under permutation of the indices i (=1,2). To determine the parameters that characterize the physical contents of the sweeps, the method of steepest descent of Fletcher and Powell (Reference 5) is used for fitting the sweep patterns. The parameters to be determined are N_i, T_i, Φ , r, a and b. Occasionally, the results of a sweep have to be rejected because of over saturation of data, broken sweep due to existence of time gap in which no signal was received on the ground, too much noise in data, or simply overshooting in the rapid descent technique. Usually, the sweep results are very useful. The scheme of electron density correction computation scheme at the end of every real sweep is shown in Figure 3.

6.3 Determination of the Plasma Flow Direction

In this section we derive expressions for the pitch and yaw of the plasma flow relative to the spacecraft coordinate system, using the currents flowing to an array of the positive ion sensors. The spacecraft velocity relative to the plasma contains components due to the spacecraft velocity and to any drift or 'bulk' motion of the plasma, (References 8, 9). To evaluate the component due to plasma motion it is necessary to know the spacecraft attitude and velocity in an external coordinate system, and this is dealt with in Section 6.4. First, however, we must derive the pitch and yaw angles of the plasma flow in the spacecraft geometric coordinates.

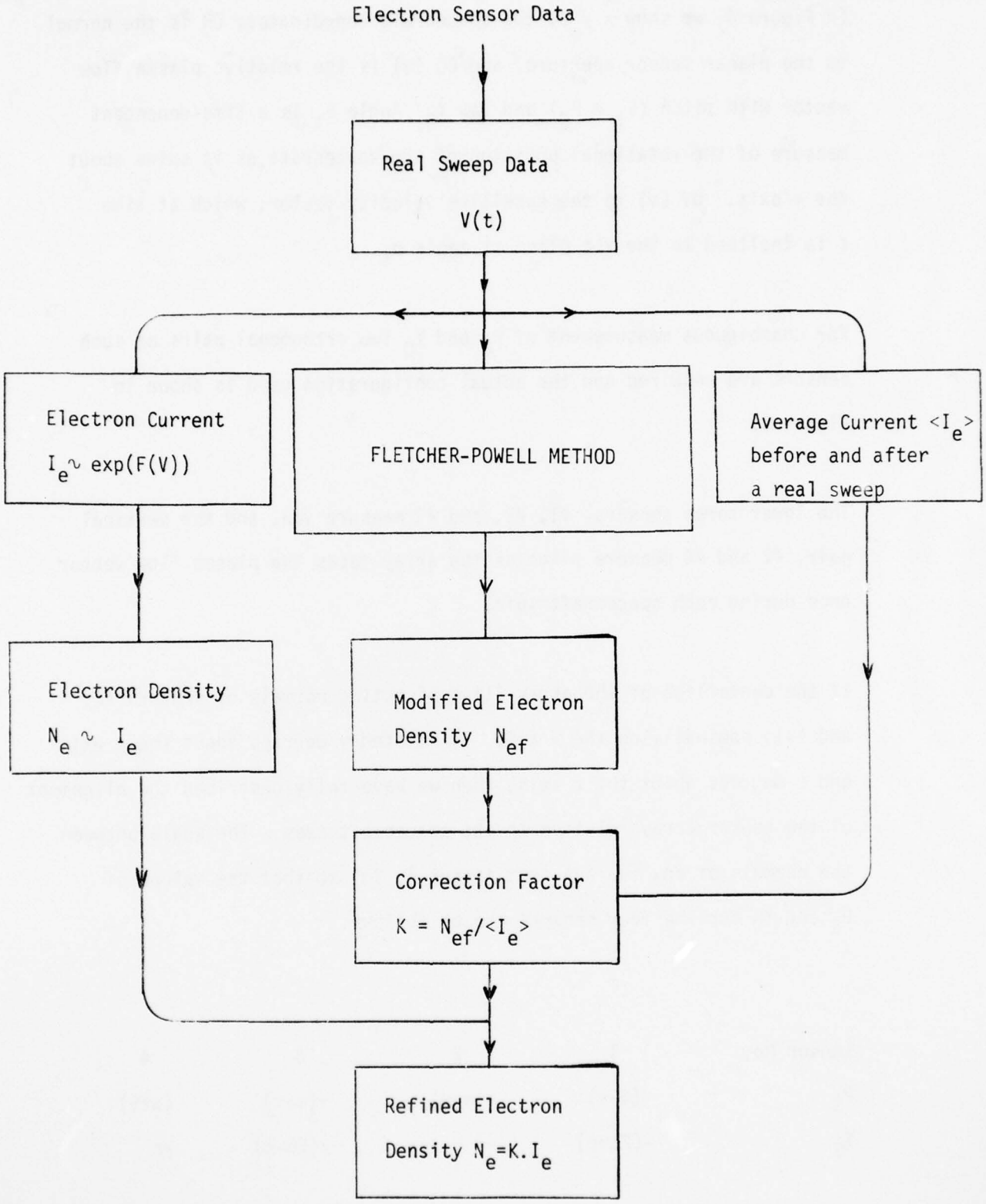

Figure 3. Scheme of Real Sweep Electron Density Computation.

In Figure 4, we show x y z, the spacecraft coordinates; ON is the normal to the planar sensor aperture, and OQ (q) is the relative plasma flow vector with pitch $(E_t + P_Q)$ and yaw Y_Q. Angle E_t is a time-dependent measure of the rotational position of the spacecraft as it spins about the y axis. OV (v) is the satellite velocity vector, which at time t is inclined to the x z plane at angle σ_t.

For unambiguous measurement of P_Q and Y_Q two orthogonal pairs of such sensors are required and the actual configuration used is shown in Figure 5.

The lower three sensors, #1, #2, and #3 measure yaw, and the vertical pair, #2 and #4 measure pitch as the array faces the plasma flow vector once during each spacecraft spin.

If the centerline of the array (line bisecting normals of sensors #2 and #4), nominally on the x axis, is rotated γ degrees about the y axis and ε degrees about the z axis, then we have fully described the alignment of the sensor array relative to the spacecraft axes. The angle between the normals of any two adjacent sensor is 2α so that the values of P_S and Y_S for the four sensors are as follows:

Sensor No.	1	2	3	4
P_S	$-(\alpha-\gamma)$	$-(\alpha-\gamma)$	$-(\alpha-\gamma)$	$(\alpha+\gamma)$
Y_S	$-(2\alpha+\varepsilon)$	$-\varepsilon$	$-(2\alpha-\varepsilon)$	$-\varepsilon$

TABLE 1. Skew Sensor Pitch and Yaw Angles

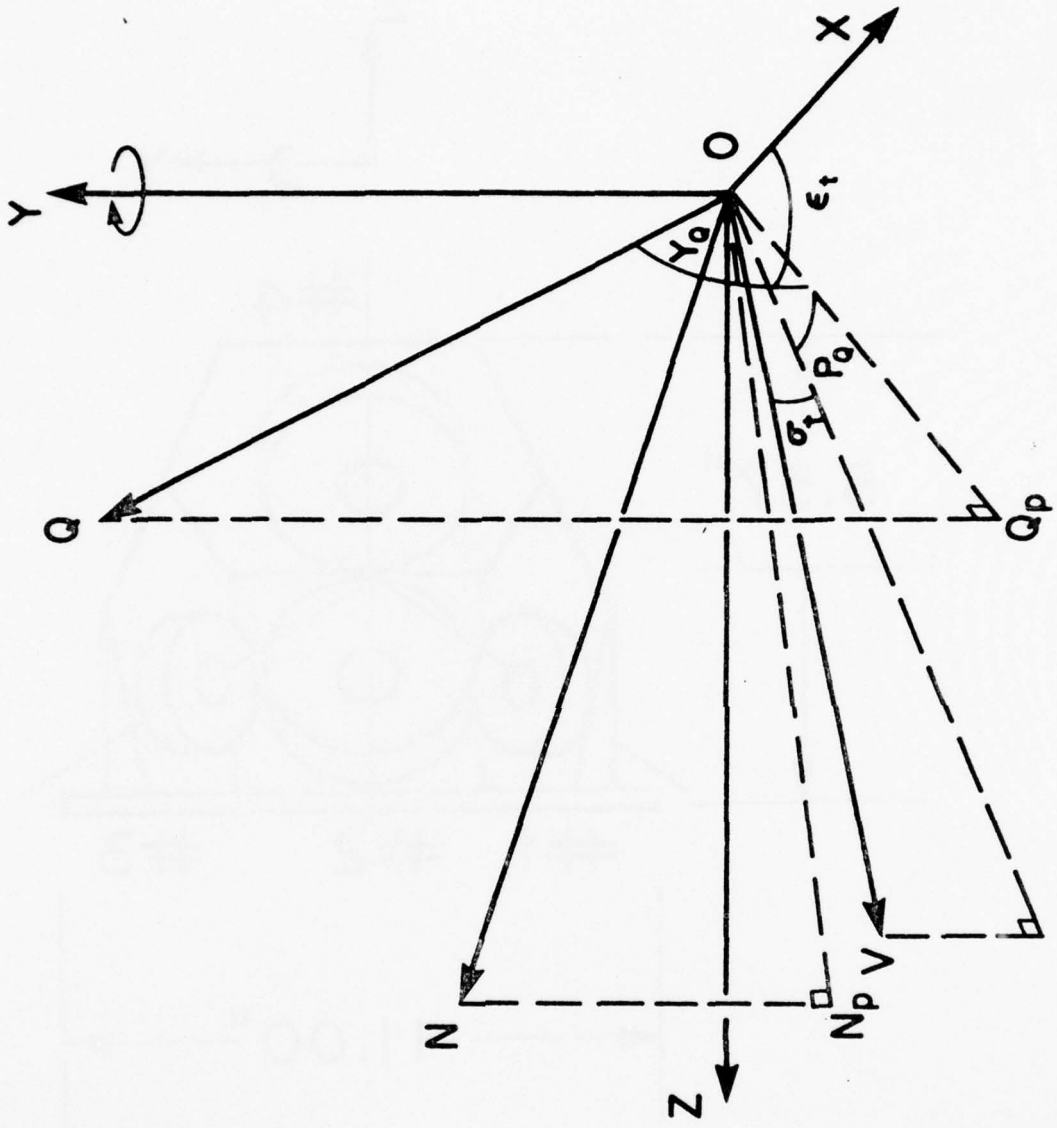

Figure 4. Geometry of Sensor in Ion Flow

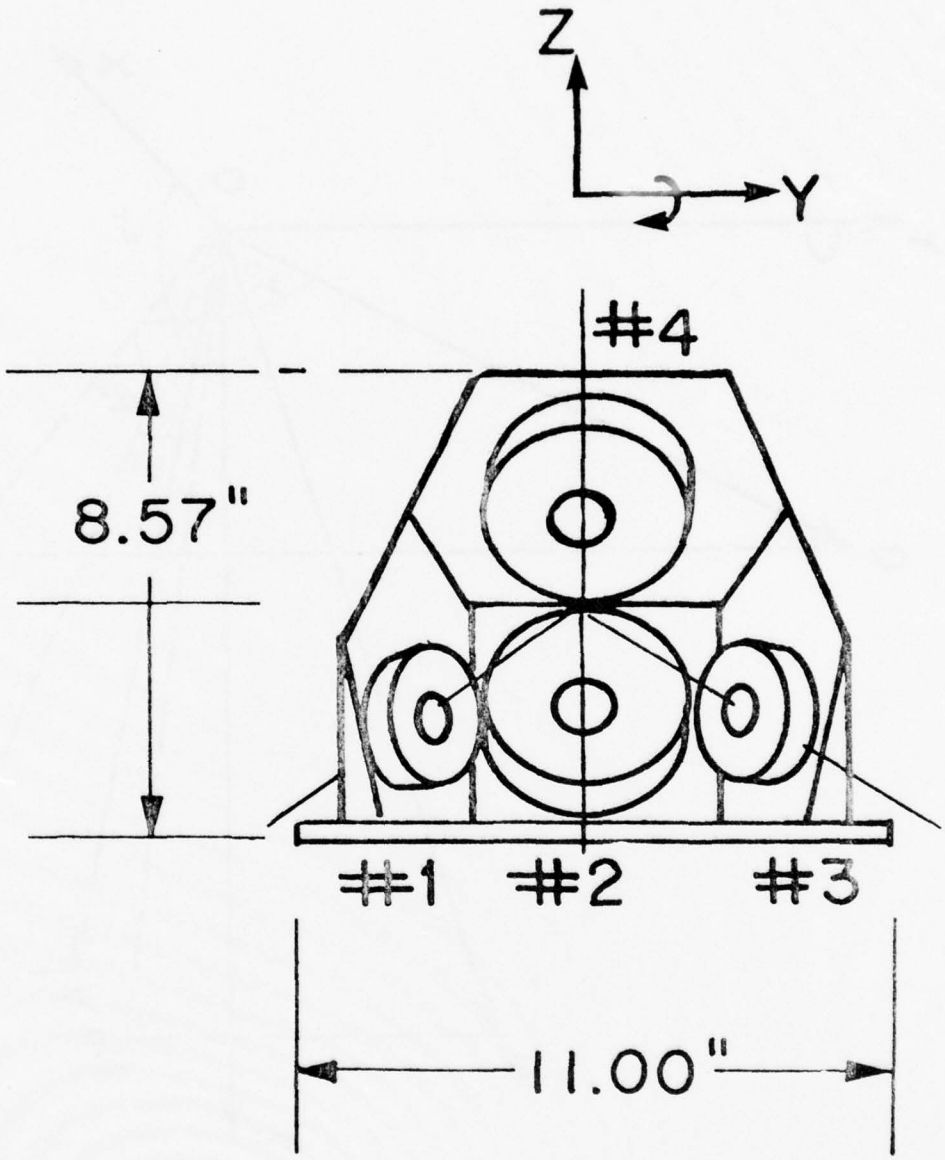

Figure 5. Front View of Ion Sensor Array

Considering again the ion flow to a single sensor, we assume that the mean thermal (isotropic) velocity of the ions is much less than the spacecraft velocity (Sagalyn and Smiddy, Reference 7) so that I, the sensor current is given by:

$$I = \xi \, Ne \, Aq \, \text{Cos} \, \phi$$

where:

ξ = transmission of the aperture

N = ambient ion density

e = electron charge

q = relative velocity between plasma and spacecraft

A = aperture area

ϕ = angle between q and aperture normal (NOQ in Figure 4)

Using the direction Cosines of OQ and ON to derive Cos ϕ, we obtain:

$$I = \xi \, Ne \, Aq \left[\text{Cos} \, Y_Q \, \text{Cos} \, Y_S \, \text{Cos}(P_Q - P_S + E_t) + \text{Sin} \, Y_Q \, \text{Sin} \, Y_S\right]$$

Let $\eta = \xi \, Ne \, Aq$

$Y = Y_Q$

$X = P_Q + \alpha - \gamma + E_t$

and P_S, Y_S are the Pitch and Yaw of the sensor normal. From the angles given in Table 1 we obtain the following relations:

$$R_{ij} = (I_i - I_j)/(I_i + I_j)$$

$$I_1 + I_3 = 2 \, I_2 \, \text{Cos} \, 2\alpha$$

Now let tan Φ = tan Y/Cos X

then:

$$R_{21} = \tan \alpha \, \tan (\alpha + \varepsilon + \Phi)$$

$$R_{23} = \tan \alpha \, \tan (\alpha - \varepsilon - \Phi)$$

$$R_{13} = -\tan 2\alpha \, \tan (\varepsilon + \Phi)$$

and $R_{24} = \dfrac{\text{Sin } \alpha \text{ Sin } (\alpha - X)}{\text{Cos } \alpha \text{ Cos } (\alpha - X) - \tan Y \tan \varepsilon}$

Define

$$\chi = \frac{R_{13} + \tan 2\alpha \tan \varepsilon}{R_{13} - \tan 2\alpha \text{ Cos } \varepsilon}$$

so that

$$R_{24} \frac{1 - \chi}{1 + \chi R_{24}} = \tan \alpha \tan (\alpha - X)$$

$$\tan (P_Q + E_t - \gamma) = \frac{-R_{24}}{\tan \alpha} \frac{1 - \chi}{1 + \chi R_{24}}$$

The choice between R_{21} and R_{23} depends on which side of the centerline the plasma flow is located.

6.4 Derivation of Plasma Velocity Vector

In Figure 6 we show the vector triangle containing the true plasma flow vector f together with v and q from Section 6.2. The angle θ, between v and q is determined knowing P_Q and Y_Q from Section 6.2.

In Figure 6 we now have:

$$f^2 = q^2 + v^2 - 2q\,v\,(\text{Cos } \sigma_t \text{ Cos } Y_Q \text{ Cos } P_Q + \text{Sin } \sigma_t \text{ Sin } Y_Q)$$

The direction cosines of the true plasma flow are given by:

$$\text{Cos } \alpha = \left[V \text{ Cos } \sigma_t \text{ Cos } E_t - q \text{ Cos } Y_Q \text{ Cos } (E_t + P_Q)\right] / f$$

$$\cos \beta = \left[V \sin \sigma_t - q \sin Y_Q\right] / f$$

$$\cos \mu = \left[V \cos \sigma_t \text{ Sin } E_t - q \cos Y_Q \sin (E_t + P_Q)\right] / f$$

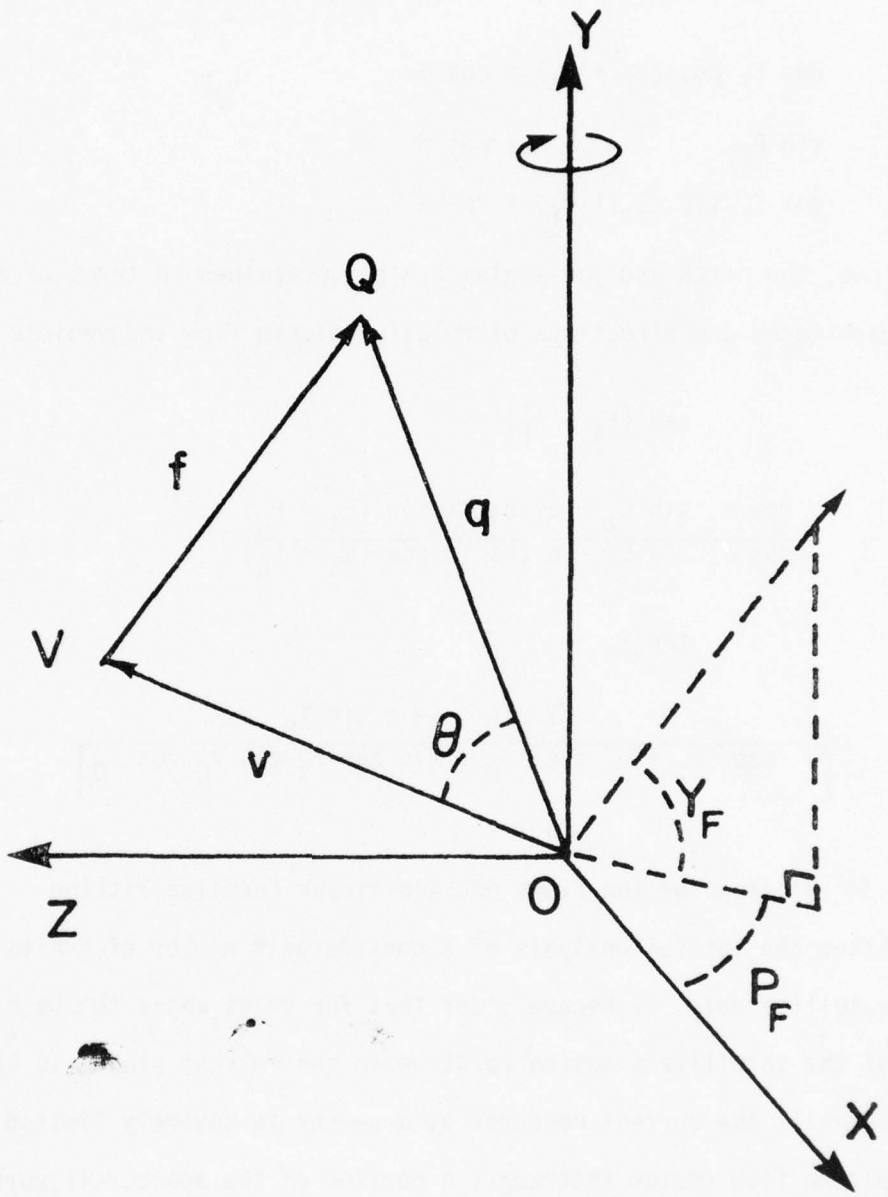

Figure 6. Definition of Ion Flow Vector

The pitch P_F and yaw Y_F angles of the true plasma flow are related to these direction cosines by:

$$\cos Y_F \cos (E_t + P_F) = \cos \alpha$$

$$\sin P_F = \cos \beta$$

$$\cos Y_F \sin (E_t + P_F) = \cos \mu$$

Thus, the pitch and yaw angles can be determined in terms of the magnitudes and directions of relative plasma flow and vehicle velocity;

$$\tan (E_t + P_F) =$$

$$\frac{V \cos \sigma_t \sin E_t - q \cos Y_Q \sin (E_t + P_Q)}{V \cos \sigma_t \cos E_t - q \cos Y_Q \cos (E_t + P_Q)}$$

$$\tan Y_F =$$

$$\frac{V \sin \sigma_t - q \sin Y_Q}{\left[V \cos \sigma_t + q \cos Y_Q - 2Vq \cos \sigma_t \cos P_Q \cos Y_Q\right]}$$

6.5 Blockage of Ion Flows and Non-linear Function Fitting

After the careful analysis of a considerable number of orbits of real satellite data, it became clear that for cases where the Mach number of the satellite's motion relative to the ambient plasma is large ($M >> 1$), the current measured by a sensor is severely limited when the plasma flow vector intercepts a portion of the spacecraft surface reaching the surface aperture. When the flow vector does not intercept the satellite surface, the current does behave similarly to that detected by an "unobstructed" sensor, as formulated by Lai et al (Reference 9).

AD-A051 126 LOGICON INC LEXINGTON MA F/G 4/1
ANALYSIS AND RESEARCH FOR INTEGRATED SYSTEMS IN PHYSICS OF THE --ETC(U)
NOV 77 J N BASS, K H BHAVNANI, B J GUZ F19628-76-C-0304
UNCLASSIFIED AFGL-TR-77-0265 NL

2 OF 2
AD
A051126

END
DATE
FILMED
4-78
DDC

For the case when the Mach number of the satellite motion relative to the ambient plasma is near or greater than 1 ($M \gtrsim 1$), the current measured by a sensor is less than that which would be measured by an "unobstructed" sensor for all directions of the flow vector.

To model exactly the shapes of the obstructions of flow to the sensor would require an algorithm that would not be efficient for the analysis of a large volume of data. Instead, the obstructions are approximated by a series of wedges centered on the sensor's apertures (Reference 10). The arrangements of the model wedges obstructing the fields of view of sensors are shown in Figures 7 and 8. As a result, the analytical expression of the current measured by a sensor looking out of the satellite spin plane becomes (Reference 10):

$$I_{out} = 1/2\, N e A (a/\pi)^{\frac{1}{2}} \int_0^\infty \nu_z \{erf[\sqrt{a}\,(\nu_z \cot \phi_1 \pm q \cos \eta)] + erf[\sqrt{a}\,(\nu_z \cot \phi_2 - q \cos \xi)]\} \exp[-a(\nu_z - q \cos \theta)^2]\, d\nu_z \quad .$$

Similarly, the analytical expression for the in-plane sensor current becomes

$$I_{in} = 1/2\, N e A (a/\pi)^{\frac{1}{2}} \int_0^\infty \nu_z \{erf[\sqrt{a}\,(\nu_z \cot \phi_1 + q \cos \eta)] + erf[\sqrt{a}\,(\nu_z \cot \phi_2 - q \cos \xi)]\} \exp[-a(\nu_z - q \cos \theta)^2]\, d\nu_z \quad .$$

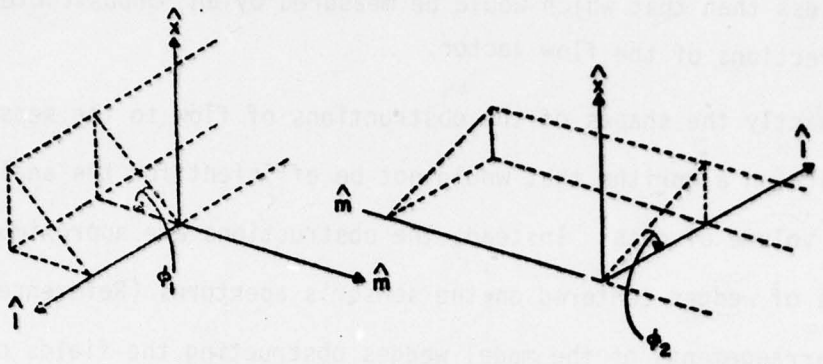

Figure 7. Orientation of the Two Wedges Used to Model the Obstruction for the Out-of-Plane Sensor's Field of View

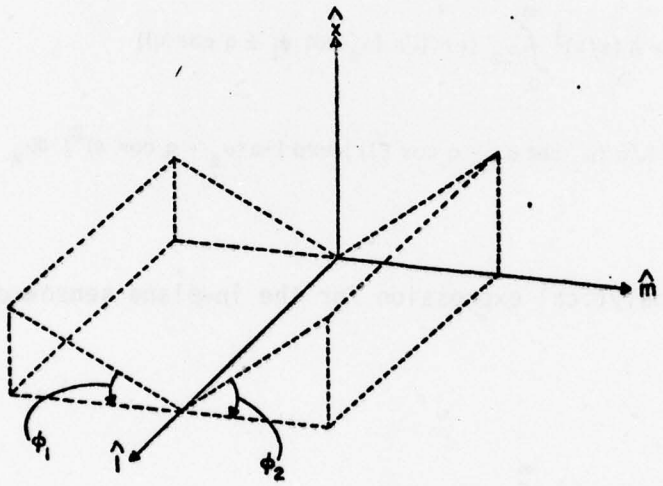

Figure 8. Orientation of the Two Wedges Used to Model the Obstruction for the In-Plane Sensor's Field of View

where $$\text{erf}(x) = \frac{2}{\sqrt{\pi}} \int_0^x \exp(-t^2)dt$$

These integrals can be calculated with good accuracy with Gaussian Quadrature. The technique to determine the plasma flow parameters is to use non-linear function data curve fitting methods. The parameters are found by a search in the vector space represented by them for the "solution" that yields a minimum in the difference between the expected and real values of the function. The search algorithm is based on the method developed by Fletcher and Powell (References 5, 6). Using the methods described in this section, we have computed the plasma flow data in many orbits (Figures 9, 10). In particular, a very high (9.8 km/s.) flow velocity of plasma was discovered to be associated with a large poleward electric field structure (see Section 7) at the plasmapause during the May 1976 magnetic storm (Reference 11).

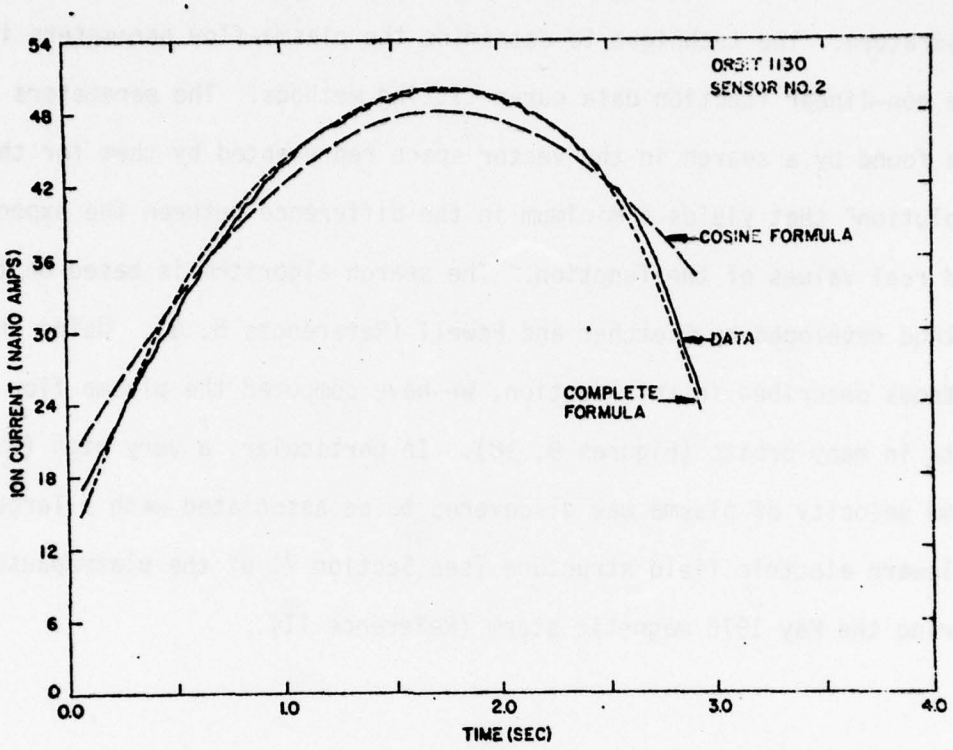

Figure 9. Comparison of the Best Fit Possible With the Unobstructed Flow Formula and the Formula Obtained Herein

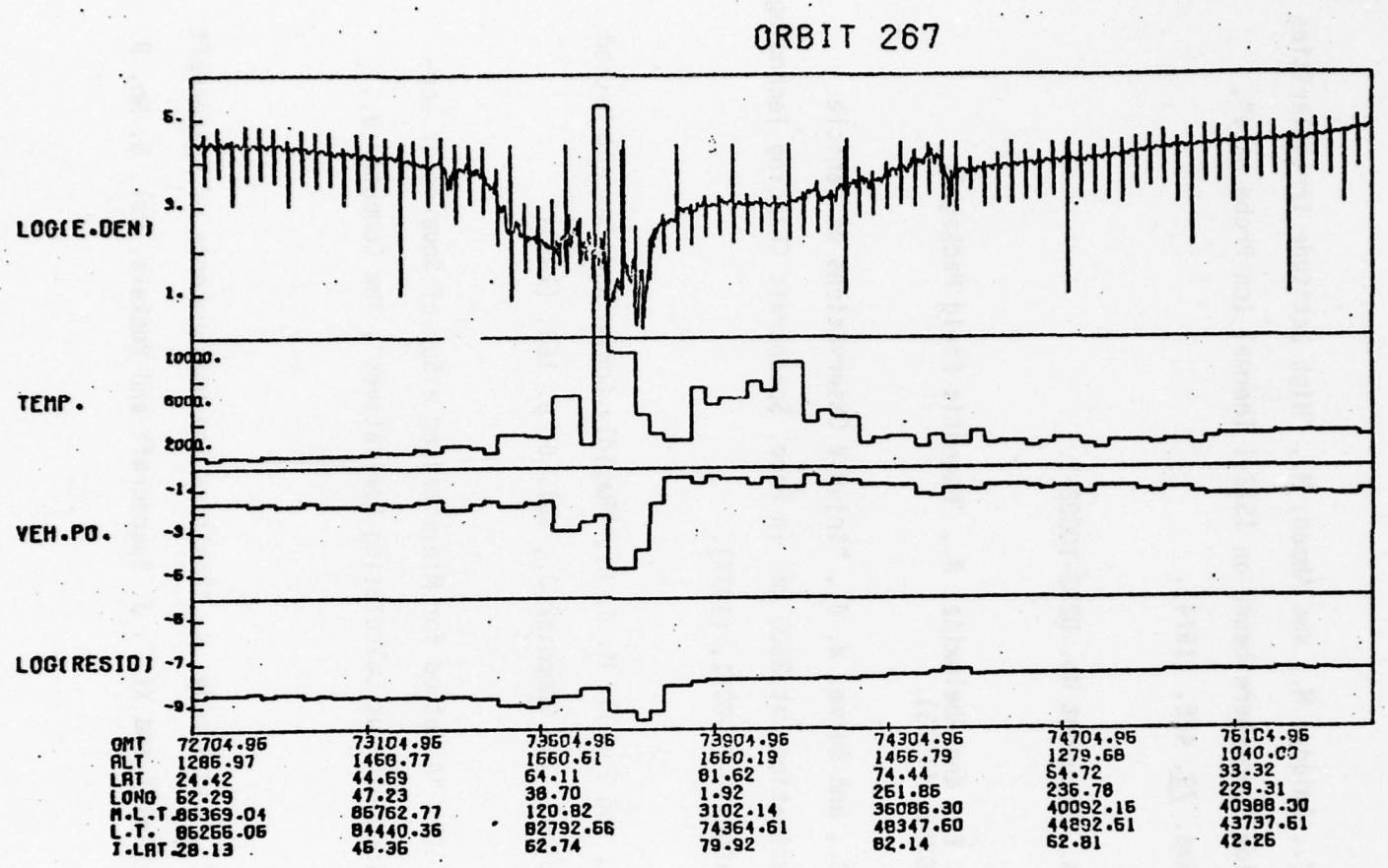

Figure 10. Plot of Geophysical Parameters Computed from Electron Sensor Data

References

1. Sagalyn, R. C., Smiddy, M., and Ahmed, M., "High Latitude Irregularities in the Top Side Ionosphere based on ISIS-I Thermal Ion Probe Data", J. Geophys. Res. 79, 425, (1974).

2. The Boeing Co., Document No. D233-10002-1.

3. McInerney, R. E., and Abelowitz, A., "Magnetic Field Package", AFCRL-TR-73-0356, (1973).

4. Sagalyn, R. C., and Burke, W. J., "Injun V Observations of Vehicle Potential Fluctuations at 2500 km" in Proc. Spacecraft Charging Technology Conference, AFGL-TR-77-0051, (1977).

5. Fletcher, R., and Powell, M. J. D., "Rapidly Convergent Descent Method for Minimization", The Computer J., Vol. 6, p. 163, (1963).

6. Powell, M. J. D., "A Method for Minimizating a Sum of Squares of Non-Linear Functions without Calculating Derivatives", The Computer J., Jan. (1965).

7. Sagalyn, R. C., and Smiddy, M. "Positive Ion Measurements of Spacecraft Attitude: Gemini X and XII", J. Spacecraft and Rockets, Vol. 6, No. 9 (1969).

8. Lai, S. T., Smiddy, M., and Wildman, P., "Satellite Sensing of Low Energy Plasma Bulk Motion", Bull. Amer. Meteor. Soc., Vol.57, No. 8, p. 108, (1976).

9. Lai, S. T., Smiddy, M., and Wildman, P., "Satellite Sensing of Low Energy Plasma Bulk Motion", Proceedings of the Seventh Conference of Aerospace and Aeronautical Meteorology and Symposium on Remote Sensing from Satellites, Amer. Meteor. Soc. & AIAA, p. 302 - 306, (1976). Also, AFGL-TR-76-0281, (1976).

10. Rich, F. J. and Wildman, P., "A Model for the Electrical Current Collected by a Planar Aperture Ion Collector With a Partially Blocked Field of View", AFGL-TR-77-0096, (1976).

11. Smiddy, M., Kelley, M., Burke, W., Rich, F., Sagalyn, R., Shuman, B., Hayes, R., and Lai, S., "Intense Poleward-Directed Electric Fields near the Ionospheric Projection of the Plasmapause", accepted for publication, J. Geophys. Res. Lett. (1977).

Section 7. Ionospheric Electric Fields

Authors: S. T. Lai

R. R. Hayes

R. Pavelle

7.0 Ionospheric Electric Fields

Initiator: M. Smiddy

Project No: 2311 Problem No: 4702

The reconnection of the magnetic field lines frozen into the solar wind with the earth's field lines at the magnetopause leads to large scale induced electric fields which are subsequently mapped down into the polar ionosphere. In order to measure the global distribution of these fields and their associated currents, the Air Force Satellite S3-2 was launched into a nearly polar orbit late in 1975.

7.1 Rotating Satellite Boom Sensor System

The satellite featured three pairs of deployable booms, each pair being orthogonal to the others. Carbon coated sensor spheres were mounted on the ends of the booms. Data were obtained from the axial pair and from one of the wire boom pairs in the satellite spin plane. The frequency of the data from the sensor was predominantly spin frequency. However, other frequencies corresponding to various oscillation modes may be present, especially during the transient response periods following boom deployment, spin orientation maneuver, etc. A comprehensive study of the mode dynamics of the rotating satellite was carried out in order to analyze all mode frequencies of the system.

Lagrangian equations of motion and Laplace transform techniques are used for computations of the transient response of the satellite system.

For full digital simulation of satellite dynamics including nonlinear mode-mode interactions and combinations of various boom deployment, a set of Lagrangian equations is solved:

$$\left[\frac{d}{dt}\left(\frac{\partial}{\partial \dot{x}_j}\right) - \frac{\partial}{\partial x_j}\right] L\left(\{x_i\}, \{\dot{x}_i\}\right) = F\left(\{x_i\},\{\dot{x}_i\}\right)$$

where $i,j = 1, \ldots N$, and $\{x_i\}$ is a set of N dynamical variables for a spinning satellite system.

Numerical solutions of these coupled nonlinear differential equations by means of Hamming's modified predictor-corrector method (Reference 1) provide the time-dependent development of the mode dynamics of the rotating satellite under specified boundary conditions. This technique is useful for detecting any mode frequency, instability side drift, excessive precession, and damping characteristics of satellite-boom systems (References 2,3,4).

7.2 Effect of Earth's Rotation

The electric field induced in the dipole sensors of a satellite is of sine wave form because of the spin of the satellite. In the regions of low latitude (equatorial) and low altitude, it is well known that the electric field is small with lack of significant plasma motion, so that the predominant electric field is due to the Earth's rotation. Two important remarks should be mentioned:

1. The electric field $\underline{E}$ measured in a moving frame is related to the electric field $\underline{E_0}$ in a rest frame by (Reference 5).

$$\underline{E} = \underline{E_0} + \underline{V} \times \underline{B}$$

where $\underline{B}$ is the magnetic field in the rest frame, and $\underline{V}$ is the velocity which is small ($V << C$) otherwise there is an additional relativistic factor in the denominator.

2. The velocity $\underline{V_r}$ in a rotating frame r is related to the velocity $\underline{V}$ in a fixed frame by (Reference 6).

$$\underline{V_r} = \underline{V} - \underline{\omega} \times \underline{r}$$

where $\underline{\omega}$ is the rotation angular velocity and $\underline{r}$ is the position vector. Thus, the induced electric field due to the Earth's rotation is

$$\underline{E} = \underline{V_r} \times \underline{B}$$

This induced field $\underline{E}$ is always subtracted out in order to bring out the genuine electric field from the processed result.

7.3 Program System for Data Reduction and Analysis

For data reduction and computation, three types of input data are required. They are 1) electric field experiment data, 2) satellite sensor attitude (OM) data, and 3) ephemeris/magnetic field (ORMAG) data. The structures of these data are tabulated in the references (References 7,8,9).
The electric field experiment data are in the fifth file of every tape of the satellite's raw data. The experiment data contain six channels of sensor signals with various high and low gains. These signals are given in telemetry counts, which can be converted to voltages by a simple conversion factor.

One unusual feature in the S3-2 electric field data is the appearance of ion (especially oxygen ion) induced DC-offsets detected by the axial booms.

Such a feature has never been detected previously, because of the relatively low sensitivity of the instruments on previous satellites. The DC-offsets vary with time and are due to variation of the contact potentials on the sensors in the ionized environment (Figure 1). No constant direct correlation exists between the offsets and spin plane dipole measurements (Figure 2).

For lower latitudes ($< 60^{o}$), where the earth's magnetic field lines are closed, the ambient electric field is vanishingly small. Therefore, any voltage that remains after subtraction of the induction field ($\underline{V} \times \underline{B}$) can be attributed to the spheres' contact potential. By deleting regions above and below 60^{o}, and by fitting a slowly varying function to this voltage, one can determine, approximately, the contact potential for an entire orbit.

The entire analysis is presently executed by means of a highly integrated system of programs as depicted in the flow chart of Figure 3. The functional form is generated for the contact potential. This function is then used in the MAIN processing system.

7.4 Program Description

Initial processing converts the measured voltage difference between spheres by the appropriate amplifier gain, removes amplifier biases, subtracts the induction field, and eliminates calibration sequences.

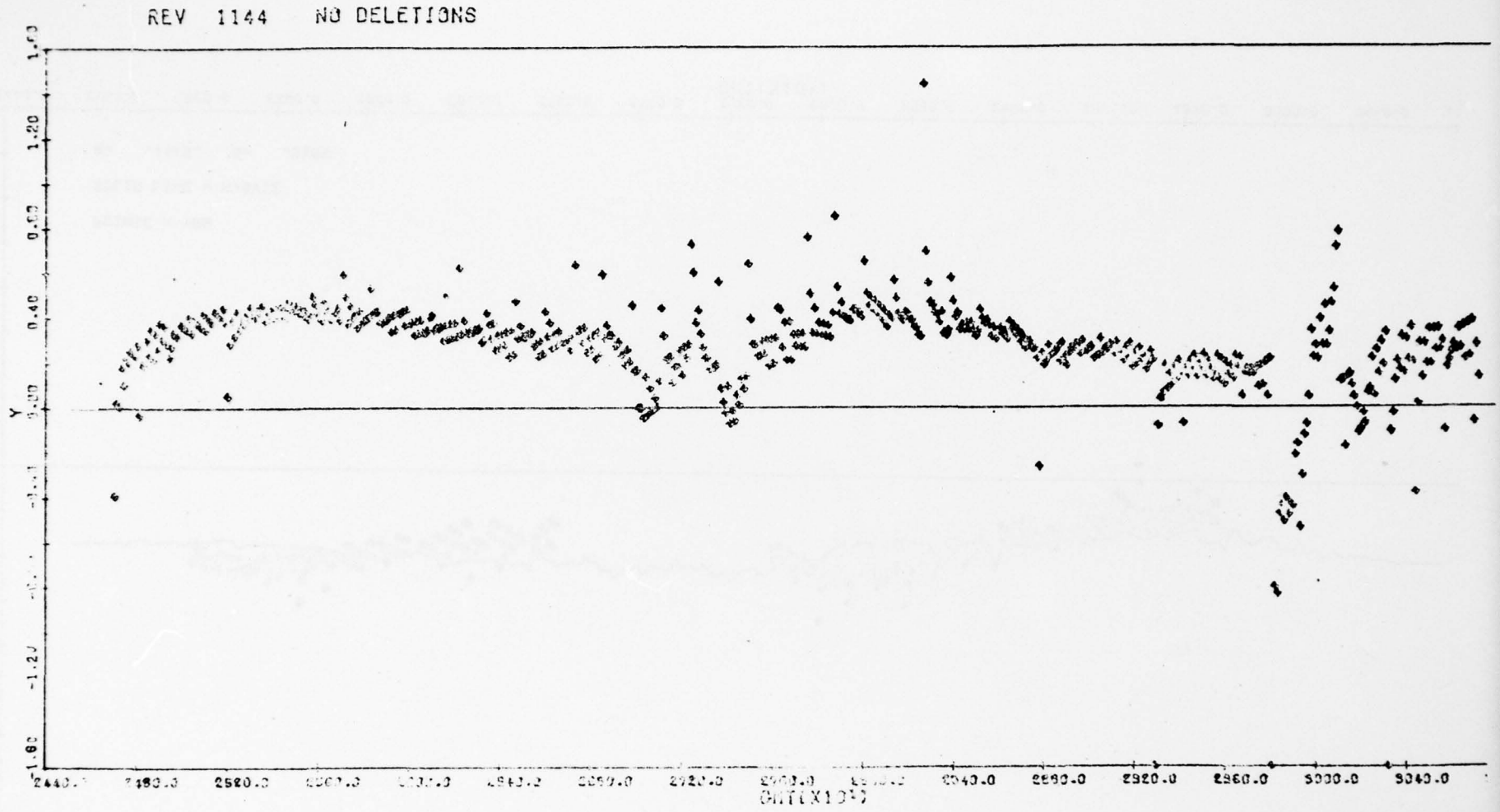

Figure 1. Channel 6 Data of $\underline{E}-(\underline{V}\times\underline{B})$. The noisy regions are due to Auroral Electric Fields.

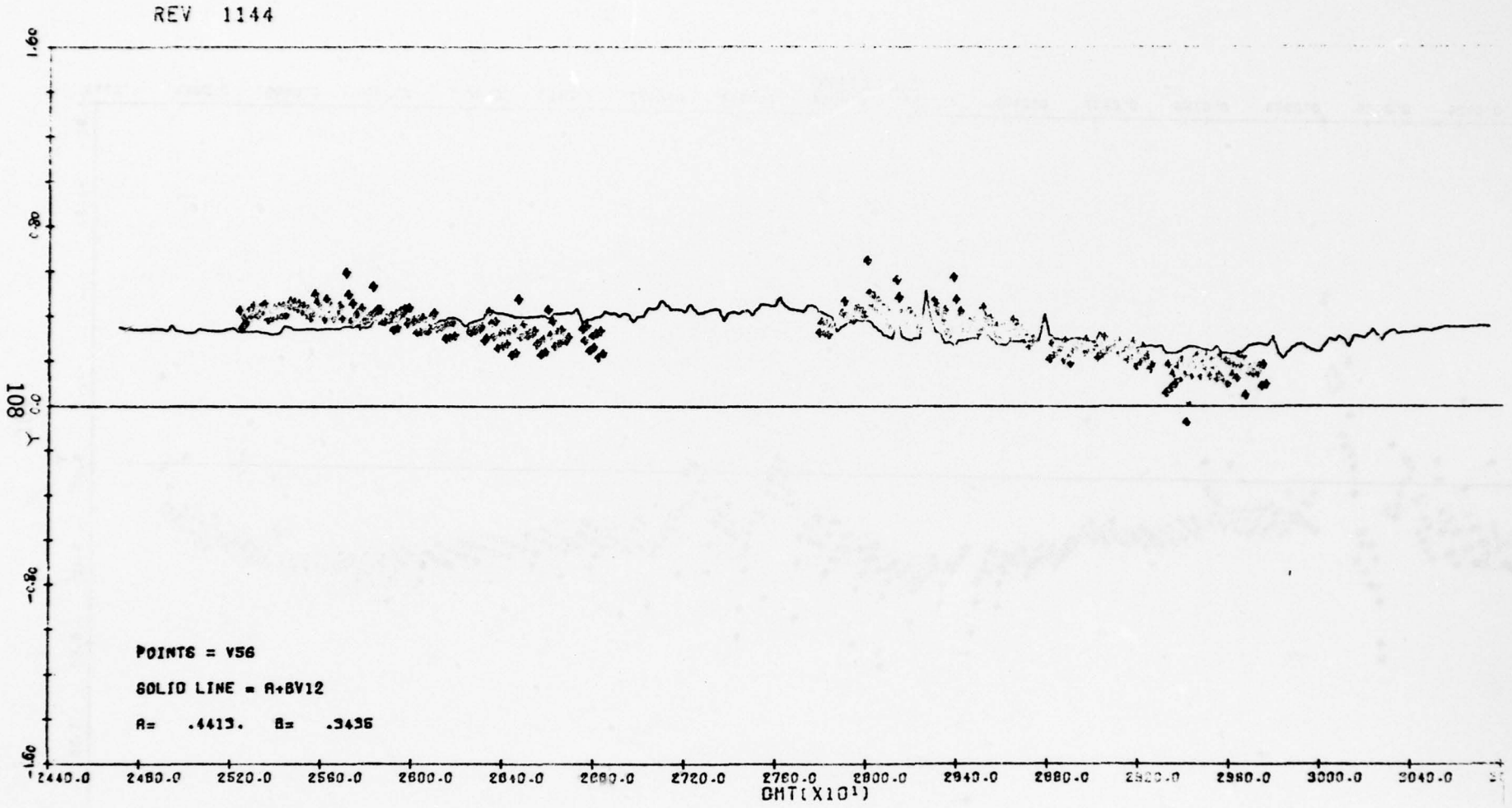

Figure 2. Correlation Between Data of Booms 5, 6 and Boom 1, 2.

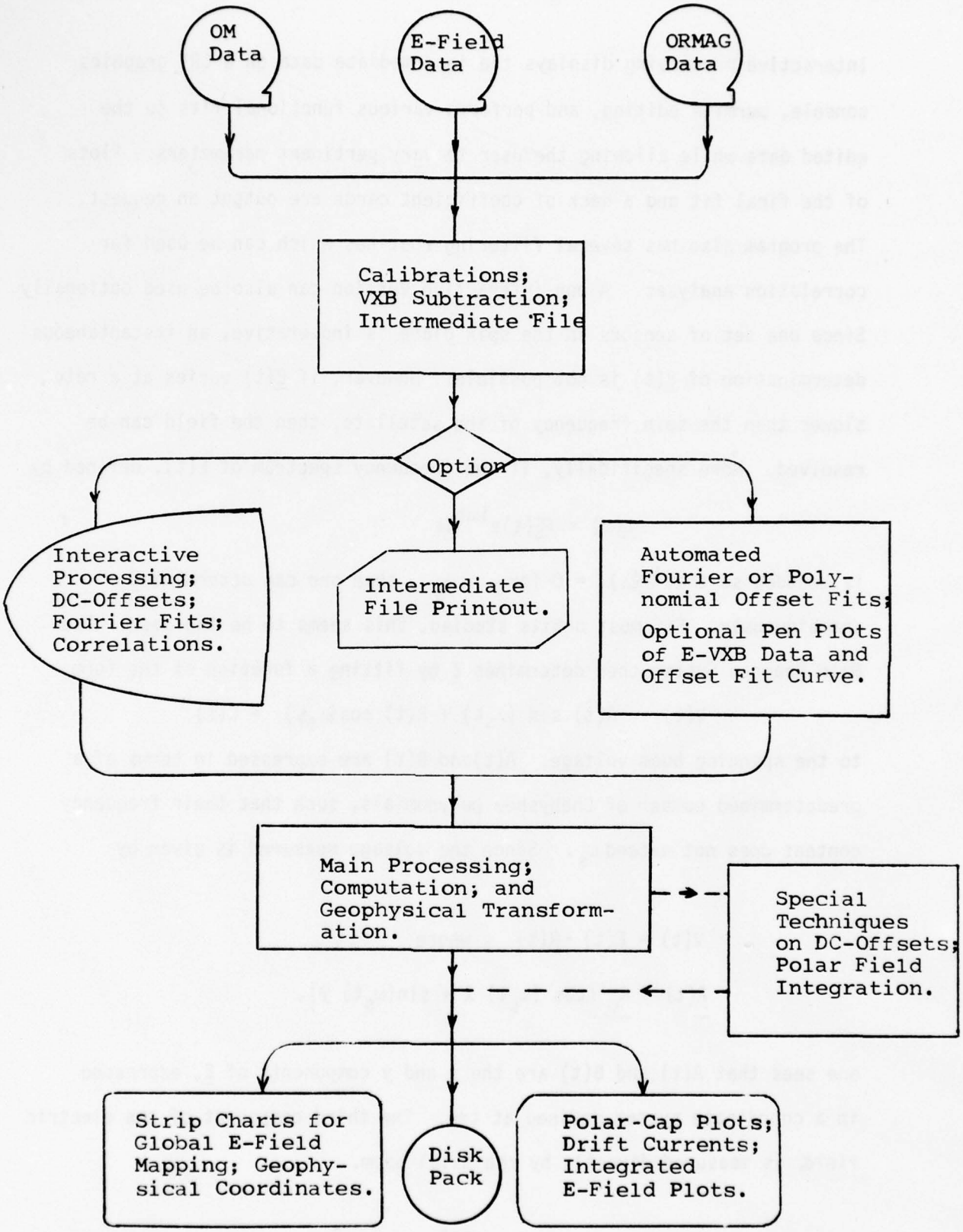

Figure 3. Flow Chart of Program System for Electric Field Analysis

Interactive processing displays the intermediate data on a CRT graphics console, permits editing, and performs various functional fits to the edited data while allowing the user to vary pertinent parameters. Plots of the final fit and a deck of coefficient cards are output on request. The program also has several filtering routines which can be used for correlation analyses. A non-interactive version can also be used optionally. Since one set of sensors in the spin plane is inoperative, an instantaneous determination of $\underline{E}(t)$ is not possible. However, if $\underline{E}(t)$ varies at a rate slower than the spin frequency of the satellite, then the field can be resolved. More specifically, if the frequency spectrum of E(t), defined by

$$\underline{\Sigma}(\omega) = \int \underline{E}(t) e^{i\omega t} dt$$

is bounded so that $|\underline{\Sigma}(\omega)| = 0$ for $\omega > \omega_s$, then one can determine $\underline{E}$ unambiguously. For most orbits studied, this seems to be the case. The Main Program System then determines $\underline{E}$ by fitting a function of the form

$$V(t) = A(t) \sin(\omega_s t) + B(t) \cos(\omega_s t) + C(t)$$

to the spinning boom voltage. A(t)and B(t) are expressed in terms of a predetermined number of Chebyshev polynomials, such that their frequency content does not exceed ω_s. Since the voltage measured is given by

$$V(t) = \underline{E}(t) \cdot \underline{R}(t) \quad , \text{where}$$

$$\underline{R}(t) = \underline{R_o} (\cos(\omega_s t)\, \hat{x} + \sin(\omega_s t)\, \hat{y}),$$

one sees that A(t) and B(t) are the x and y components of $\underline{E}$, expressed in a coordinate system defined at t=o. The third component of the electric field, is measured directly by the axial boom.

After subtraction of the induction field ($\underline{V} \times \underline{B}$) and determination of the empirical offset, resultant vectors are transformed to various physical coordinate systems, written on a disc file, and plotted as strip charts and polar plots. In the strip charts, the ionospheric electric field magnitude and components are plotted for a whole orbit in Earth centered inertial geomagnetic, satellite local vertical, or optionally solar magnetic coordinates. A typical plot is shown in Figure 4. In the polar plots, the electric field geomagnetic components in the polar caps are mapped on a background of invariant latitude and magnetic local time (Figure 5, 6). For dawn-dusk orbits, the integration $\int \underline{E} \cdot \underline{V} dt$ of the polar cap electric fields is also plotted (Figure 7).

7.5 Results and Discovery

Using the techniques outlined in this section, many orbits of satellite data have been processed and the electric fields mapped. In particular, the largest electric field structure ever detected at low altitudes in the ionosphere has been discovered (References 10, 11). The event took place during the May 1976 magnetic storm and the field structure was in the evening sector near the ionospheric projection of the plasmapause (Figure 8, 9). The largest pulse was 280 mV/m, directed toward magnetic north at an altitude of 1460 km with a hundred kilometer latitudinal extent. A very high drift velocity (about 9.8 km/sec) of the plasma flow (see Sec. 7) was associated with the pulse, and the flow directed westward along L shells.

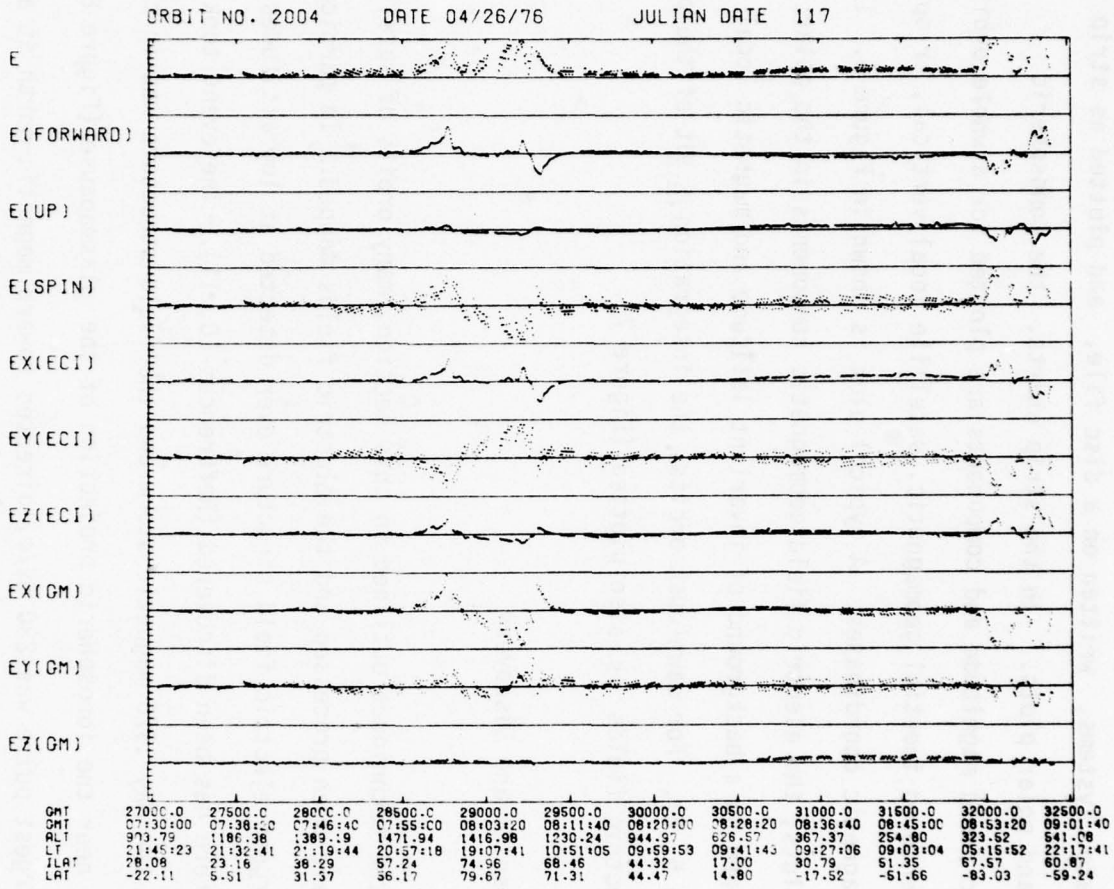

Figure 4. Strip Chart of Computed Ambient Electric Field Durig an Orbit

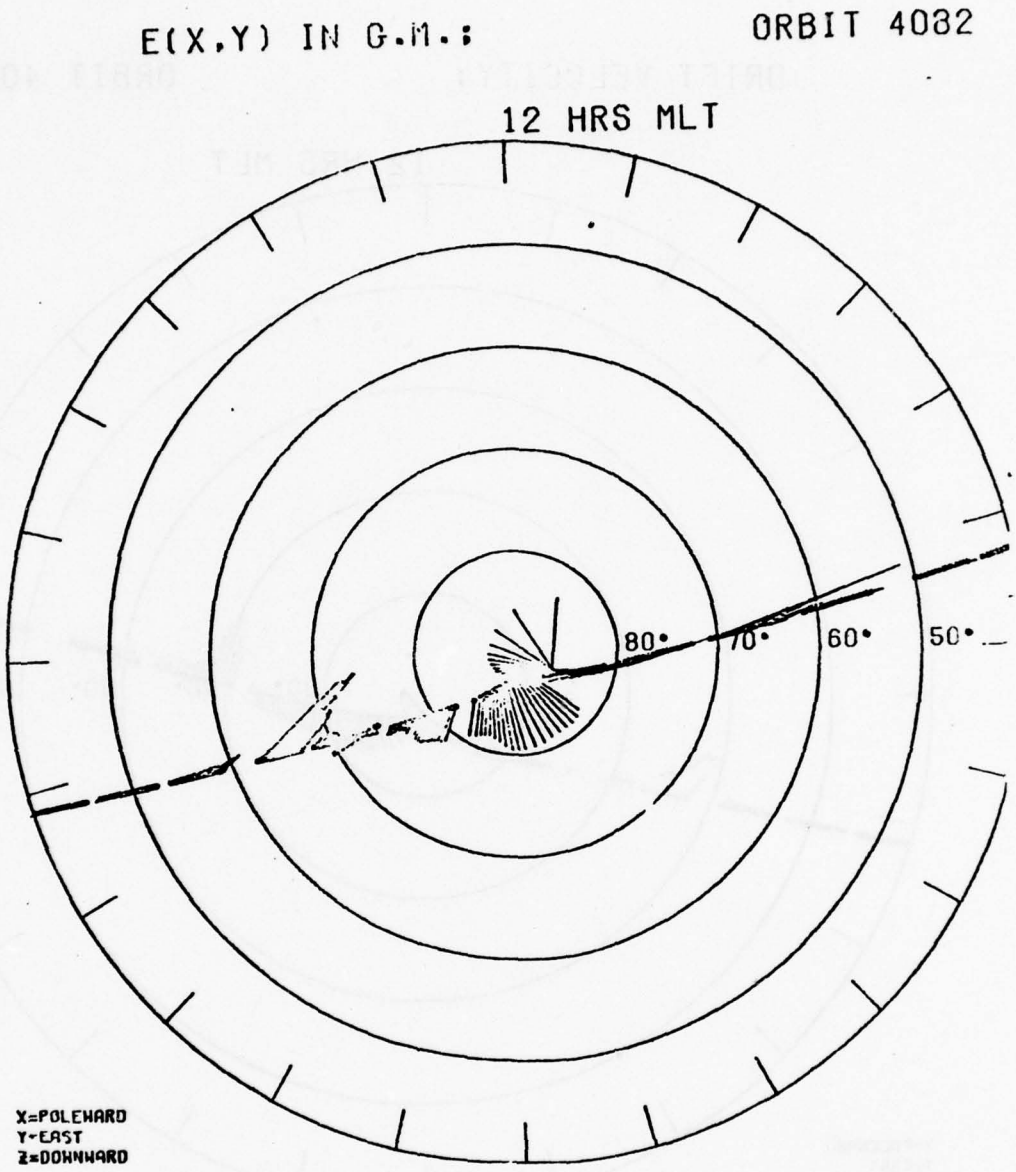

Figure 5. Geomagnetic Components of Electric Field Mapped on a Background of Invariant Latitude and Magnetic Local Time

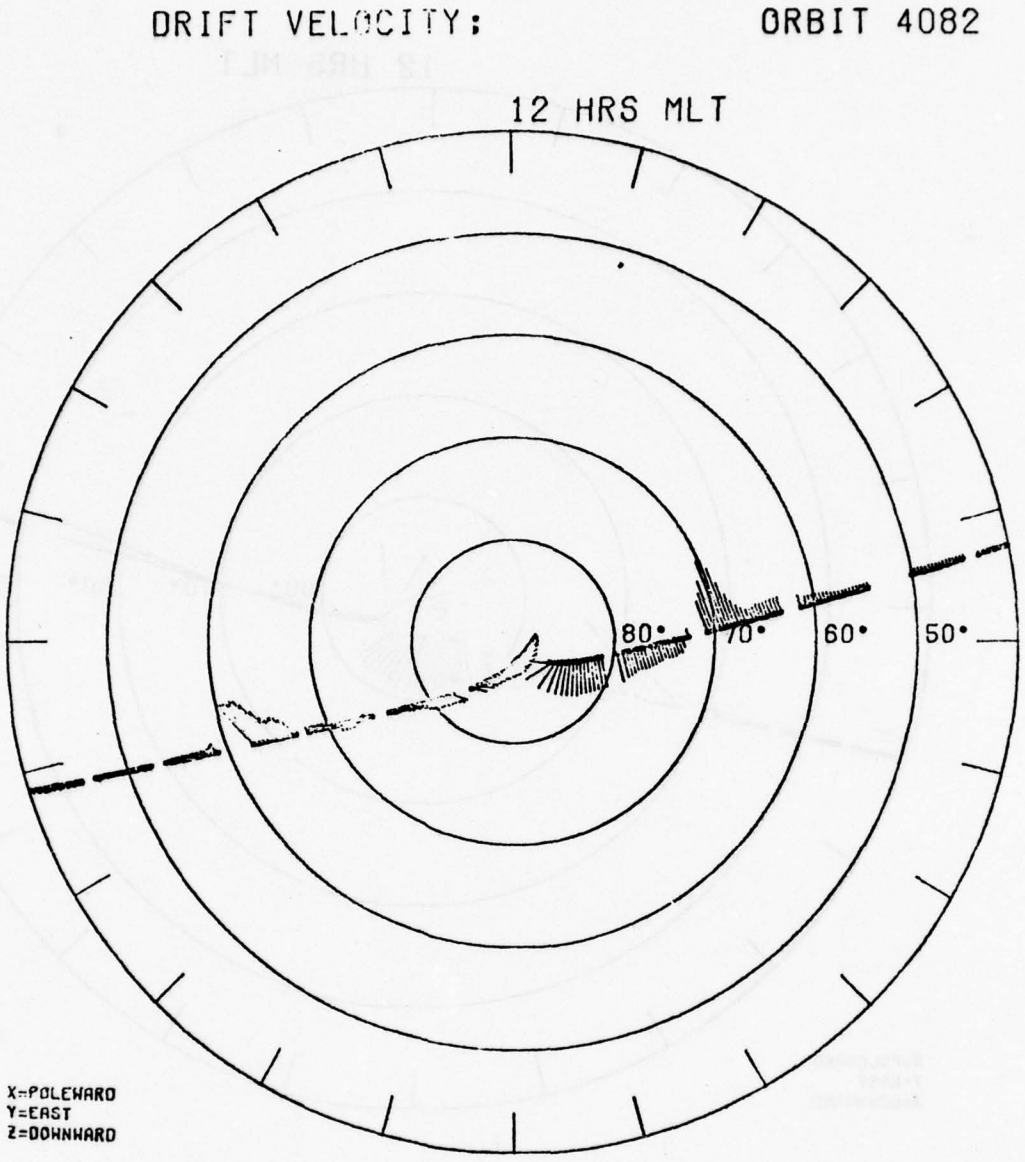

Figure 6. Polar Drift Velocity Mapped on a Background of Invariant Latitude and Magnetic Local Time.

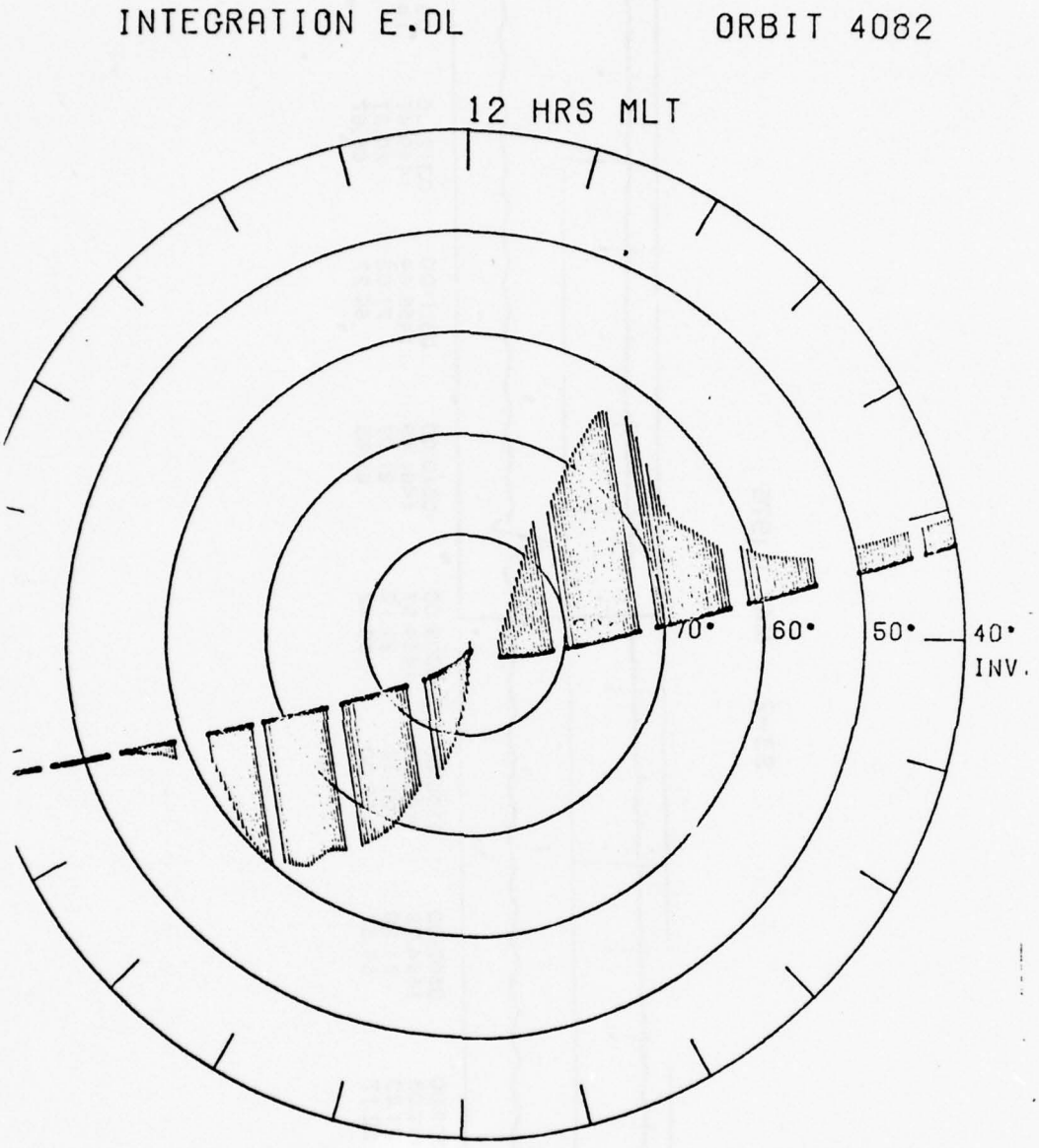

Figure 7. Plot of Polar Cap Integrated Electric Field for a Dawn-Dusk Orbit.

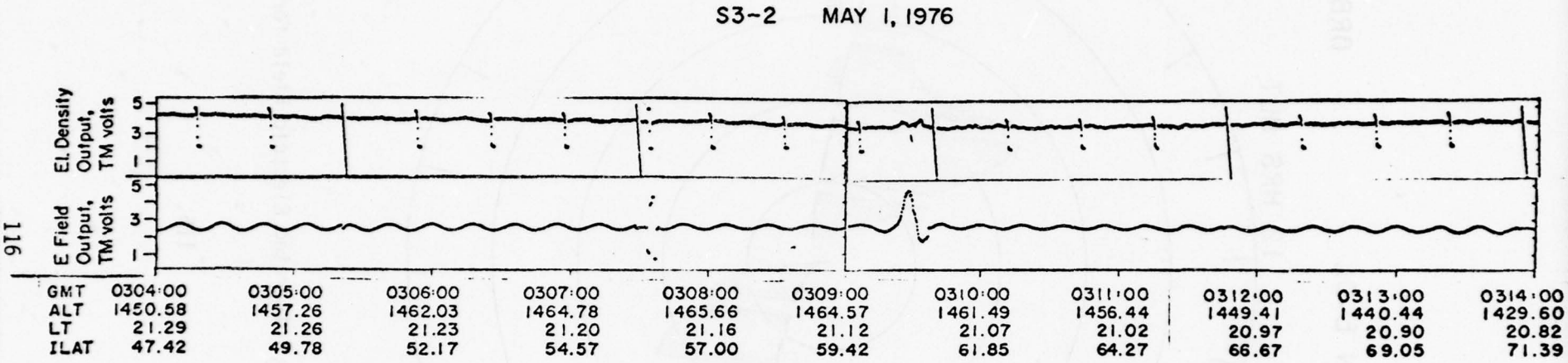

Figure 8. Electric Field Pulse during the May 1976 Magnetic Storm. The smoothly varying sine wave is primarily due to the $\underline{V} \times \underline{B}$ field.

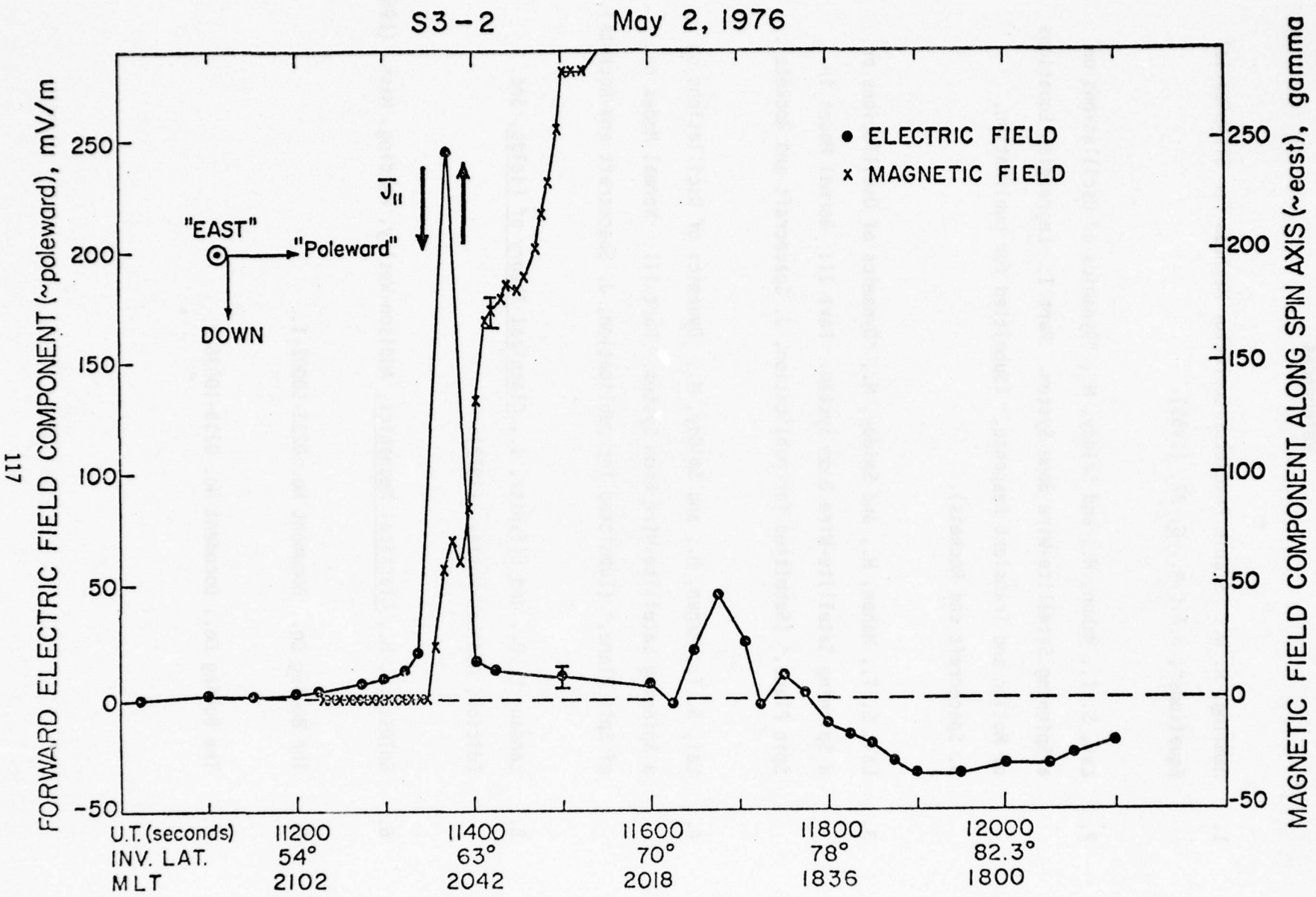

Figure 9. Electric and Magnetic Fields Measured by Satellite S3-2 during the May 1976 Magnetic Storm.

References

1. Hamming, R. W., "Stable Predictor-Corrector Methods for Differential Equations", J.A.C.M., 6, 37, (1959).

2. Lai, S. T., Mahon, H., and Smiddy, M., "Dynamics of Oscillations on a Spinning Satellite-Wire Boom System. Part I: Lagrangian Equations of Motion and Transient Response," (Submitted for publication, J. Spacecraft and Rockets).

3. Lai, S. T., Mahon, H., and Smiddy, M., "Dynamics of Oscillations on a Spinning Satellite-Wire Boom System. Part II: Normal Modes in Spin Plane," (Submitted for publication, J. Spacecraft and Rockets).

4. Lai, S. T., Mahon, H., and Smiddy, M., "Dynamics of Oscillations on a Spinning Satellite-Wire Boom System. Part III: Normal Modes out of Spin Plane," (Submitted for publication, J. Spacecraft and Rockets).

5. Landau, L. D., and Lifshitz, I., Classical Theory of Fields, 3rd Edition, Addison-Wesley, (1973).

6. Goldstein, H., Classical Mechanics, Addison-Wesley, Reading, Mass. (1950).

7. The Boeing Co., Document No. D233-10002-1.

8. The Boeing Co., Document No. D233-10036-2.

9. McInerney, R. E., and Abelowitz, A., "Magnetic Field Package", Air Force Report No. AFCRL-TR-73-0356, (1973).

10. Smiddy, M., Kelley, M., Sagalyn, R. C., Wildman, P., Burke, W., Rich, F. J., Hayes, R., and Lai, S. T., "Sub-Auroral Electric Field Observations during a Magnetic Storm," Trans. Amer. Geophys. U., Vol. S-8, No. 6, p. 482, (1977).

11. Smiddy, M., Kelley, M., Burke, W., Rich, F., Sagalyn, R., Shuman, B. Hayes, R., and Lai, S., "Intense Poleward-Directed Electric Fields near the Ionospheric Projection of the Plasmapause," accepted for publication, J. Geophys. Res. Lett. (1977).

Section 8. Multi-Spectral Measurements Program

Authors: J. N. Bass

K. H. Bhavnani

D. C. Schwank

8.0 Multi-Spectral Measurements Program

Initiator: E. Robinson

Project No: 2123 Problem No: 4937

This program consists of a series of rocket flights in which the payload separates into 2 stages - a sensor module which will contain sensing instrumentation and a target module which the sensing instruments will be viewing. There will be six radars tracking the vehicle - 3 for each module. An attitude control system will orient the sensor to point at the target. Each flight will last approximately 600 seconds.

8.1 System Studies

The data reduction system designed according to SUA specifications is shown schematically in Figure 1. After decommutation the input is in the form of digital tapes, 2 from the sensor module (TL1, TL2) and 1 from the target module.

The data must be unpacked and separated to form a number of individual raw data bases for further processing. Individual raw data bases are then further reduced through demodulation and filtering, background and/or dark count determination and subtraction, and application of pre-flight calibration data. Attitude, trajectory, and target data are merged with sensor data in a single file for correlative analysis (i.e., raw or reduced sensor data vs. altitude). Geophysical environmental data,

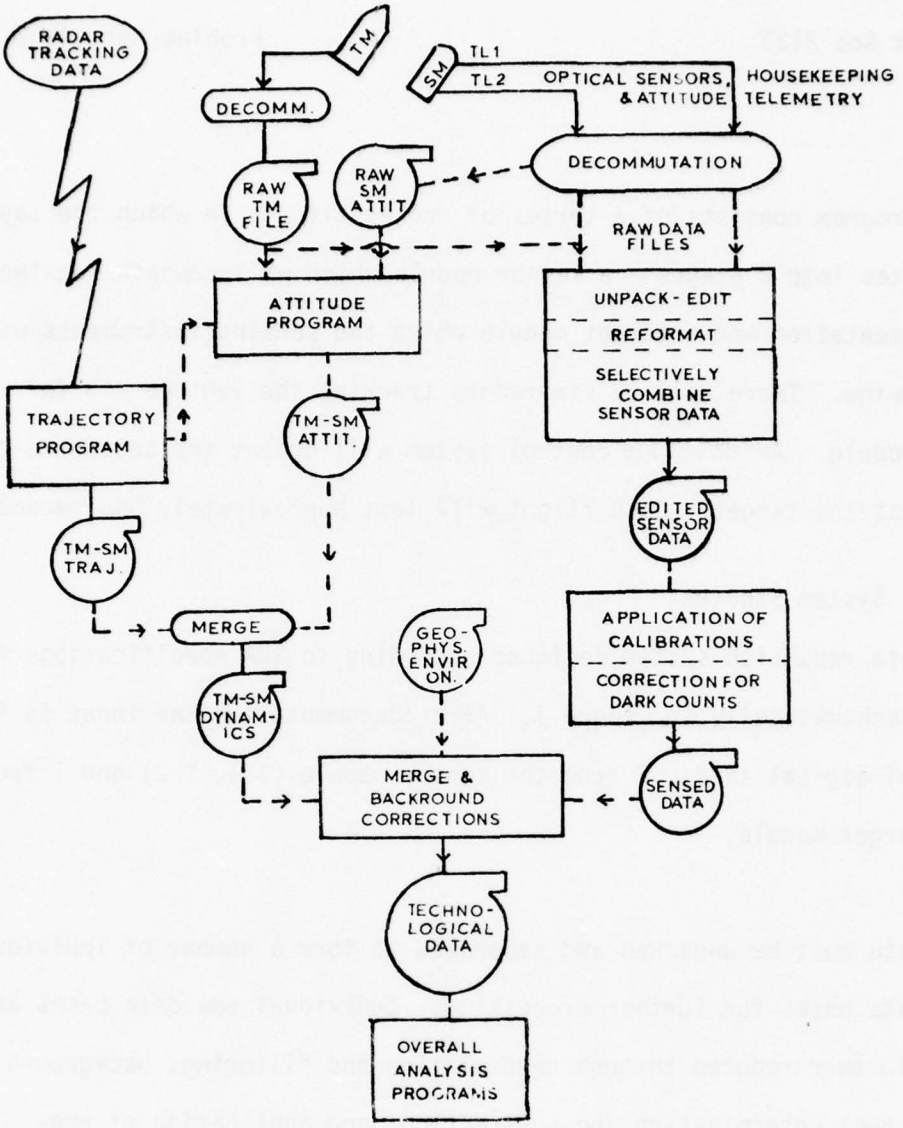

Figure 1. Comprehensive Data Processing System For Creating and Analyzing Data Bases from an Experimental Flight

such as solar, lunar and stellar positions may also be used in the data analysis, although not necessarily merged into the final data base. Section 8.3 describes the preliminary file design.

In the initial phases of the data reduction a quick-look study is carried out covering the raw data before calibrations and using preliminary attitude and trajectory information. Sample plots and printouts are generated for review by the experimenters. This phase is expected to last 20 days.

8.1.1 Ultraviolet Sensors

The UV instrumentation will consist of 3 photometers to provide spatial resolution and a spectrometer for spectral resolution.

8.1.1.1 Photometers

There will be two medium-sensitivity photometers (MSP) and one high-sensitivity photometer (HSP). Each will contain a square array (10x10) of 100 picture elements (pixels) each with a field-of-view of $.2^{o}x.2^{o}$ and a filter wheel of 4 filters. Readings will be .1 sec sample-and-hold.

8.1.1.2 Spectrometer

The spectrometer consists of a linear array of 36 spectral elements (specels) each responding to a different wavelength band depending on the position of the source in the $1.5^{o}x1.5^{o}$ field of view. As with the photometers the data is .1 sec sample-and-hold.

8.1.2 IR Sensors

The first MSMP flight payload will contain 4 infrared instruments: a full-field radiometer to measure radiation in 2 wavelength regions (SWIR and MWIR), 2 CVF spectrometers to measure distribution from 2 to 5 μm and from 7-22 μm, and a spatial radiometer to provide a spatial map of both SWIR and MWIR.

8.1.2.1 Full-Field Radiometer

The input from the full-field radiometer consists of 4 prime data channels (a high gain and a low gain signal for each of the two wavelength regions) plus a 50 Hz reference sine wave signal, each sampled at 1,000 Hz. The data signals consist of amplitude-modulated signals at a carrier frequency of 50 Hz. These are to be input into the demodulation/filtering software developed by the Optical Physics Division of AFGL and shown schematically in Figure 2[1]. This software package has been incorporated into the full data reduction system. Briefly, the output of the multipliers contains a d.c. component, which contains the primary useful information, plus components at multiples of the carrier frequency (50 Hz). The higher frequencies are subsequently filtered out with the low-pass filters.

8.1.2.2 CVF Spectrometers

The input of each spectrometer consists of high-gain and low-gain data channels plus an amplitude-modulated square wave spectral position reference signal (Fig. 3[1]). The fall-off from a 10 volt peak in both data and reference channel marks the beginning of each new spectral scan. Pre-flight calibrations will provide information on the wavelength

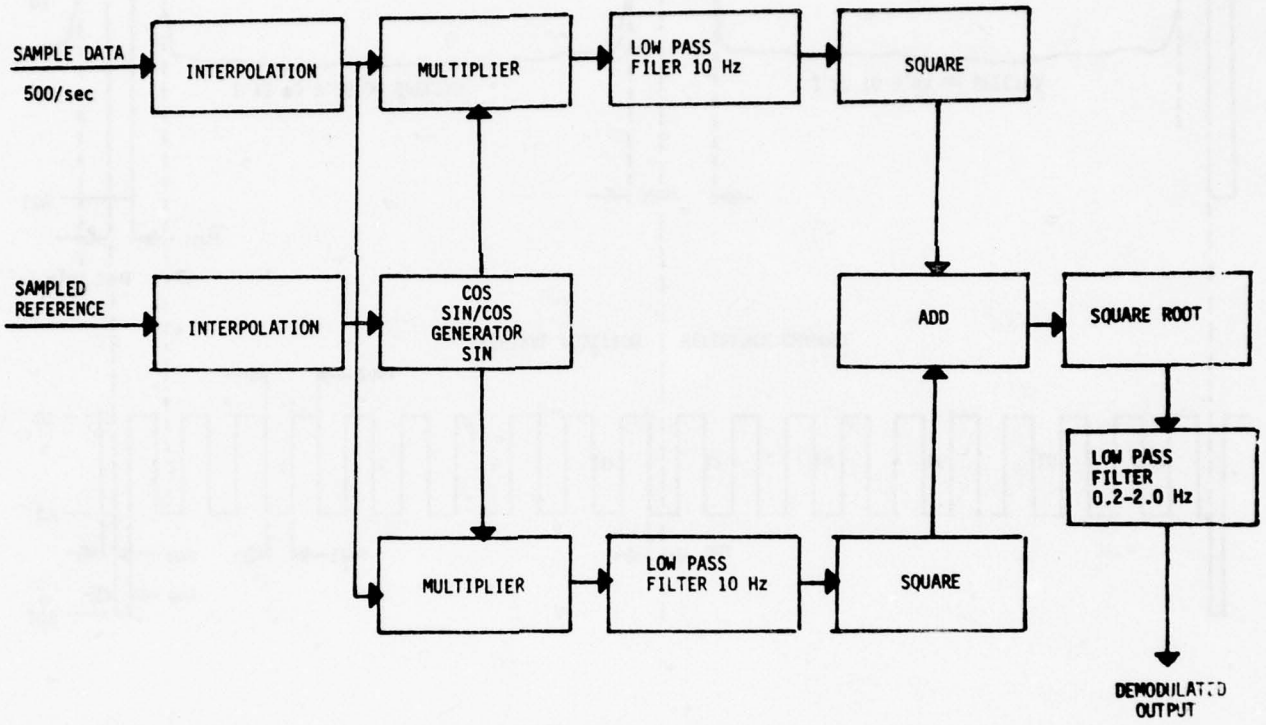

Figure 2. Demodulation of Radiometer Signal

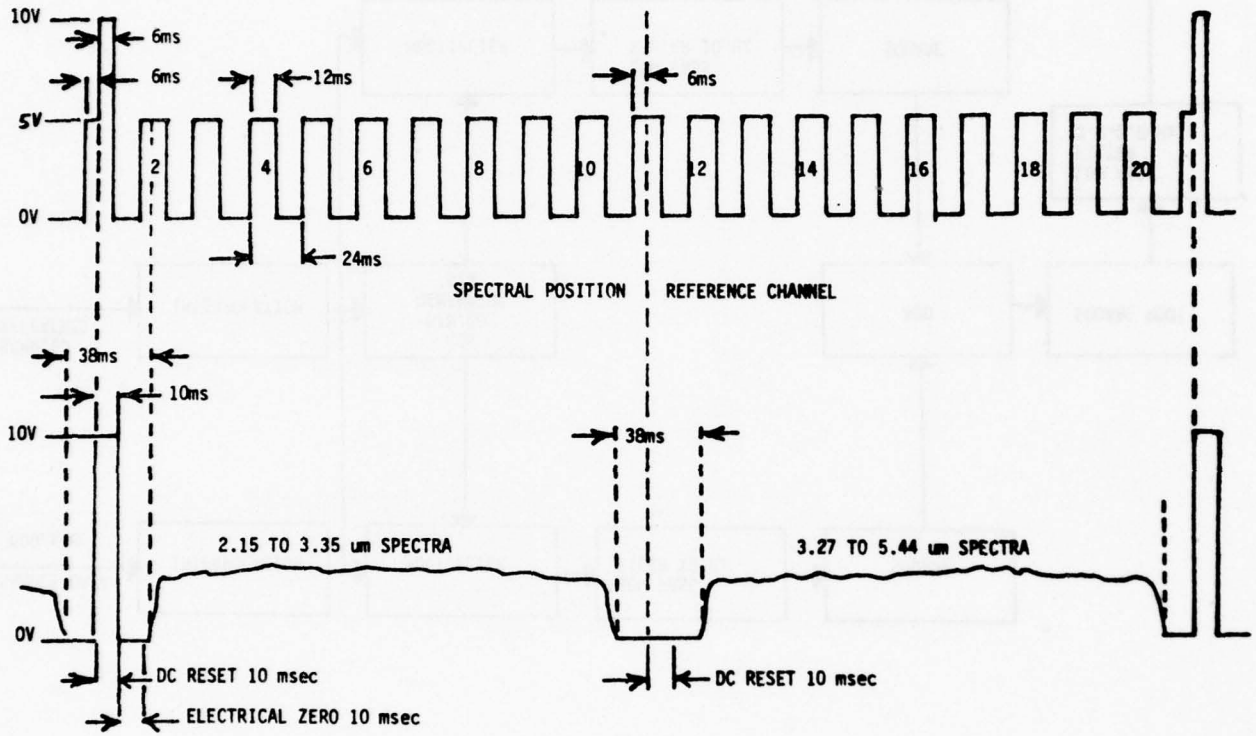

Figure 3. CVF Spectrometer Data Channels

for each positive and negative transition in a scan. All signals are sampled at 2,000 Hz.

8.1.2.3 Spatial Radiometer

The spatial radiometer measures the spatial distribution in the SWIR and MWIR regions. This is done with 4 vertical arrays of 10 detectors each, 2 arrays per wavelength region, designated as small ($.2^{o}$x$.2^{o}$ field-of-view) and large ($.4^{o}$x$.4^{o}$). The detectors sweep horizontally over a 6^{o} range, 1 sweep/sec, 250 data points/sweep for each detector. This is the only instrument whose data is to be transmitted via TL2. All other sensor data is via TL1.

8.1.3 Attitude/Trajectory Data

The following parameters are required to define the attitude and trajectory for full analysis of the data. The appropriate attitude/trajectory raw data are to be processed separately to produce a data base with the required parameters to be merged with the sensor. The trajectory will be processed by the AFGL trajectory determination system, possibly including programs DRIVEA, DRIVEB, and DRIVEC.[2]

The appropriate raw attitude parameters are to be taken from the sensor and target telemetry tapes and processed by SUA's attitude determination group to produce a tape containing the required attitude parameters. The trajectories are also required for this phase.

The principal feature of the attitude requirements is the sensor coordinate system (Figs. 4 and 5). The z' axis corresponds to the line-of-sight for the instrument while the x' and y' axes define the

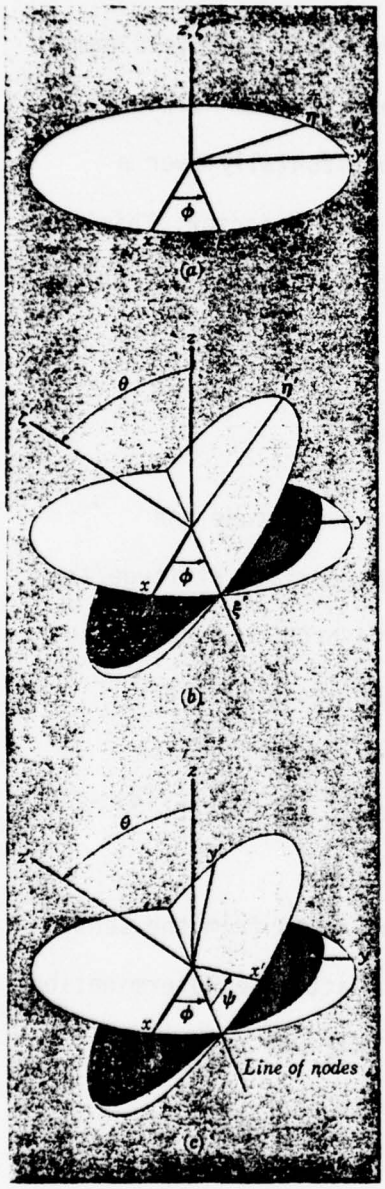

Figure 4. Transformation from ECI(xyz) coordinates to sensor (x'y'z') coordinates.

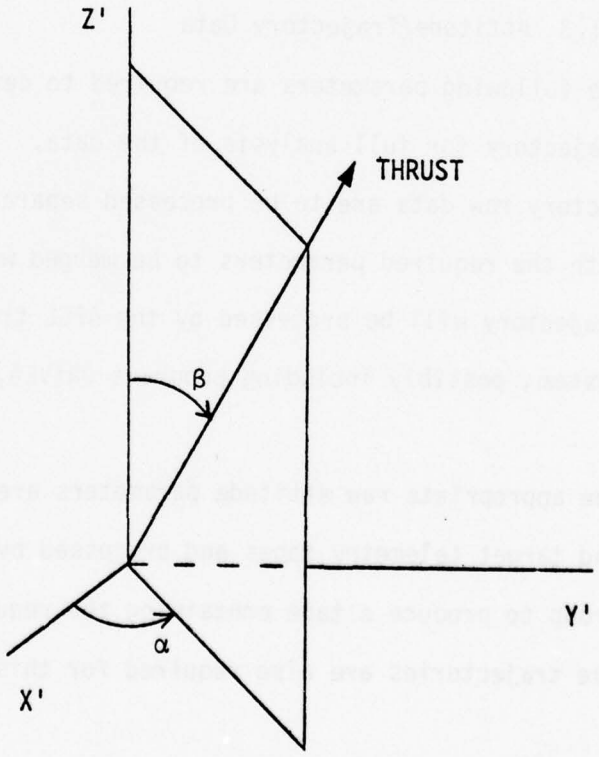

Figure 5. Thrust Vector in Sensor Coordinate System.

orientation of the sensor plane. It will be necessary to define a coordinate system for each instrument. This will require alignment data relative to the sensor module's body axis, including definition of the x' and y' axes. Knowledge of the sensor coordinate system permits one to know where the target and stars are in the sensor's field of view and thus facilitates interpretation of the data.

ATTITUDE DATA

(1) Angles relating sensor coordinate system x'y'z' (z' = line of sight) to ECI system xyz (Figure 4[3]) (0.2^{o} accuracy)

a) Right ascension of line of sight = $\phi - \frac{\pi}{2}$

b) Declination of line of sight = $\frac{\pi}{2} - \theta$

c) Rotation angle of x' axis from line of nodes = ψ

(2) Thrust vector direction (α,β) in sensor coordinate system (Figure 5) and roll angle of target (1^{o} accuracy)

(3) Target nozzle position (λ,μ) (Figure 6) in sensor plane (0.2^{o} accuracy)

(4) Earth limb view angles (0.2^{o} accuracy)

a) Angles relating sensor coordinate system to <u>local</u> vertical (z) - east (x) - north (y) coordinate system (Figure 4)

1) View azimuth from true north = $\pi-\phi$

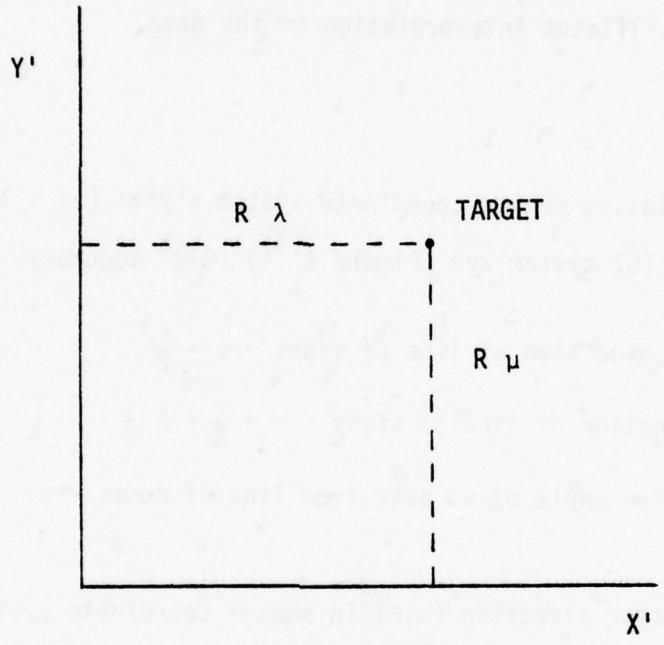

Figure 6. Target Position in Sensor Plane.

R=Target-Sensor Slant Range.

2) Elevation rel. to horizontal = $\frac{\pi}{2} - \theta$

3) Skew angle = ψ

b) Angle (δ) between los and hard earth tangent (Figure 7)

c) Tangent height (BT') (Figure 7)

d) Distance (OB) along los from sensor to point nearest earth surface (Figure 7)

(5) Angle between target thrust and target velocity.

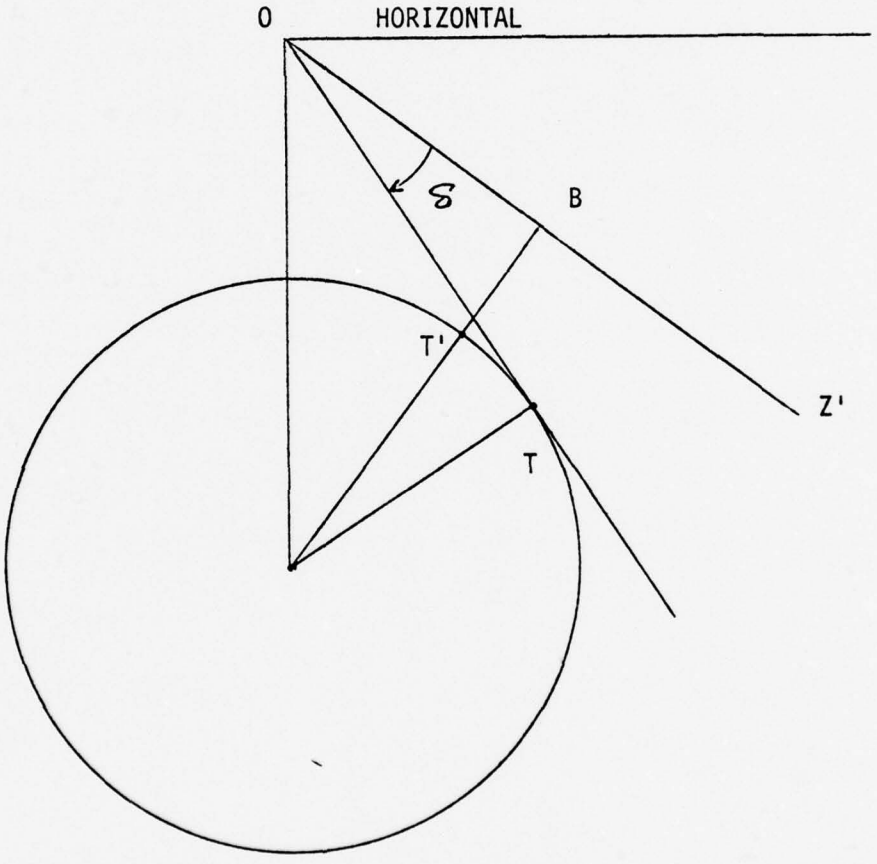

Figure 7. Earth's Limb View Angles

TRAJECTORY DATA

(1) Position and velocity of both vehicles in ECI coordinates

(2) Target-sensor slant angle

(3) Altitude of both vehicles

8.2 Calibration Data Processing

Data processing support is necessary for some pre-flight calibrations. These calibrations can be conveniently conducted using the existing telemetry system along with a few manually entered values indicating pertinent experiment parameters. Programs to summarize and present the results of calibration tests are required, and to some extent, are similar to the programs used in the flight data reduction.

8.2.1 UV Photometers

Pre-flight calibrations have been carried out at AFGL for the medium sensitivity photometers MSP-1 and MSP-3. Figures 8 and 9[1] show the data processing plan. In each experiment a beam of known wavelength is mounted on a rotating gimbal so that it scans the entire array of pixels. During a scan the gimbal stops when the beam points at the center of a pixel, defining the stationary gimbal data to be used to determine its peak sensitivity. Cross-talk (response of pixels not illuminated) can also be noted. Moving gimbal data permits measurement of each pixel's field of view.

8.2.1.1 Program PHCLFG

PHCLFG (Photometer Calibration, Fixed Gimbal) was written to provide calibration data for the UV photometers associated with MSMP.

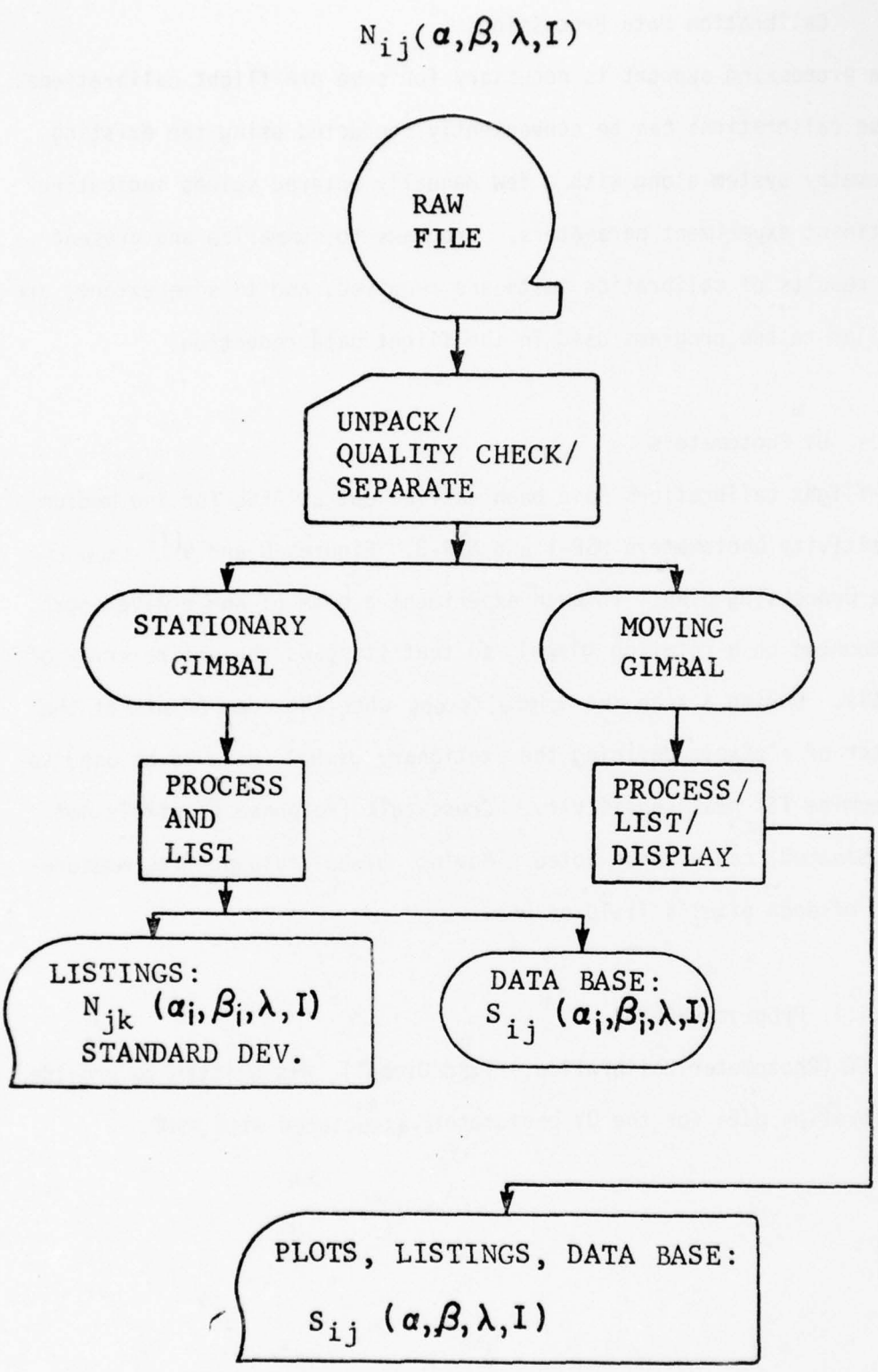

Figure 8. General flow of UV Photometer Calibrations

N_{ij} = Counts/sec by Pixel #i with Filter #j

α = Gimbal Azimuth

β = Gimbal Elevation

α_i, β_i = Gimbal position when beam focused on Pixel #i

I = Beam Intensity

$S_{ij} = N_{ij} / I$ = SENSITIVITY for Pixel #i with Filter #j

λ = Wavelength

Figure 9. UV Photometer Calibrations: Legend

Functional Description

Dark Count: Initially, many frames of dark count are taken. The average and standard deviation for each pixel is calculated and printed out.

Normal Data: At each fixed gimbal position, the average count (dark count subtracted) and standard deviation for each of the 100 pixels is calculated and printed out. A header provides relevant housekeeping data including filter positions, the type of light source, the actual pixel position being illuminated and the number of frames included in the averaging.

Summary: After all 100 pixels have been illuminated, a summary sheet is printed. This sheet contains the average count, minus dark count, for each pixel while it was illuminated.

8.2.2 Honeywell Spatial Radiometer

Pre-flight tests have been conducted at AFGL and Honeywell Radiation Center to determine the response of each detector as a function of source radiance, angle, and wavelength. The original data processing plan is shown in Figures 10 and 11[1]. As a result of changes in instrument design it has been possible to avoid extensive data processing in the spectral response (V vs λ) calibrations. The irradiance calibrations

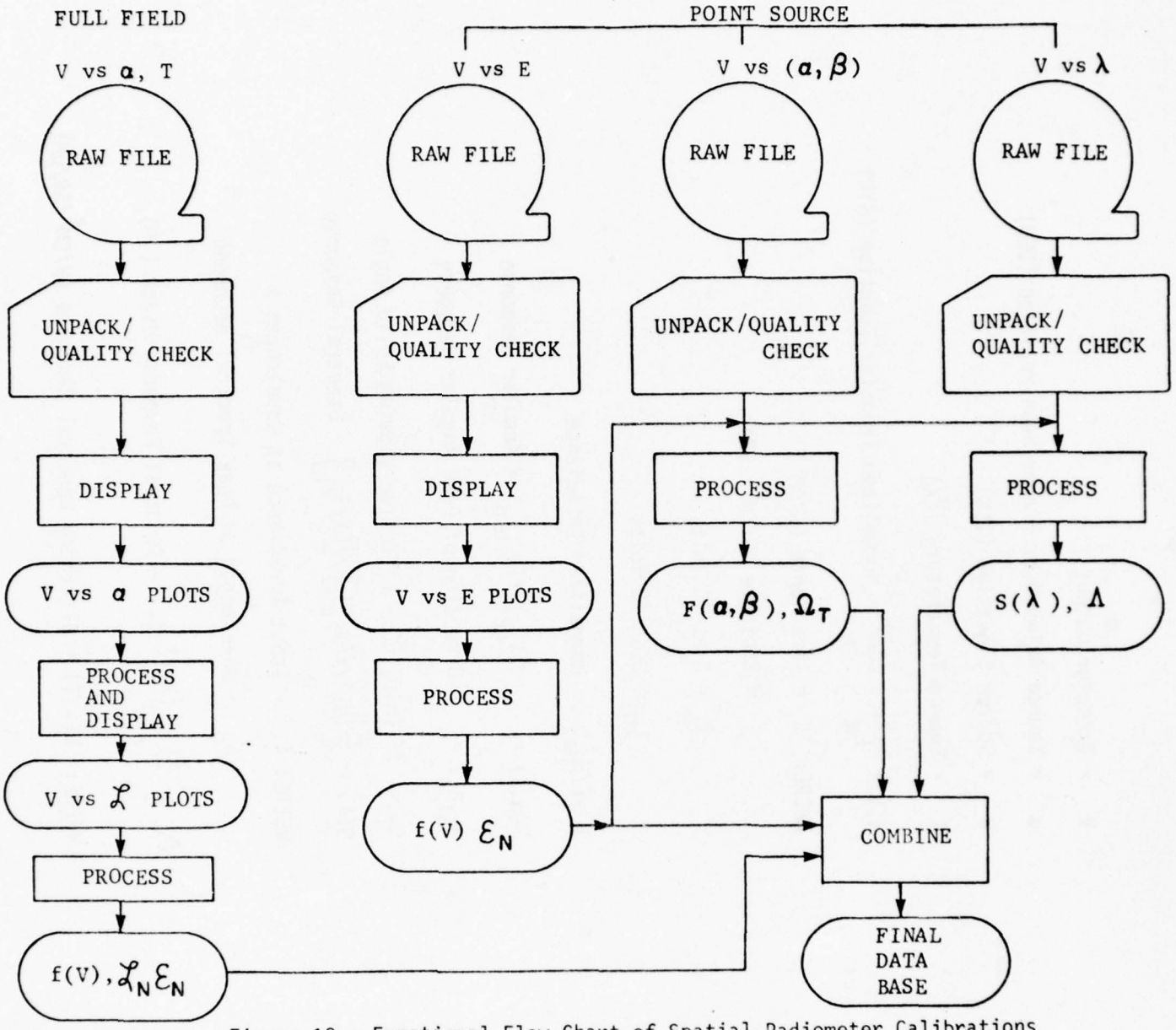

Figure 10. Functional Flow Chart of Spatial Radiometer Calibrations

V = Detector Output

α = Source Azimuth or Mirror Scan Position (DEG)

β = Source Elevation (DEG)

T = Source Temperature (^{o}K)

$f(V) = \frac{L(V)}{L_N} = \frac{E(V)}{E_N}$ = Normalized Transfer Function (NTF)

WHERE: E = Irradiance (W/CM^2)

L = Radiance (W/CM^2 /SR)

E_N = E at 10 Volts

L_N = L at 10 Volts

$E = E/E_{MAX}$ = Normalized Irradiance

$F(\alpha,\beta) = f(V_{\alpha\beta})/f(V_{\alpha_o\beta_o})$ = Angular Response

α_o, β_o = Direction of Peak Angular Response

$\Omega_T = \int F(\alpha,\beta)\, d\Omega$ = Effective Viewing Solid Angle

$S(\lambda) = \left[f(V_\lambda)/f(V_{\lambda_o})\right] / \left[E\lambda/E_{\lambda_o}\right]$ = Spectral Response

WHERE: E_λ = Input Irradiance at Wavelength λ

λ_o = Wavelength of Peak Spectral Response

$\Lambda = \frac{S(\lambda)L(\lambda,T)}{L(\lambda_o,T)}\, d\lambda$ = Spectral Response Width (μM)

WHERE: $L(\lambda,T)$ = Blackbody Spectral Radiance ($W/CM^2/SR/\mu M$)

Figure 11. Honeywell Spatial Radiometer Calibrations Legend

(V vs. E) have also been reduced in scope for the first flight. Hence, this section will concentrate on the full-field and point source (angular response) calibrations. Much of the software developed for these would be useful for the other calibrations.

8.2.2.1 Full-Field Calibrations - Program FLFIELD

Program FLFIELD reads an input data tape and determines the full-field response in volts for both backward and forward sweep directions (ramp up and ramp down) for all 40 detectors. Initially it was planned to use a 7-track digital tape prepared by AFGL's decommutation center from analog tapes recorded during the experiments; however, problems associated with saturation of the more sensitive detectors at higher radiances forced use of the Honeywell 9-track digital tapes, also recorded during the experiments. Tables of temperatures and radiances correlated to experiment numbers recorded on these tapes were supplied by experimentors to be input to FLFIELD.

Results are printed and plotted for convenient review by the experimenters. They are also written to disk for permament file and archive storage. A feature of the program allows direct access to these permanent files in a lieu of tapes if different plotting parameters (such as scale changes) are requested.

8.2.2.2 Angular Calibrations - FOVPEAK, FOVPLOT

These programs process input data from 7-track tapes produced by AFGL Decommutation Center from analog raw data tapes. Saturation problems

associated with the full-field calibrations did not occur here. Time jumps in the data are used to separate different experiments each of which is characterized by a value of the elevation β as supplied in a table to be input.

Program FOVPEAK scans the data and produces an output file containing the (α_o,β_o) and value (in volts) of the peak response for each detector. This is then used by program FOVPLOT, together with the full-field results, to map out $F(\alpha,\beta)$. Plots of $F(\alpha_o,\beta)$ and $F(\alpha,\beta_o)$ are produced. For the first flight these are to be analyzed by the experimenter to estimate the field of view solid angle Ω. It is expected that this quantity will be deduced more rigorously in future flights.

8.3 File Design for Flight Data Base

The final flight data base design was conceived to meet a number of objectives:

1) All information expected to be required for extended study of the performance of any instrument will be in one file. Thus, for each instrument, pertinent Link 1, Link 2, Link 4, trajectory, attitude, and reduced data will be available simultaneously so as to facilitiate further processing and analyses.

2) Files will be separate per instrument. However, the slower data rate for the UV instruments allows for combining all 4 instruments on one file. For convenience in processing, a file should readily fit on one magnetic tape.

3) Since the significant resolution of the bulk of the data is limited to 1 bit in 14, the final data base will use packing of CDC 60-bit words with scaling and offset for efficient utilization of storage.

4) Since many variables are required much less frequently than the basic 1000 Hz frame rate, these variables will be stored commutated.

5) File design for different instruments will be as similar as possible so that common generating and user routines can be used from instrument to instrument.

Tables 1 - 5 on the following pages show the file format that is proposed per instrument. Each word is 15 bits long, and the range dictates the scale and offset that will apply. The telemetered data are described in Reference 4. Trajectory and attitude data are generated by SUA and may be obtained from separate files or stored commutated. Raw signals will be accessible for checking purposes, but the final analyses will be based on the smoothed background signals (SM BKGD) and the calibrated and background removed signals (CABR). The file contents are subject to considerable change, but these specifications have been reviewed with the researchers and present the scope of the problem.

Table 6 quantifies the size of each data base. For each IR instrument a reduction in the output subframe rate is proposed either by averaging or taking one of two samples. Assuming 15 bit values or 4 per CDC word, the worst case of 9.45×10^6 values with the Honeywell Spatial Radiometer can be stored on one 9-track 1600 bpi tape.

MSMP ENVIRONMENTAL DATA BASE 9/7/77

OUTPUT FILES

UV PHOTOMETERS AND SPECTROMETER FILE

WORD 2 IS A COMMUTATOR (100 X 1) WHICH CONTAINS (BY SFID): TIME,1; TARGET HKPG, 2-11; SENSOR HKPG, 12-20; SP CABR, 21-56; SP BKGD, 57-92; MSP HKPG, 93-99; SP HKPG, 100.
WORD 3 IS A COMMUTATOR WHICH CONTAINS: (OPTIONAL) TRAJ & ATT, 1-46; SP RAW, 47-82; MSP-1 HKPG, 83-89; MSP-3 HKPG, 90-96; SP HKPG, 97-100.

WORD	SFID	SYMBOL	DESCRIPTION		RANGE
1			SFID (100 SUBFRAMES/FRAME)		1/100
2	1		TIME FROM LAUNCH (SEC)		0/600
			T < 65 SEC	T > 65 SEC	
2	2		TIMER EVENTS	TIMER EVENTS	
2	3			ENGINE OXIDIZER PRESS (VOLTS)	0/5
2	4			ENGINE CHAMBER PRESS (VOLTS)	0/5
2	5			ENGINE FUEL PRESS (VOLTS)	0/5
2	6		TIMER EVENTS		
2	7		ENGINE GN2 PRESS (VOLTS)		0/5
2	8		ENGINE REGUL PRESS (VOLTS)		0/5
2	9		ENGINE FUEL TEMP (VOLTS)		0/5
2	10		ENGINE OXIDIZER TEMP (VOLTS)		0/5
2	11		ENGINE GN2 TEMP (VOLTS)		0/5
2	12		ORD FUNCTION MON (VOLTS)		0/5
2	13		DLD FUNCTION MON (VOLTS)		0/5
2	14		B7A BATTERY (VOLTS)		0/5
2	15		B8A BATTERY (VOLTS)		0/5
2	16		K5 LOGIC RELAY (VOLTS)		0/5
2	17		K6 LOGIC RELAY (VOLTS)		0/5
2	18		K8 LOGIC RELAY (VOLTS)		0/5
2	19				
2	20				
2	21-56		SP CABR (PHOTONS/CM2/SEC/A)		
2	57-92		SP SM BKGD (PHOTONS/CM2/SEC/A)		
2	93		MSP FILTER #		

Table 1. UV Instruments Data Base

2	94	HSP TEMP A (VOLTS)	0/5
2	95	HSP TEMP B (VOLTS)	0/5
2	96	HSP TEMP C (VOLTS)	0/5
2	97	HSP H.V.COM'D (VOLTS)	0/5
2	98	HSP LAMP VOLT (VOLTS)	0/5
2	99	HSP CORONA VOLT (VOLTS)	0/5
2	100	SP TEMP A (VOLTS)	0/5
		TRAJECTORY & ATTITUDE (WORD 3, SFID 1-46)-OPTIONAL	
3	1	RT ASCEN OF GREENWICH (DEG)	0/360
3	2-4	GEOC POS COMPONENTS(SENSOR) (KM)	2500/6500
3	5-7	GEOC VEL COMPONENTS(SENSOR) (KM/SEC)	-2/2
3	8-10	GEOC ACCEL COMPONENTS(SENSOR) (KM/SEC2)	-.5/.5
3	11	GEOD ALT ABOVE SUB-EARTH PT(SENSOR) (KM)	0/300
3	12-14	GEOC POS COMPONENTS(TARGET) (KM)	2500/6500
3	15-17	GEOC VEL COMPONENTS(TARGET) (KM/SEC)	-2/2
3	18-20	GEOC ACCEL COMPONENTS(TARGET) (KM/SEC2)	-.5/.5
3	21	GEOD ALT ABOVE SUB-EARTH PT(TARGET) (KM)	0/300
3	22	TARGET RANGE (SCS) (KM)	0/15
3	23-25	TARGET POS (SCS) (KM)	-15/15
3	26-28	TARGET VEL (SCS) (KM/SEC)	-.5/.5
3	29-31	TARGET ACCEL (SCS) (KM/SEC2)	-.01/.01
3	32-34	EULERIAN ANGLES DEF ECI TO SCS (DEG)	0/360
3	35-37	EULERIAN ANGLES DEF VEN TO SCS (DEG)	0/360
3	38-39	THRUST DIRECTION IN SCS (DEG)	0/360
3	40	ROLL ANGLE OF TARGET (DEG)	0/360
3	41-42	TARGET NOZZLE POS IN SENSOR PLANE (DEG)	-10/10
3	43	ANGLE BETWEEN LOS & HARD EARTH TANGENT (DEG)	-90/90
3	44	TANGENT HT OF LOS FROM NEAREST EARTH SURF. (KM)	0/300
3	45	DISTANCE ALONG LOS TO PT NEAREST EARTH SURF. (KM)	0/2500
3	46	TARGET THRUST-VEL ANGLE (DEG)	0/180
3	47-82	SP RAW (COUNTS)	16 BITS
3	83	MSP-1 FILTER #	
3	84	MSP-1 TEMP A (VOLTS)	0/5
3	85	MSP-1 TEMP B (VOLTS)	0/5
3	86	MSP-1 TEMP C (VOLTS)	0/5
3	87	MSP-1 H.V.COM'D (VOLTS)	0/5
3	88	MSP-1 LAMP VOLT (VOLTS)	0/5
3	89	MSP-1 CORONA DET (VOLTS)	0/5

Table 1. UV Instruments Data Base (continued)

3	90	MSP-3 FILTER #	
3	91	MSP-3 TEMP A (VOLTS)	0/5
3	92	MSP-3 TEMP B (VOLTS)	0/5
3	93	MSP-3 TEMP C (VOLTS)	0/5
3	94	MSP-3 H.V.COM'D (VOLTS)	0/5
3	95	MSP-3 LAMP VOLT (VOLTS)	0/5
3	96	MSP-3 CORONA VOLT (VOLTS)	0/5
3	97	SP TEMP B (VOLTS)	0/5
3	98	SP H.V.COM'D (VOLTS)	0/5
3	99	SP LAMP VOLT (VOLTS)	0/5
3	100	SP CORONA DETECTOR (VOLTS)	0/5
4		MSP CABR (PHOTONS/CM2/SEC)	
5		MSP SM BKGD (PHOTONS/CM2/SEC)	
6		MSP RAW (COUNTS)	15 BITS
7		MSP-1 CABR (PHOTONS/CM2/SEC)	
8		MSP-1 SM BKGD (PHOTONS/CM2/SEC)	
9		MSP-1 RAW (COUNTS)	15 BITS
10		MSP-3 CABR (PHOTONS/CM2/SEC)	
11		MSP-3 SM BKGD (PHOTONS/CM2/SEC)	
12		MSP-3 RAW (COUNTS)	15 BITS

Table 1. UV Instruments Data Base (continued)

FULL-FIELD RADIOMETER (NR-5) FILE

WORD 2 IS A COMMUTATOR (50 X 1) WHICH CONTAINS (BY SFID): TIME,1; TARGET HKPG, 2-11; SENSOR HKPG, 12-20; FFR HKPG, 21-27; UNASS, 28-50.
WORD 3 IS A COMMUTATOR (50 X 1) WHICH CONTAINS: (OPTIONAL) TRAJ & ATT, 1-46; UNASS, 47-50.

WORD	SFID	SYMBOL	DESCRIPTION		RANGE
1			SFID (50 SUBFRAMES/FRAME)		1/50
2	1		TIME FROM LAUNCH (SEC)		0/600
			T < 65 SEC	T > 65 SEC	
2	2		TIMER EVENTS	TIMER EVENTS	
2	3			ENGINE OXIDIZER PRESS (VOLTS)	0/5
2	4			ENGINE CHAMBER PRESS (VOLTS)	0/5
2	5			ENGINE FUEL PRESS (VOLTS)	0/5
2	6		TIMER EVENTS		
2	7		ENGINE GN2 PRESS (VOLTS)		0/5
2	8		ENGINE REGUL PRESS (VOLTS)		0/5
2	9		ENGINE FUEL TEMP (VOLTS)		0/5
2	10		ENGINE OXIDIZER TEMP (VOLTS)		0/5
2	11		ENGINE GN2 TEMP (VOLTS)		0/5
2	12		ORD FUNCTION MON (VOLTS)		0/5
2	13		DLD FUNCTION MON (VOLTS)		0/5
2	14		B9A BATTERY (VOLTS)		0/5
2	15		B10A BATTERY (VOLTS)		0/5
2	16		C2 CAP MONITOR (VOLTS)		0/5
2	17				
2	18		K14 LOGIC RELAY (VOLTS)		0/5
2	19				
2	20				
2	21		PT-1 TEMP (VOLTS)		0/10
2	22		PT-2 TEMP (VOLTS)		0/10
2	23		DT-C TEMP (VOLTS)		0/10
2	24		DT-H TEMP (VOLTS)		0/10
2	25		TB TEMP (VOLTS)		0/10
2	26		BB TEMP (VOLTS)		0/10
2	27		FP TEMP (VOLTS)		0/10
2	28-50				
TRAJECTORY & ATTITUDE (WORD 3, SFID 1-46)-OPTIONAL					
3	1		RT ASCEN OF GREENWICH (DEG)		0/360
3	2-4		GEOC POS COMPONENTS(SENSOR) (KM)		2500/6500
3	5-7		GEOC VEL COMPONENTS(SENSOR) (KM/SEC)		-2/2
3	8-10		GEOC ACCEL COMPONENTS(SENSOR) (KM/SEC2)		-.5/.5
3	11		GEOD ALT ABOVE SUB-EARTH PT(SENSOR) (KM)		0/300
3	12-14		GEOC POS COMPONENTS(TARGET) (KM)		2500/6500
3	15-		GEOC VEL COMPONENTS(TARGET) (KM/SEC)		-2/2

Table 2. Full-Field Radiometer (NR-5) Data Base

3	17-20	GEOC ACCEL COMPONENTS(TARGET) (KM/SEC2)	-.5/.5
3	21	GEOD ALT ABOVE SUB-EARTH PT(TARGET) (KM)	0/300
3	22	TARGET RANGE (SCS) (KM)	0/15
3	23-25	TARGET POS (SCS) (KM)	-15/15
3	26-28	TARGET VEL (SCS) (KM/SEC)	-.5/.5
3	29-31	TARGET ACCEL (SCS) (KM/SEC2)	-.01/.01
3	32-34	EULERIAN ANGLES DEF ECI TO SCS (DEG)	0/360
3	35-37	EULERIAN ANGLES DEF VEN TO SCS (DEG)	0/360
3	38-39	THRUST DIRECTION IN SCS (DEG)	0/360
3	40	ROLL ANGLE OF TARGET (DEG)	0/360
3	41-42	TARGET NOZZLE POS IN SENSOR PLANE (DEG)	-10/10
3	43	ANGLE BETWEEN LOS & HARD EARTH TANGENT (DEG)	-90/90
3	44	TANGENT HT OF LOS FROM NEAREST EARTH SURF. (KM)	0/300
3	45	DISTANCE ALONG LOS TO PT NEAREST EARTH SURF. (KM)	0/2500
3	46	TARGET THRUST-VEL ANGLE (DEG)	0/180
3	47-50		
4		CABR (SIGNAL 1 LO) (W/CM2/SR)	E-12/E-4
5		CABR (SIGNAL 1 HI) (W/CM2/SR)	E-12/E-4
6		CABR (SIGNAL 2 HI) (W/CM2/SR)	E-12/E-4
7		CABR (SIGNAL 2 LO) (W/CM2/SR)	E-12/E-4
8		SM BKGD (SIGNAL 1 LO) (W/CM2/SR)	E-12/E-4
9		SM BKGD (SIGNAL 1 HI) (W/CM2/SR)	E-12/E-4
10		SM BKGD (SIGNAL 2 HI) (W/CM2/SR)	E-12/E-4
11		SM BKGD (SIGNAL 2 LO) (W/CM2/SR)	E-12/E-4
12		RAW-DEMOD & FLTRD (SIGNAL 1 LO) (VOLTS)	0/10
13		RAW-DEMOD & FLTRD (SIGNAL 1 HI) (VOLTS)	0/10
14		RAW-DEMOD & FLTRD (SIGNAL 2 HI) (VOLTS)	0/10
15		RAW-DEMOD & FLTRD (SIGNAL 2 LO) (VOLTS)	0/10
16		RAW (SIGNAL 1 LO) (VOLTS)	-10/10
17		RAW (SIGNAL 1 HI) (VOLTS)	-10/10
18		RAW (REFERENCE) (VOLTS)	-10/10
19		RAW (SIGNAL 2 HI) (VOLTS)	-10/10
20		RAW (SIGNAL 2 LO) (VOLTS)	-10/10

Table 2. Full-Field Radiometer (NR-5) Data Base (continued)

CVF SPECTROMETER NS-6 FILE

WORD 2 IS A COMMUTATOR (100 X 1) WHICH CONTAINS (BY SFID): TIME,1; TARGET HKPG, 2-11; SENSOR HKPG, 12-20; SCAN #, 21; NS-6 HKPG, 22-28; UNASS, 29-50; (OPTIONAL) TRAJ & ATT, 51-96; UNASS, 97-100.

WORD	SFID	SYMBOL	DESCRIPTION	RANGE
1			SFID (100 SUBFRAMES/FRAME)	1/100
2	1		TIME FROM LAUNCH (SEC)	0/600
			T < 65 SEC / T > 65 SEC	
2	2		TIMER EVENTS / TIMER EVENTS	
2	3		ENGINE OXIDIZER PRESS (VOLTS)	0/5
2	4		ENGINE CHAMBER PRESS (VOLTS)	0/5
2	5		ENGINE FUEL PRESS (VOLTS)	0/5
2	6		TIMER EVENTS	
2	7		ENGINE GN2 PRESS (VOLTS)	0/5
2	8		ENGINE REGUL PRESS (VOLTS)	0/5
2	9		ENGINE FUEL TEMP (VOLTS)	0/5
2	10		ENGINE OXIDIZER TEMP (VOLTS)	0/5
2	11		ENGINE GN2 TEMP (VOLTS)	0/5
2	12		DRD FUNCTION MON (VOLTS)	0/5
2	13		DLD FUNCTION MON (VOLTS)	0/5
2	14		39A BATTERY (VOLTS)	0/5
2	15		B10A BATTERY (VOLTS)	0/5
2	16		C3 CAP MONITOR (VOLTS)	0/5
2	17			
2	18		K14 LOGIC RELAY (VOLTS)	0/5
2	19			
2	20			
2	21		SCAN #	1/1200
2	22		PT TEMP (VOLTS)	0/10
2	23		DT-C TEMP (VOLTS)	0/10
2	24		DT-W TEMP (VOLTS)	0/10
2	25		TB TEMP (VOLTS)	0/10
2	26		BB TEMP (VOLTS)	0/10
2	27		FP TEMP (VOLTS)	0/10
2	28			
2	29-50			
			TRAJECTORY & ATTITUDE (WORD 2, SFID 51-96)-OPTIONAL	
2	51		RT ASCEN OF GREENWICH (DEG)	0/360
2	52-54		GEOC POS COMPONENTS(SENSOR) (KM)	25000/-6500
2	55-57		GEOC VEL COMPONENTS(SENSOR) (KM/SEC)	-2/2
2	58-60		GEOC ACCEL COMPONENTS(SENSOR) (KM/SEC2)	-.5/.5
2	61		GEOD ALT ABOVE SUB-EARTH PT(SENSOR) (KM)	0/300
2	62-		GEOC POS COMPONENTS(TARGET) (KM)	25000/

Table 3. CVF Spectrometer NS-6 Data Base

	64		6500
2	65-	GEOC VEL COMPONENTS(TARGET) (KM/SEC)	-2/2
	67		
2	68-	GEOC ACCEL COMPONENTS(TARGET) (KM/SEC2)	-.5/.5
	70		
2	71	GEOD ALT ABOVE SUB-EARTH PT(TARGET) (KM)	0/300
2	72	TARGET RANGE (SCS) (KM)	0/15
2	73-	TARGET POS (SCS) (KM)	-15/15
	75		
2	76-	TARGET VEL (SCS) (KM/SEC)	-.5/.5
	78		
2	79-	TARGET ACCEL (SCS) (KM/SEC2)	-.01/ .01
	81		
2	82-	EULERIAN ANGLES DEF ECI TO SCS (DEG)	0/360
	84		
2	85-	EULERIAN ANGLES DEF VEN TO SCS (DEG)	0/360
	87		
2	88-	THRUST DIRECTION IN SCS (DEG)	0/360
	89		
2	90	ROLL ANGLE OF TARGET (DEG)	0/360
2	91-	TARGET NOZZLE POS IN SENSOR PLANE (DEG)	-10/10
	92		
2	93	ANGLE BETWEEN LOS & HARD EARTH TANGENT (DEG)	-90/90
2	94	TANGENT HT OF LOS FROM NEAREST EARTH SURF. (KM)	0/300
2	95	DISTANCE ALONG LOS TO PT NEAREST EARTH SURF. (KM)	0/2500
2	96	TARGET THRUST-VEL ANGLE (DEG)	0/180
2	97-		
	100		
3		% OF SCAN	0/100
4		WAVELENGTH (MU)	2/6
5		CABR (SIGNAL-LO) (W/CM2/SR/MU)	E-12/ E-4
6		CABR (SIGNAL-HI) (W/CM2/SR/MU)	E-12/ E-4
7		SM BKGD (SIGNAL-LO) (W/CM2/SR/MU)	E-12/ E-4
8		SM BKGD (SIGNAL-HI) (W/CM2/SR/MU)	E-12/ E-4
9		RAW (SIGNAL-LO) (VOLTS)	-10/10
10		RAW (SIGNAL-HI) (VOLTS)	-10/10
11		POSITION REFERENCE (VOLTS)	-10/10

Table 3. CVF Spectrometer NS-6 Data Base (continued)

CVF SPECTROMETER HS-3 FILE

WORD 2 IS A COMMUTATOR (100 X 1) WHICH CONTAINS (BY SFID): TIME,1; TARGET HKPG, 2-11; SENSOR HKPG, 12-20; SCAN #, 21; HS-3 HKPG, 22-28; UNASS, 29-50; (OPTIONAL) TRAJ & ATT, 51-96; UNASS, 97-100.

WORD	SFID	SYMBOL	DESCRIPTION		RANGE
1			SFID (100 SUBFRAMES/FRAME)		1/100
2	1		TIME FROM LAUNCH (SEC)		0/600
			T < 65 SEC	T > 65 SEC	
2	2		TIMER EVENTS	TIMER EVENTS	
2	3			ENGINE OXIDIZER PRESS (VOLTS)	0/5
2	4			ENGINE CHAMBER PRESS (VOLTS)	0/5
2	5			ENGINE FUEL PRESS (VOLTS)	0/5
2	6		TIMER EVENTS		
2	7		ENGINE GN2 PRESS (VOLTS)		0/5
2	8		ENGINE REGUL PRESS (VOLTS)		0/5
2	9		ENGINE FUEL TEMP (VOLTS)		0/5
2	10		ENGINE OXIDIZER TEMP (VOLTS)		0/5
2	11		ENGINE GN2 TEMP (VOLTS)		0/5
2	12		ORD FUNCTION MON (VOLTS)		0/5
2	13		DLD FUNCTION MON (VOLTS)		0/5
2	14		B9A BATTERY (VOLTS)		0/5
2	15		B10A BATTERY (VOLTS)		0/5
2	16		C4 CAP MONITOR (VOLTS)		0/5
2	17		K13 LOGIC RELAY (VOLTS)		0/5
2	18		K14 LOGIC RELAY (VOLTS)		0/5
2	19				
2	20				
2	21		SCAN#		1/1200
2	22		PRE-TEMP (VOLTS)		0/10
2	23		JET TEMP (VOLTS)		0/10
2	24		CF-C TEMP (VOLTS)		0/10
2	25		CF-W TEMP (VOLTS)		0/10
2	26		BAF TEMP (VOLTS)		0/10
2	27		OPT TEMP (VOLTS)		0/10
2	28				
2	29-50				
TRAJECTORY & ATTITUDE (WORD 2, SFID 51-96)-OPTIONAL					
2	51		RT ASCEN OF GREENWICH (DEG)		0/360
2	52-54		GEOC POS COMPONENTS(SENSOR) (KM)		25017 / 6523
2	55-57		GEOC VEL COMPONENTS(SENSOR) (KM/SEC)		-2/2
2	58-60		GEOC ACCEL COMPONENTS(SENSOR) (KM/SEC2)		-.5/.5
2	61		GEOD ALT ABOVE SUB-EARTH PT(SENSOR) (KM)		0/360
2	62-		GEOC POS COMPONENTS(TARGET) (KM)		25017

Table 4. CVF Spectrometer HS-3 Data Base

	64		6500
2	65-	GEOC VEL COMPONENTS(TARGET) (KM/SEC)	-2/2
	67		
2	68-	GEOC ACCEL COMPONENTS(TARGET) (KM/SEC2)	-.5/.5
	70		
2	71	GEOD ALT ABOVE SUB-EARTH PT(TARGET) (KM)	0/300
2	72	TARGET RANGE (SCS) (KM)	0/15
2	73-	TARGET POS (SCS) (KM)	-15/15
	75		
2	76-	TARGET VEL (SCS) (KM/SEC)	-.5/.5
	78		
2	79-	TARGET ACCEL (SCS) (KM/SEC2)	-.01/
	81		.01
2	82-	EULERIAN ANGLES DEF ECI TO SCS (DEG)	0/360
	84		
2	85-	EULERIAN ANGLES DEF VEN TO SCS (DEG)	0/360
	87		
2	88-	THRUST DIRECTION IN SCS (DEG)	0/360
	89		
2	90	ROLL ANGLE OF TARGET (DEG)	0/360
2	91-	TARGET NOZZLE POS IN SENSOR PLANE (DEG)	-10/10
	92		
2	93	ANGLE BETWEEN LOS & HARD EARTH TANGENT (DEG)	-90/90
2	94	TANGENT HT OF LOS FROM NEAREST EARTH SURF. (KM)	0/300
2	95	DISTANCE ALONG LOS TO PT NEAREST EARTH SURF. (KM)	0/2500
2	96	TARGET THRUST-VEL ANGLE (DEG)	0/180
2	97- 100		
3		% OF SCAN	0/100
4		WAVELENGTH (MU)	2/6
5		CABR (SIGNAL-LO) (W/CM2/SR/MU)	E-12/ E-4
6		CABR (SIGNAL-HI) (W/CM2/SR/MU)	E-12/ E-4
7		SM BKGD (SIGNAL-LO) (W/CM2/SR/MU)	E-12/ E-4
8		SM BKGD (SIGNAL-HI) (W/CM2/SR/MU)	E-12/ E-4
9		RAW (SIGNAL-LO) (VOLTS)	-10/10
10		RAW (SIGNAL-HI) (VOLTS)	-10/10
11		POSITION REFERENCE (VOLTS)	-10/10

Table 4. CVF Spectrometer HS-3 Data Base (continued)

HONEYWELL SPATIAL RADIOMETER FILE

WORD 2 IS A COMMUTATOR (25 X 1) WHICH CONTAINS (BY SFID): TIME, 1; TARGET HKPG, 2-11; SENSOR HKPG, 12-20; SWEEP #, 21; UNASS, 22-25.
WORD 3 IS A COMMUTATOR WHICH CONTAINS: (OPTIONAL) TRAJ, 1-25.
WORD 4 IS A COMMUTATOR WHICH CONTAINS: (OPTIONAL) TRAJ & ATT, 1-21; UNASS, 22-25.

WORD	SFID	SYMBOL	DESCRIPTION	RANGE
1			SFID (25 SUBFRAMES/FRAME)	1/25
2	1		TIME FROM LAUNCH (SEC)	0/600
			T < 65 SEC / T > 65 SEC	
2	2		TIMER EVENTS / TIMER EVENTS	
2	3		ENGINE OXIDIZER PRESS (VOLTS)	0/5
2	4		ENGINE CHAMBER PRESS (VOLTS)	0/5
2	5		ENGINE FUEL PRESS (VOLTS)	0/5
2	6		TIMER EVENTS	
2	7		ENGINE GN2 PRESS (VOLTS)	0/5
2	8		ENGINE REGUL PRESS (VOLTS)	0/5
2	9		ENGINE FUEL TEMP (VOLTS)	0/5
2	10		ENGINE OXIDIZER TEMP (VOLTS)	0/5
2	11		ENGINE GN2 TEMP (VOLTS)	0/5
2	12		DRD FUNCTION MON (VOLTS)	0/5
2	13		DLD FUNCTION MON (VOLTS)	0/5
2	14		B11A BATTERY (VOLTS)	0/5
2	15		C1 CAP MONITOR (VOLTS)	0/5
2	16		K10 LOGIC RELAY (VOLTS)	0/5
2	17		K11 LOGIC RELAY (VOLTS)	0/5
2	18			
2	19			
2	20			
2	21		SWEEP #	1/600
2	22-25			
			TRAJ & ATT (WORD 3, SFID 1-25 AND WORD 4, SFID 1-21)-OPTIONAL	
3	1		RT ASCEN OF GREENWICH (DEG)	0/360
3	2-4		GEOC POS COMPONENTS(SENSOR) (KM)	25000/6500
3	5-7		GEOC VEL COMPONENTS(SENSOR) (KM/SEC)	-2/2
3	8-10		GEOC ACCEL COMPONENTS(SENSOR) (KM/SEC2)	-.5/.5
3	11		GEOD ALT ABOVE SUB-EARTH PT(SENSOR) (KM)	0/300
3	12-14		GEOC POS COMPONENTS(TARGET) (KM)	25000/6500
3	15-17		GEOC VEL COMPONENTS(TARGET) (KM/SEC)	-2/2
3	18-20		GEOC ACCEL COMPONENTS(TARGET) (KM/SEC2)	-.5/.5
3	21		GEOD ALT ABOVE SUB-EARTH PT(TARGET) (KM)	0/300
3	22		TARGET RANGE (SCS) (KM)	0/15

Table 5. Honeywell Spatial Radiometer Data Base

3	23-25	TARGET POS (SCS) (KM)	-15/15
4	1-3	TARGET VEL (SCS) (KM/SEC)	-.5/.5
4	4-6	TARGET ACCEL (SCS) (KM/SEC2)	-.01/.01
4	7-9	EULERIAN ANGLES DEF ECI TO SCS (DEG)	0/360
4	10-12	EULERIAN ANGLES DEF VEN TO SCS (DEG)	0/360
4	13-14	THRUST DIRECTION IN SCS (DEG)	0/360
4	15	ROLL ANGLE OF TARGET (DEG)	0/360
4	16-17	TARGET NOZZLE POS IN SENSOR PLANE (DEG)	-10/10
4	18	ANGLE BETWEEN LOS & HARD EARTH TANGENT (DEG)	-90/90
4	19	TANGENT HT OF LOS FROM NEAREST EARTH SURF. (KM)	0/300
4	20	DISTANCE ALONG LOS TO PT NEAREST EARTH SURF. (KM)	0/2500
4	21	TARGET THRUST-VEL ANGLE (DEG)	0/180
4	22-25		
5	1-8	HK1-HK8	
5	9-16	TMP1-TMP8	
5	17-25		
6		MIRROR POS	
7-46		CABR FROM EACH OF 40 DETECTORS	
47-86		SM BKGD FROM EACH OF 40 DETECTORS	
87-126		RAW FROM EACH OF 40 DETECTORS	

Table 5. Honeywell Spatial Radiometer Data Base (continued)

	Frame rate	Subframe rate	Number of Subframes per frame	Number of values per subframe	Number of values (Assuming 600 sec. flight)
UV Photometers & Spectrometer	10 Hz	1000 Hz	100	12	$7.2 * 10^6$
Full-Field Radiometer	10 Hz	500 Hz*	50	20	$6 * 10^6$
CVF	20 Hz	2000 Hz	100	11	$13.2 * 10^6$
Spectrometer	10 Hz	1000 Hz*	100	11	$6.6 * 10^6$
Honeywell Spatial	10 Hz	250 Hz	25	126	$18.9 * 10^6$
Radiometer	5 Hz	125 Hz$	25	126	$9.45 * 10^6$

Note: On 7-track tape (800 bpi) can fit
$2* 10^6$ 60-bit words.
On 9-track tape (1600 bpi) can fit
$4.75 * 10^6$ 60-bit words.

* Averaging two successive values

$ Taking every other sample

Table 6. Estimate of Volume of Data per Instrument based on Data Base Specifications of Tables 1 - 5.

References

1. Kotelly, J. C. (SUA), "MSMP Data Management Plan" (Unpublished).

2. "Analysis and Programming for Research in Physics of the Upper Atmosphere", Logicon, Inc., Final Report, AFGL-TR-76-0231, Sept., 1976.

3. Goldstein, H., Classical Mechanics, Addison-Wesley, Reading, Ma., 1950.

4. Miller, W. B., "MSMP Telemetry Data", AFGL Tech Data No. 77-1, March, 1977.

Section 9. General Programs

Author: K. H. Bhavnani

9.0 Packing-Unpacking Programs

Initiator: E. Robinson

Project No: 2123 Problem No: 4937

Two general subroutine systems were developed for efficient packing/unpacking and input/output of fixed length records. They have been employed in various instances where large quantities of data in repeating format must be stored and processed. Subroutine PACKER handles records consisting of an independent variable (such as time) requiring a full CDC 60-bit word, and a fixed number of NB-bit words where NB is a sub-multiple of 60.

Subroutine PACKUP handles records consisting of a fixed number of variable bit length words, the only requirement on the bit length being that packed data must fit 60-bit boundaries. All unpacked data are taken to be contained in the rightmost bits of CDC words; therefore it is incumbent on the user to scale his data depending upon range and resolution limits so as to always represent them as non-negative integers.

User's guide listings for the available routines are provided on the next two pages.

9.1 Functional Description

Packing and blocking procedures are used in order to optimize for storage and speed. BUFFER IN-OUT is used since this is faster than Fortran binary read-write, and to allow simpler information interchange with other computer installations if required. 510-word blocking is used since this is an accepted block length for 800 bpi tapes, and to remain within the 512-word binary blocking of SCOPE 3.4 even if Fortran binary read-writes were desired for some reason.

```
C     SUBROUTINE PACKER      PACKLIB,ID=LOGICON.                MAY, 1977
C
C  SUBROUTINE PACKER PROCESSES FIXED LENGTH RECORDS CONSISTING OF
C  TIME AND THE FIXED RIGHTMOST 'NB' BITS OF 'LD' DATA WORDS. THESE ARE
C  PACKED INTO 'NW' CDC-WORD RECORDS, AND INPUT-OUTPUT TO SEQUENTIAL FILES.
C
C  THE FIRST WORD (EG. TIME) IS STORED UNCHANGED, AND THE RIGHTMOST NB BITS
C  OF THE LD DATA WORDS ARE PACKED FROM LEFT TO RIGHT INTO CDC 60-BIT WORDS,
C  WITH THE UNUSED PART OF THE LAST CDC WORD OF EACH RECORD ZERO-FILLED.
C  EACH RECORD THUS CONSISTS OF  NW = 1 + LD*NB/60 (ROUNDED-UP) CDC WORDS.
C  AN INTEGRAL NUMBER 'NR' OF THESE RECORDS ARE BLOCKED INTO 510 CDC WORDS.
C  THE FIRST WORD OF EACH BLOCK IS A CONTROL WORD WHICH DEFINES NB, NW & NR.
C  THE UNUSED WORDS AT THE END OF EACH BLOCK ARE ALSO ZERO-FILLED.
C  ACTUAL I-O IS ACCOMPLISHED BY BUFFER IN-OUT STATEMENTS USING ODD PARITY.
C
C  ALL ROUTINE CALLS ARE OF THE FORM
C     CALL XYTP(ITAPE, TIME, IARRAY, LN, LARRAY), RETURNS(E,F)
C        WHERE
C  ITAPE IS THE LOGICAL FILE NUMBER (FROM 1 TO 10 ALLOWED)
C  IARRAY AND LARRAY MUST HAVE DIMENSION LD
C  LN MAY TAKE ON ANY VALUE FROM 1 TO LD
C  E IS THE END-OF-FILE RETURN,     F IS THE PARITY ERROR RETURN
C
C  THE LIST OF AVAILABLE ROUTINES FOLLOWS:
C
C     CALL NUTP(ITAPE, NB, LD)
C  ESTABLISHES CONTROL INFORMATION FOR WRITING OR READING.
C  NB MUST BE A PROPER SUB-MULTIPLE OF 60
C
C     CALL OLTP(ITAPE)
C  FOR READING PREVIOUSLY PREPARED FILES, CONTROL INFORMATION MAY BE
C  INITIALIZED FROM THE BLOCK THAT IS NEXT IN POSITION.
C
C     CALL PKTP(ITAPE, TIME, IARRAY, LN)
C  TIME AND THE FIRST LN WORDS FROM IARRAY ARE PACKED OUT.
C
C     CALL UPTP(ITAPE, TIME, IARRAY, LN, 0), RETURNS(E,F)
C  TIME AND THE FIRST LN WORDS ARE UNPACKED INTO IARRAY.
C
C     CALL WRTP(ITAPE, TIME, IARRAY, LN, LARRAY)
C  LARRAY SHOULD CONTAIN LN INTEGERS, EACH HAVING A VALUE FROM 1 TO LD.
C  THE CORRESPONDING IARRAY LOCATIONS ONLY REPLACE EXISTING PACKED DATA.
C
C     CALL ROTP(ITAPE, TIME, IARRAY, LN, LARRAY), RETURNS(E,F)
C  TIME AND THE SELECTED LN WORDS ONLY ARE UNPACKED INTO IARRAY(1-LD).
C
C     CALL OUTP(ITAPE, TIME, IARRAY)
C  TIME AND NW PRE-PACKED WORDS ARE COPIED OUT FROM IARRAY.
C
C     CALL INTP(ITAPE, TIME, IARRAY, 0, 0), RETURNS(E,F)
C  TIME AND ALL NW PACKED WORDS ARE COPIED AS IS INTO IARRAY.
C
C     CALL BSTP(ITAPE)
C  BACKSPACE OF ONE RECORD ONLY WHEN READING A FILE.
C
C     CALL ENTP(ITAPE)
C  THE LAST BLOCK IS WRITTEN TO TAPE FOLLOWED BY AN END-OF-FILE.
C
C     CALL RETP(ITAPE)
C  INDICES ARE RESET BY ONE TO ALLOW A NEW FILE TO ACCESS THESE ROUTINES.
C
```

```
C     SUBROUTINE PACKUP      PACKLIB,ID=LOGICON.                    MAY, 1977
C
C  SUBROUTINE PACKUP PROCESSES FIXED LENGTH RECORDS CONSISTING OF
C  THE VARIABLE RIGHTMOST 'NB' BITS OF 'LD' DATA WORDS. THESE ARE
C  PACKED INTO 'NW' CDC-WORD RECORDS, AND INPUT-OUTPUT TO SEQUENTIAL FILES.
C
C  THE LD DATA WORDS ARE PACKED FROM LEFT TO RIGHT INTO CDC 60-BIT WORDS,
C  WITH ALL PACKED DATA EXCEPT THE LAST TERMINATING ON 60-BIT BOUNDARIES,
C  AND THE UNUSED PART OF THE LAST CDC WORD OF EACH RECORD ZERO-FILLED.
C  AN INTEGRAL NUMBER 'NR' OF THESE RECORDS ARE BLOCKED INTO 510 CDC WORDS.
C  THE FIRST WORD OF EACH BLOCK IS A CONTROL WORD WHICH DEFINES NW & NR.
C  THE UNUSED WORDS AT THE END OF EACH BLOCK ARE ALSO ZERO-FILLED.
C  ACTUAL I-O IS ACCOMPLISHED BY BUFFER IN-OUT STATEMENTS USING ODD PARITY.
C
C  ALL ROUTINE CALLS ARE OF THE FORM
C     CALL XYFL(ITAPE, IARRAY, LN) RETURNS(E,F)
C       WHERE
C  ITAPE IS THE LOGICAL FILE NUMBER (FROM 1 TO 10 ALLOWED)
C  IARRAY AND LARRAY MUST HAVE DIMENSION LD
C  LN MAY TAKE ON ANY VALUE FROM 1 TO LD
C  E IS THE END-OF-FILE RETURN,     F IS THE PARITY ERROR RETURN
C
C  THE LIST OF AVAILABLE ROUTINES FOLLOWS:
C
C     CALL NUFL(ITAPE, IARRAY, LD)
C  ESTABLISHES CONTROL INFORMATION FOR WRITING OR READING.
C  IARRAY PROVIDES THE VALUE NB FOR EACH DATA WORD.
C
C     CALL OLFL(ITAPE, IARRAY, LD)
C  FOR READING PREVIOUSLY PREPARED FILES, USE OF OLFL RATHER THAN NUFL
C  VERIFIES THE PACKING INFORMATION AGAINST NW FROM THE NEXT BLOCK.
C
C     CALL PKFL(ITAPE, IARRAY, LN)
C  THE FIRST LN WORDS FROM IARRAY ARE PACKED OUT.
C
C     CALL UPFL(ITAPE, IARRAY, LN), RETURNS(E,F)
C  THE FIRST LN WORDS ARE UNPACKED INTO IARRAY.
C
C     CALL OUFL(ITAPE, IARRAY)
C  NW PRE-PACKED WORDS ARE COPIED OUT FROM IARRAY.
C
C     CALL INFL(ITAPE, IARRAY, 0), RETURNS(E,F)
C  ALL NW PACKED WORDS ARE COPIED AS IS INTO IARRAY.
C
C     CALL BSFL(ITAPE)
C  BACKSPACE OF ONE RECORD ONLY WHEN READING A FILE.
C
C     CALL ENFL(ITAPE)
C  THE LAST BLOCK IS WRITTEN TO TAPE FOLLOWED BY AN END-OF-FILE.
C
C     CALL REFL(ITAPE)
C  INDICES ARE RESET BY ONE TO ALLOW A NEW FILE TO ACCESS THESE ROUTINES.
C
```

The first word in each block is the control word. For PACKER this contains zeroes in the first (leftmost) 12 bits, block length (510) in the second 12 bits, bit length NB in the third 12 bits, number of CDC words per packed record in the fourth 12 bits, and the number of packed records in the block in the rightmost 12 bits. This information is sufficient to initialize the routines for unpacking a previously prepared tape.

For PACKUP the control word information differs only in that the total bit length for all the variables is stored in the third 12-bit field. Initialization before packing or unpacking requires that the number of data words and the bit length per word be provided. A feature of this system is that a tape prepared by PACKER can be read by PACKUP, the latter comprising more general but somewhat (30%) slower programs.

The routines allow various tape input-output operations after initialization. Pack (write) or unpack (read) may be performed in 3 ways:

1) an array of the first N data words
2) individually selected words from an array
3) Bulk transfer of the full packed record

An ENTP or ENFL operation is necessary at the end of writing to tape, to ensure that the last block is output.

Simultaneous use of either of these routines is restricted to two tapes. RETP or REFL returns control area storage for a new file after a file has completed using the routines. Logical tape numbers are restricted to 1-10. Finally, in PACKUP the maximum number of data words is restricted to 50.

9.2 Logical Procedures and Performance

The main performance consideration is that compared to binary unpacked READ/WRITE to tape, savings of the order of 75% can be obtained in file storage re-

quirements for packable data. As shown below, data transfer times using PACKER or PACKUP are also superior to binary unpacked Fortran read-writes.

Each of the subroutine calls requires only a few lines of compact code. The program is optimized in FORTRAN IV by the exclusive use of inline functions such as AND, SHIFT, etc. Indexing is avoided where this is advantageous. A variety of test runs were conducted leading to the present implementation of the programs. Comparative execution times are discussed below, based on 10,000 operations of the type indicated. Packing or unpacking times for the same type commands are comparable, and the average values are given.

BUFFER IN (OUT) 510 words	3.5 secs
Binary READ(WRITE) 510 words	40.0 secs
All the following handle time and 48 data words.	
Binary READ (WRITE) - No Packing	8.0 secs
All the following handle packed data (12 bits).	
PKFL or UPFL	7.0 secs
PKTP or UPTP	5.0 secs
PKTP (UPTP) w. Binary READ/WRITE instead of BUFFER IN/OUT	5.5 secs
PKTP (UPTP) w/o blocking	11.5 secs
PKTP (UPTP) using LBYTX, etc.	19.0 secs
WRTP or RDTP	9.0 secs
WRTP (RDTP) replace 4 of the 48 data words	1.7 secs
OUTP or INTP (direct transfer of the packed words)	1.0 secs

9.3 Job Setup and Program Restrictions

These routines require about 3K octal core memory

When in frequent use, EDITLIB has been used to store the binaries on permanent file.

Program halts due to violation of restrictions occur under the following conditions:

STOP PACKER ERROR occurs if logical Tape number < 1 or > 10
or More than 2 logical files initialized
or NB (bits/word) is not a sub-multiple of 60.

STOP PACKUP ERROR occurs if
Logical Tape number < 1 or > 10
or More than 2 logical files initialized
or Packed words do not fit 60-bit boundaries
or Number of data words > 50
or Number CDC words calculated in OLFL > control word info.

STOP BACKSPACE ERROR occurs if a BUFFER-IN after backspace results in an end-of-file or a parity error.
The BUFFER- IN/OUT operations allow for end-of-file and parity error returns. Following parity error on a read operation, the subroutines are set to bring in and process the next block on an ensuing unpack call. However, a BSTP or BSFL backspace call allows the first record only of the block with the parity error to be unpacked if desired.

Section 10. Astronomical Ephemerides

Authors: K. H. Bhavnani

R. R. Hayes

10.0 New JPL Planetary Ephemeris (DE-96)

Initiator: L. Telford

Project No: 4643 Problem No: 4844

The JPL ephemeris system became unworkable when all copies of the old JPL DE19 tapes proved unreadable for 1977 and beyond. JPL has gone through various official releases of Ephemeris Tape systems. The latest version was accordingly obtained from JPL[1,2]. This BCD tape DE-96 was converted to binary using Fortran code provided on the same tape. The new version obsoletes the old JPL binaries, is based on updated planetary observational data, and uses improved interpolation techniques to compact data through the year 2000 on about half a reel as compared to three reels for the previous version.

Routines to process the new tape were incorporated into System II of the JPL Ephemeris Processing System. This produces the annual tape for Prospect Hill Radio Observatory. Results duplicated the earlier version for 1976 to within 0.5 seconds of arc. A 1977 PHRO tape was then created. This revision can also be incorporated in System I - the general Ephemeris Processing System, if planetary observations are required.

10.1 Implementation at AFGL

A 7-track even parity magnetic tape which constitutes the export or users' package for DE-96 was requested from JPL. This encoded form is originally prepared on a Univac 1108, but is as machine-independent as possible with instructions[2] as to how to adapt and use the tape. There are two files on the tape:

File 1 contains in card image form all the Fortran software needed for conversion of the encoded ephemeris file to binary, and for use of the binary tape. Twelve programs and subroutines are included.

File 2 contains the encoded ephemeris in 550 records of 24000 characters each.

1) File 1 was punched out to obtain a card deck for further work.

2) File 2 was Buffered-In in even parity 2400 word blocks and written out with SCOPE 3.4 binary writes to Tape JPLE96 for intermediate storage.

3) The deck of programs was debugged for Fortran errors on the CDC-6600.

4) Program BCDEPH and subroutine RCI were run using JPLE96 to create the compact binary tape JPL 96B which is the exclusive data base hereafter. The range of the data is from December 16, 1944 to January 25, 2000.[1] JPL achieves compaction by providing Chebyshev coefficients for polynomials which can be interpolated for the ephemeris of a particular body.

5) Program XSHORT and subroutines LH, SECCAL and VIGSEC may be used to create a short copy of JPL96B over a selected range of epochs. This feature was tested but not used in the further development.

6) The main user subroutine is READE which reads and interpolates the binary ephemeris file. Double precision is provided and has not been eliminated though it is not required on the CDC-6600. READE in turn requires subroutines XSTATE, XINTRP and LH. The description of subroutine READE is reproduced from Reference 2 on the following two pages.

READE

Purpose: Read and interpolate the binary ephemeris file. Many users have a subroutine by the same name that reads earlier JPL ephemeris files. This routine can be used in its place without change. The binary file must be on unit 12.

Use: The user must have the four statements

```
DOUBLE PRECISION  AU, RE, TPD, EMRAT, TABOUT, NUT, JED, TSEC
COMMON/CETBL1/AU, RE, TPD, EMRAT
COMMON/CETBL2/ICW, ICENT, IREQ(13)
COMMON/CETBL4/TABOUT(6, 12),NUT(4)
```

in his program.

Then the call

```
CALL READE (JED, TSEC, IERR)
```

provides the interpolation, according to the following rules:

AU is the scale factor that multiplies the output quantities. If AU = 0, all distance units are in kilometers. If AU = any other number, the distance unit is (astronomical unit)*AU.

RE is not used.

TPD is the time unit. If TPD = 0, time units are seconds. If TPD = any other number, time units are days*TPD.

EMRAT is the earth-moon mass ratio. If EMRAT = 0, the value 81.3007 is assumed.

ICW is a flag word. ICW ≠ 2 forces a new raw data read on the next call to READE. The subroutine sets ICW to 2.

ICENT is the center number of the coordinate system. All vectors are referenced to earth mean equator and equinox of 1950.0. The bodies corresponding to center numbers are:

Number	Body
1	Mercury
2	Venus
3	Earth
4	Mars
5	Jupiter
6	Saturn
7	Uranus
8	Neptune
9	Pluto
10	Sun
11	Moon

Reproduced from "JPL Export Ephemeris DE-96 Users Guide", January 1976.

IREQ is what kind of interpolation is requested for each body. The meaning is:

IREQ(I) = 0, no interpolation
= 1, position only
= 2, position and velocity

For I = 1 through 11, the body designation is the same as for ICENT. IREQ(12) refers to the Earth-Moon barycenter, and IREQ(13) refers to nutations.

The calling sequence arguments JED and TSEC specify the ephemeris epoch at which interpolation is wanted. The ephemeris date is taken to be JED + TSEC/86400. Any combination of JED and TSEC is permissible, but for highest precision it is recommended that JED be the most recent midnight at or before the requested epoch and that TSEC be the number of ephemeris seconds elapsed between then and the interpolation epoch.

Output:

For I = 1 - 12, interpolated quantities requested in IREQ(I) are in TABOUT(1, I) - TABOUT(3, I) for position vectors and in TABOUT(4, I) - TABOUT(6, I) for velocity vectors.

NUT(1) contains $\delta\psi$, the nutation in longitude
NUT(2) contains $\delta\varepsilon$, the nutation in obliquity
NUT(3) contains $\delta\dot{\psi}$, and
NUT(4) contains $\delta\dot{\varepsilon}$.

The units of nutations are radians and radians/time unit.

IERR is a status flag.

IERR = 0, normal return.
= 1, epoch earlier than earlist epoch on file.
= 2, epoch later than last epoch on file.
= 3, IREQ(I) < 0 or IREQ(I) > 2
= 4, Illegal value for ICENT

Necessary Modifications: None

Reproduced from "JPL Export Ephemeris DE-96 Users Guide", January 1976.

7) Program TSTRDE was employed to exercise the binary ephemeris file using subroutines READE and SECCAL. Output was matched to a microfiche copy of a JPL run.

8) System II of the JPL Ephemeris Processing System produces an annual tape for Prospect Hill Radio Observatory. This program was modified to operate with the new JPL96B binary ephemeris file. Code for reading and interpolating the obsoleted binary file was removed from subroutines EPHEMI, EPHE1 and INTRPL of System II and replaced by one call to READE in EPHE1 along with the required labelled common and double precision statements. Provision for entering ET-UT in seconds was added.

This revised System II is operational and has been used satisfactorily to produce PHRO ephemeris tapes for 1977 and 1978. Modification of System I for planetary ephemerides at AFGL can be carried out when required.

References

(1) "JPL Development Ephemeris Number 96", Jet Propulsion Laboratory, Technical Report 32-1603; February, 1976.

(2) "JPL Export Ephemeris DE-96 Users Guide", Jet Propulsion Laboratory; January, 1976. Contact: Dr. X. X. Newhall